SHOWING WIDELY DIFFERENT LATERAL SWAY IN ANGLED-PLANE AND PARALLEL-PLANE SCISSOR LINKAGES THROUGH EQUATIONS OF MECHANICS

A Thesis Submitted in
Partial Fulfillment of the Requirements
for the Degree of

DOCTOR OF PHILOSOPHY

By

SUNIL KUMAR SINGH

(Roll No.136103011)

DEPARTMENT OF MECHANICAL ENGINEERING
INDIAN INSTITUTE OF TECHNOLOGY GUWAHATI
GUWAHATI (ASSAM)-781039

JANUARY, 2020

CERTIFICATE

It is certified that the work contained in the thesis entitled **"Showing widely different lateral sway in angled-plane and parallel-plane scissor linkages through equations of mechanics"**, by **Sunil Kumar Singh** has been carried out under my supervision and that this work has not been submitted elsewhere for a degree.

(Sangamesh Deepak R)

January, 2020

Assistant Professor

Department of Mechanical Engineering

Indian Institute of Technology Dharwad

(Formerly at Indian Institute of Technology Guwahati)

DECLARATION

I, Sunil Kumar Singh (Roll no: 136103011) declare that the present written submission is my thoughts in my own words. I have adequately cited and referenced the original sources, where other's ideas have been involved. I also declare that I have adhered to all principles of academic honesty and integrity and have neither fabricated nor falsified any idea/data/fact/source in my submission. I understand that any violation of the above will be cause for disciplinary action by the Institute and can also evoke penal action from the sources which have thus not been properly cited or from whom proper permission has not been taken when needed.

(Sunil Kumar Singh)
Roll No. 136103011

Date:

Dedicated to my parents

Shri. Ram Raj Singh

Smt. Dharm Shati Devi

Acknowledgment

First and foremost, I express my great appreciation to my mentor **Dr. Sangamesh Deepak R.** for his invaluable guidance and fruitful discussion through my Ph.D. duration. His kindness, dedication, and attention to the details have been a source of great inspiration to me. My heartfelt thanks to my mentor for his unlimited support and patience that he has shown towards me. I am also very thankful for his consistent efforts to help me in better ways to improve my writing and learning skills. I thank him from the bottom of my heart for always being there with me during my journey as a research scholar at IIT Guwahati. I would like to express my gratitude to my mentor, Dr. Sangamesh Deepak R., for saying yes to me and giving me a chance to pursue doctoral research under him.

I also would like to express my great appreciation and thanks to **Dr. Arup Nandy** for his unconditional support as an administrative supervisor during the absence of Dr. Sangamesh Deepak R. (currently at IIT Dharwad). I also would like to thank him for his helpful suggestions and comments on the thesis.

I would like to thank my doctoral committee members: **Prof. Uday Shanker Dixit**, **Prof. Poonam Kumari** and **Prof. Arbind Kumar Singh** for sparing time out of their busy schedule to evaluate my progress and enrich this work with their valuable suggestions and feedbacks. I also extend my sincere thanks to the HOD of the mechanical department, all the staff members from ME office, Central Workshop, and Academic Office members for helping me out in all sorts of ways during my stay at IIT Guwahati.

I wish to express my deep gratitude to **(Late) Dr. A. N. Reddy**, who provide me academic and mental support at the time of my PhD journey.

I also would like to thank the reviewers of our paper for valuable and helpful comments.

I am also thankful to my friends Visal Agrawal, Ashish Rajak, Saipraneeth, Tushar Semwal, Prateek Rathod, Shahnawaz Ahamed, and other colleagues who provided their support in writing a part of reports such as SOAS, APS and thesis literature.

I am also thankful to my friends Manish Kumar Dubey, Bebabrata Gayan, Visal Agrawal, Ashish Rajak who supported me at the time of course work and comprehensive viva.

My deepest gratitude goes to my family members for their continuous love and support throughout my studies. The opportunities that they have given me and their unlimited sacrifices are the reasons where I am and what I have accomplished so far. They have been and will remain my ultimate source of inspiration to achieve every possible height in my journey.

Sunil Kumar Singh

ABSTRACT

In an exercise of prototyping a scissor linkage, based on naked-eye observation, it was noted that there is a significant difference in lateral sway of parallel-plane scissor linkage and angled-plane scissor linkage. However, there is no literature documenting any mechanics-based investigation on this difference in lateral sway characteristics. Typically, the more the number of variables defining a mathematical model, it would be harder to think through the model. Hence, we posed the following question: to a single degree of freedom ideal scissor linkage, what non-idealities could be added such that it is possible to deduce the significant difference in lateral sway characteristics while keeping the number of additional degrees of freedom due to non-idealities as small as possible. By ideal scissor linkage, we mean that the links are rigid, revolute joints are perfect without any misalignment or offsets in joint-axes, and the linkage has just one degree of freedom. The posed question is the motivation of the thesis. The deduction of the significant difference in lateral sway characteristics through equations of mechanics under the presence of revolute-joint-misalignment as the non-ideality constitutes the central and the original contribution of the thesis.

In rigid-multibody dynamics, there is a well-known kinematic mathematical model of non-linear equations where variables are translational and rotational variables of the bodies, and non-linear equations come from the constraints defining joints between the bodies. The constraints of a revolute-joint have five scalar equations. Among the five scalar equations, two equations relate to alignment of the joint. We mathematically quantify a misalignment in the revolute joint as violation of the two equations related to joint-alignment. The actual misalignment in practice could depend on various factors such as clearance in the joint, axial length of the bearing, and deformation of the bearing-surface due to loads. However, in the mathematical model, we would only say that the misalignment cannot exceed a pre-stated plus-minus limit. This lets us retain the mathematical model in the domain of kinematics. The lateral sway is also mathematically quantified as the sum of displacements of extreme points in their laterally swaying directions. With the mathematically quantified lateral sway as the objective function, translational and rotational coordinates of bodies as variables, constraints of revolute joint (with

slack variables incorporated) as equality constraints, and plus-minus bounds on slack variables, we have an optimization problem. A numerical solution to the optimization problem (maximization of lateral sway) did bring out the significant difference in lateral sway between parallel-plane and angled-plane scissor linkage. However, we could not get the analytical solution to the problem even after linearization. Nevertheless, from the linearized analytical problem, we could deduce bounds on maximum lateral sway, and these bounds were themselves sufficient to show the contrasting characteristics. One such result is that as the number of repeating units in the scissor linkage is increased, the lateral sway would follow a geometric series in the case of angled-plane scissor linkage and an arithmetic sequence in the case of parallel-plane scissor linkage. Further, in reasonably chosen cases, the numerically obtained maximized lateral sway respected the bounds deduced in the linearized analytical study.

There are also some auxiliary contributions and attempts. Bamboo is more famous as a structural material. Scissor linkages built primarily out of bamboo strips that are demonstrated in the thesis showcase greater opportunities in bamboo-crafts. The prototyping exercise also involved static balancing the scissor linkage. There are more than one static balancing methods. In order to rationally rank them, we explored if the frictional effort in different methods could be used. All these auxiliary results are tied to the main contribution in the sense that all these results have roots in the prototyping exercise.

Original Contributions

The central and major contribution of the thesis

Under the terms and assumptions stated in Appendix A, for $0 \leq \theta \leq 80^\circ$ and small displacements,

1. if $\phi \neq 0$, i.e., if the scissor linkage is angled, then the magnitude of maximum possible lateral displacement $|\mathcal{C}_{max}|$ is bounded as given next:

$$|\mathcal{C}_{max}| \leq l\epsilon r \frac{1-r^i}{1-r}$$

where

$$r = \frac{1}{\left(1 + 2\frac{l}{c}\sin\frac{\phi}{2}\cos\theta\right)}$$

2. if $\phi = 0$, i.e., if the scissor linkage is parallel, then the magnitude of maximum possible lateral displacement $|\mathcal{C}_{max}|$ is bounded as given next:

$$i\epsilon l \sin(\theta) \leq |\mathcal{C}_{max}| \leq i\epsilon l$$

3. The bounds in the previous items when plotted with $l = 30\,cm$, $c = 4\,cm$, $\epsilon = 0.01$, would result in a plot shown in figure (1). From this, it is evident that the lateral sway of parallel-plane scissor could be significantly different and much more than the lateral sway of angled-plane scissor linkage. Thus, the degree of freedom arising out of misalignment in revolute joints would lead to lateral deflection that has a widely different magnitude between parallel-plane scissor linkage and angled-plane scissor linkage.

4. Verification of the above bounds through a numerical model of the scissor linkages that do not have the restriction of small motion.

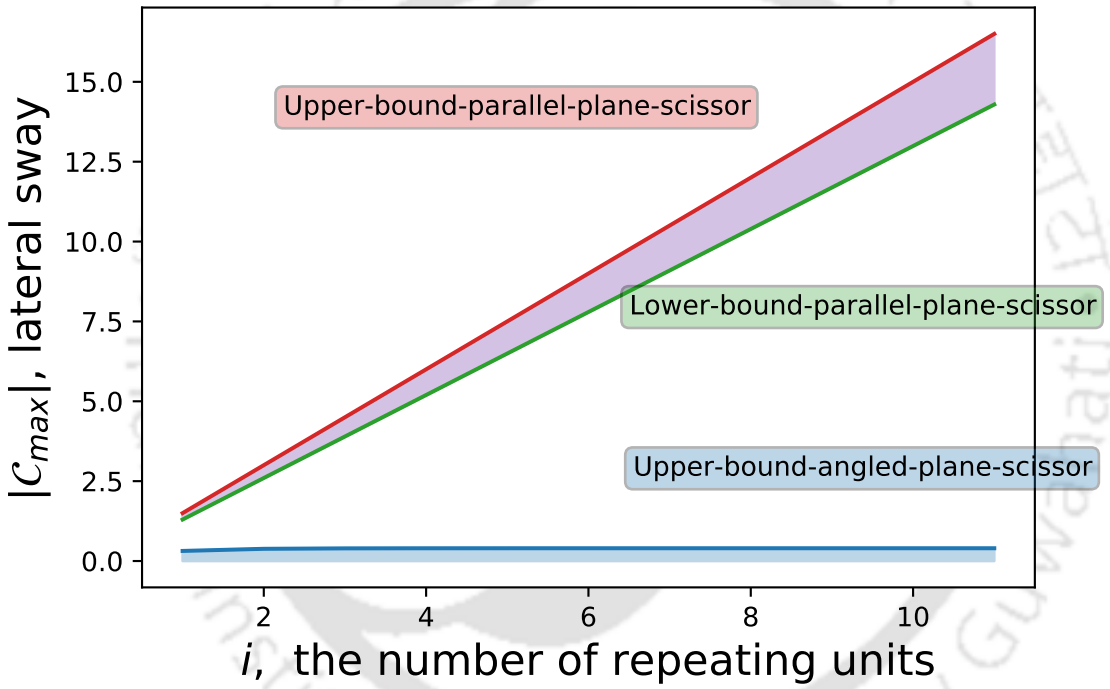

Figure 1: The regions where maximum lateral sway would lie for parallel-plane scissor linkage and angled-plane scissor linkage.

5. To our knowledge, this is the first time that a successful mechanics-based mathematical explanation has been given to show that there could be significantly different lateral sway characteristics between parallel-plane and angled-plane scissor linkage.

Minor contributions

1. When static-balancing a linkage, often there are multiple ways of static balancing. We have explored if the frictional effort could be used to rationally choose between the multiple ways.

2. We fabricated a scissor-linkage prototype that is primarily made of bamboo strips. This could be significant in bamboo-crafts, which primarily make structural products. The design exploration for the prototype is only in the domain of mechanism design and static balancing. It is this prototype that binds the entire thesis since the problems of lateral sway and choosing among multiple static balancing methods were observed while making this prototype.

Contents

List of Figures

List of Tables

Nomenclature

Chapter 1

Symbol	Definition
a, b	bearing surface length
F, f	forces
k	proportionality constant
n	number of rigid bodies
θ_m	misalignment angel of shaft
δ	clearance gap
τ	torque

Chapter 4

Symbol	Definition
c	connector length
l	link length
N	number of scissor unit
r	position vector
R	rotation matrix
s_1, s_2	slack variables
x, y, z	Cartesian co-ordinates of bodies
u, v, w	unit vector of bodies in Cartesian co-ordinates
θ	angle between ground and scissor link
ϕ	angle between two scissor linkage
ϵ	permissible misalignment
Subscripts	
i, j	index notations refers bodies
0	reference body such as ground
(k, i)	index notation (k) refers bodies and notation (i) refers unit of scissor linkage
Superscripts	
i, j	index notations refers frames

Chapter 5

Symbol	Definition
l_c	connector length
l	link length
θ	angle between ground and scissor link
ϕ	angle between two scissor linkage
ϵ	permissible misalignment
Superscripts	
a, b, c	different planes
P, Q, R	different corners

Chapter 6

Symbol	Definition
k	spring constant
f	free-length of springs
α_p	proportionality constant
l	link length
N_h, N_v	number of horizontal and vertical springs
f_h, f_v	free -length of horizontal and vertical springs
F	force
F_h, F_v	horizontal and vertical forces
W	weight applied
τ	torque on the link
f_P, f_Q, f_R	forces at point at P, Q, R
θ	angle subtended by the links from the ground
ϕ, ψ, γ	angle from the ground with action of forces

Chapter 1

Introduction

1.1 Motivation

We intended to prototype a platform whose vertical height can be changed. Further, we wanted the platform to be loaded with a constant weight, with the weight being statically balanced by springs. For prototyping, we constrained ourselves to primarily make use of bamboo along with very readily available components available in the market, such as tie rods and channels. The intent behind this is that the prototype we make should be able to inspire even people in remote locations, especially in regions where bamboo is abundant and there is thrust on bamboo crafts, to attempt making machines that undergo motion. It may be noted that bamboo has been successfully used in making structures such as houses and types of furniture. Nevertheless, its usage for linkages and machines that execute motion is rare.

Scissor linkage was the obvious choice for a vertical lift. Figure (1.1) is one such scissor lift that is popularly used in the industry. It consists of scissor linkage in two parallel planes. We call such scissor linkage a parallel-plane scissor linkage.

Inspired by the design of figure (1.1), we fabricated a similar linkage with the constraints of fabrication we had imposed. The resulting prototype is shown in figure (1.2).

Source : https://upload.wikimedia.org/wikipedia/commons/6/62/Hebebuehne Scissorlift.jpg,
Last accessed : 30 January 2020,
Image license : GNU Free Documentation License

Figure 1.1: An example of scissor lift used in industry.

The fabricated model in figure (1.2) does have the capability to execute the required vertical upward and downward motion. However, in addition to it, it also has undesirable lateral sway, as shown in figure (1.3). A video demonstrating the same could be seen in [1].

In our exploration to reduce the lateral sway, we found that if the scissor linkage were to be placed in three planes in the form of the triangular prism as shown in figure (1.4), then the lateral sway would be significantly minimized. A video demonstrating the same is shown in [2]. Even though lateral deflection characteristics of triangular-prism-shaped scissor linkages are not studied, such scissor linkages are nevertheless known in the literature [3, 4]. We later also found that angled-plane scissor linkage shown in figure (1.5) has resistance against lateral sway similar to triangular-prism-shaped scissor linkage. In fact, we can consider triangular-prism-shaped scissor linkage as an over-constrained angled-plane scissor linkage. What it means is that triangular-prism-shaped scissor linkage cannot exceed the maximum lateral sway of angled-plane scissor linkage. Thus, from the kinematic linkage point of view, angled-plane scissor linkage is more fundamental than triangular-prism-shaped scissor linkage. Therefore, in our analytical and numerical investigation, we

Figure 1.2: Fabricated parallel-plane scissor mechanism.

Figure 1.3: Lateral sway in the fabricated parallel-plane scissor linkage.

focus only on contrasting lateral sway characteristics between angled-plane scissor linkage and parallel-plane scissor linkage.

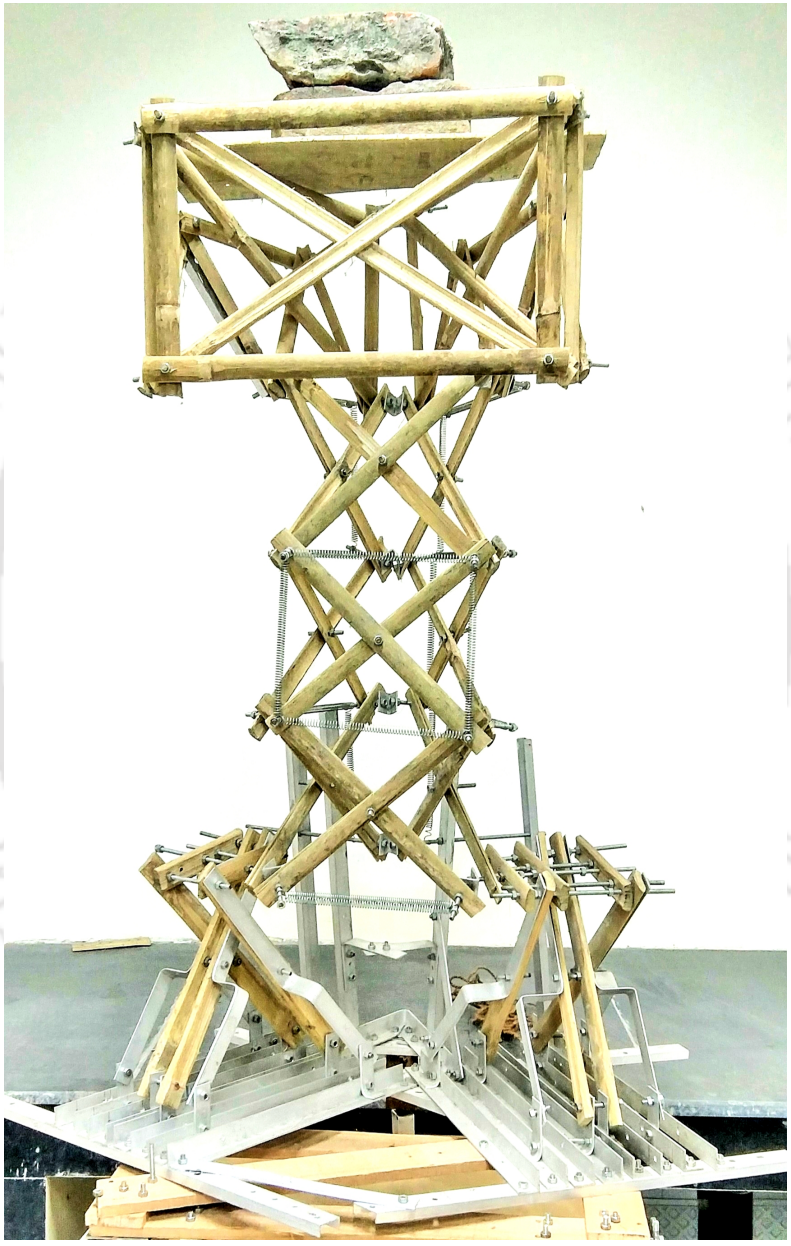

Figure 1.4: Significantly small lateral sway in triangular-prism-shaped scissor linkage.

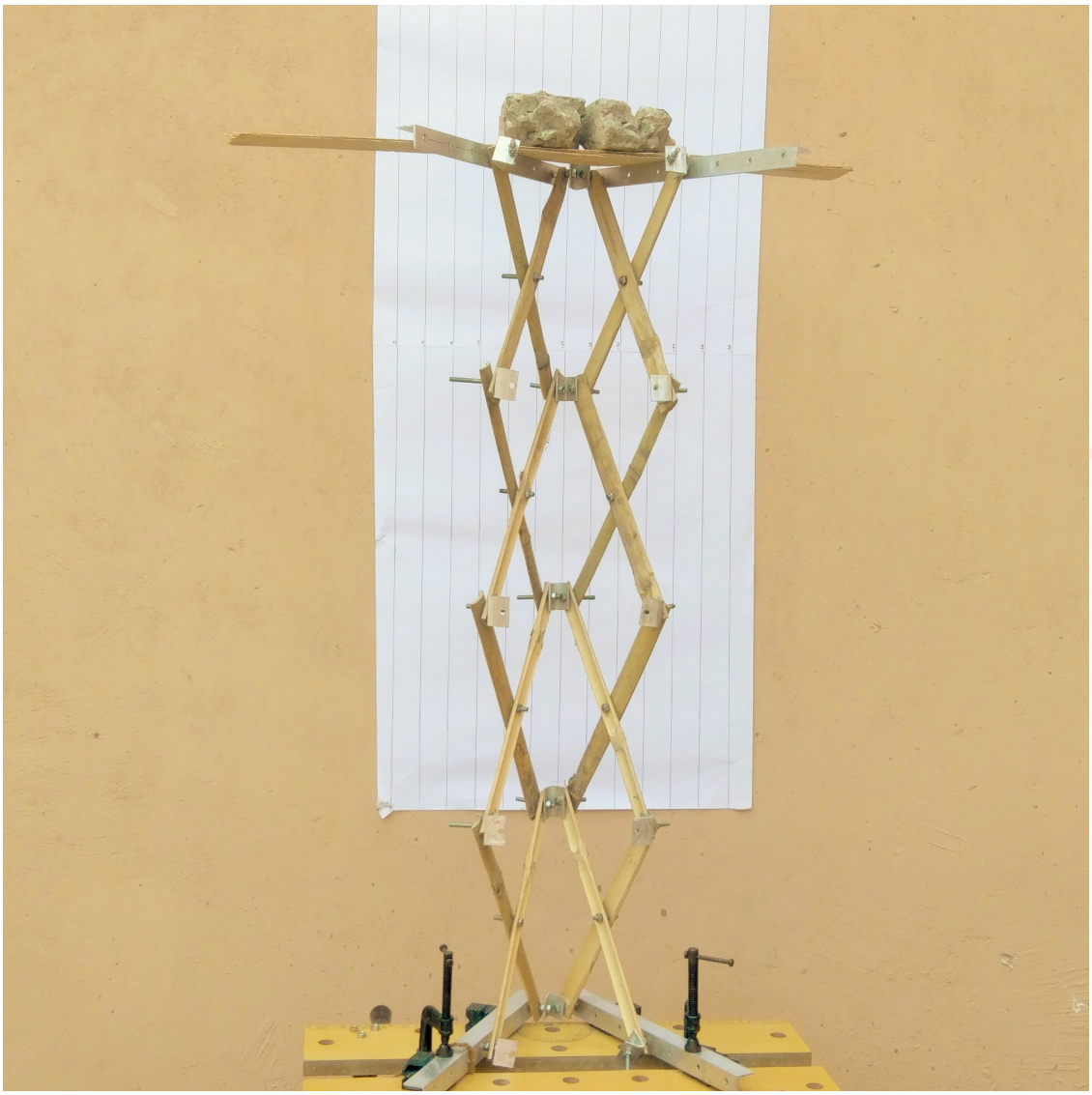

Figure 1.5: Angled-plane scissor linkage.

1.2 Rigid link scissor linkage with misaligning revolute joints as the object of investigation

Let us summarize what we have observed in practice in table (1.1). Our aim is to obtain these situations theoretically, i.e., based on the equation of mechanics. Obtaining situation 1 in table (1.1) through equations of mechanics is easy. Let us consider the scissor linkages that are ideal in the sense that the links are rigid and the revolute joints are perfect. By perfect revolute joint, we mean that apart from relative rotation about the axis of the revolute joint, no other relative motion between the bodies of the revolute pair is possible. Further, the joints are arranged as per the kinematic description of the linkage. Such a linkage would have only one-degree of freedom with the possible motion being extension and retraction of the scissor linkage. In such an ideal scissor linkage, lateral sway is not possible. Thus, from the theoretical point of view, demonstrating situation 1 of table (1.1) is easy.

Now to demonstrate situation 2 and 3 of table (1.1) theoretically, we have to introduce some non-ideality to the linkage, which allows it to have lateral sway. Let us list down some possible non-idealities:

1. non-rigidity of links,
2. offsets in revolute joints,
3. misalignment in revolute joints.

We could incorporate all these non-idealities into a theoretical model and investigate. We could also incorporate advanced material behaviour models on force-displacement relations. However, we are seeking to do the analytical investigation through equations of mechanics to demonstrate situation 2 and 3 in table (1.1). Hence, it would be prudent to keep the number of variables in the theoretical model as small as possible. Otherwise, instead of finding theoretical insights, we might get overwhelmed by a large number of variables. We choose the misalignment of the revolute joint as the only non-ideality. We also make an assumption that the maximum possible limit on misalignment is prestated in order to keep our theoretical investigation in the realm of kinematics. In reality, the maximum possible misalignment is a function of material behaviour of the linkage and load on the linkage.

The choice of non-ideality is perhaps influenced by our intuition, but it did not take us long to verify through numerical simulation that our choice of non-ideality could demonstrate situation 2 and 3 in table (1.1). What was challenging was the analytical investigation for which we had to linearize the equations and could find only bounds on the maximum possible lateral sway.

What we have shown through the equation of mechanics is that the misalignment as non-ideality would lead to the situation shown in table (1.2). However, we have not ruled out the possibility of another non-ideality leading to lateral sway characteristics shown in table (1.2). Further, we are not in a position to say whether the non-ideality of misalignment is present in the practical prototype since we have not made any measurement on the practical prototype. The measurements are non-trivial since we have to measure three-dimensional rotation to estimate misalignment in the revolute joint. We acknowledge that practical measurements would have been valuable. However, within the constraints of the thesis work, we could accomplish only so much. The practical measurement can be taken up as future work. In spite of the lack of practical measurement, what is presented in the thesis and its related publication is **the first-ever explanation based on mechanics of different lateral sway characteristics between parallel-plane scissor linkage and angled-plane scissor linkage.**

Table 1.1: Summary of practical observation.

Situation	Linkage-type	Practical prototype
1 (See fig. (1.1))	Parallel-plane	No lateral sway
2 (See fig. (1.3)	Parallel-plane	Lateral sway present
3 (See fig. (1.5))	Angled-plane	Significantly smaller lateral sway

Table 1.2: Based on the equation of mechanics, could we show the occurrence of the three situations shown in table (1.1).

Linkage-type	Ideal Condition	Non-ideality
Parallel-plane	No lateral sway	Lateral sway present
Angled-plane	No lateral sway	Significant smaller lateral sway

1.3 Modelling of scissor linkage in the presence of misaligning revolute joints

Figure (1.6) shows a single-plane scissor linkage. As shown in figure (1.6), we can think of the scissor linkage as a stack of multiple units. Parallel-plane scissor linkage is formed when two single-plane linkages are placed in parallel planes with connectors attached between the single-plane scissor linkages. The connectors are necessary to synchronize the motion between two single-plane scissor linkages. The linkage was illustrated in figure (1.2). Similarly, if three single-plane scissor linkages are placed in the form of triangular prism along with connectors between them, then a triangular-prism-shaped scissor linkage is formed. The linkage was illustrated in figure (1.4). Furthermore, if two single-plane scissor linkages are placed in non-parallel planes with connectors between them as illustrated in figure (1.5), then they are called as angled-plane scissor linkage.

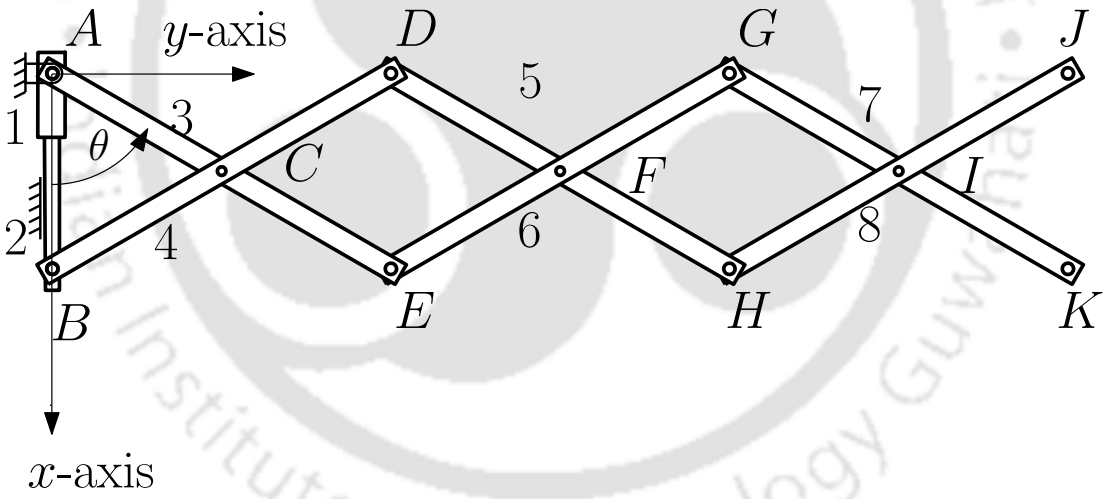

Figure 1.6: Single-plane scissor linkage.

The scissor linkages we are considering are essentially multibody systems. There is a well-known modelling of rigid multibody systems wherein for each rigid body, a local coordinate frame is assigned. Variables are then assigned to specify the position and orientation of the local frames. Normally, three variables to represent the position vector of the origin of the local frame and four variables called as Euler parameters to represent the orientation of the local frame are used. Thus, if there are n rigid bodies, there would be $7n$ variables.

Each joint in the multibody system would introduce equality non-linear constraints among the variables. Further, there are constraint equations related to Euler parameters as well. Thus, we have a system of equality constraints over the variables.

Mathematically, misalignment is a violation of certain constraint equations. Hence, to model misalignment, we introduce slack variables in the constraint equations. Furthermore, to limit misalignment, we introduce upper and lower limits on the slack variables. These upper and lower limits constitute a set of inequalities. It may be noted that modelling of misalignment is not new [5, 6].

Furthermore, we also define a function that represents the lateral sway of the scissor linkage. We seek to maximize this function without violating equality constraints as well as the upper and the lower bounds on the slack variables. Thus, the mathematical paradigm that is used to analyze the scissor linkage is constrained optimization, and the function is the objective function. As we will later present, even though the upper and lower limits for slack variables that represent misalignment are kept the same, the maximized objective functions turn out to be very different for angled-plane scissor linkage and parallel-plane scissor linkage.

1.4 Our impressions on the reasons for misalignment

Note: The contents of this section are speculative in nature. Further, any of the contributions of the thesis is not dependent on any of the contents of this section.

Since the revolute joint is being formed on a thin strip, bearing length becomes insufficient. As figure (1.7) illustrates, when clearance is present, the maximum misalignment is inversely proportional to bearing length. Further, as figure (1.8) illustrates, if the hole in the joint undergoes deformation due to misaligning torque, the misalignment is approximately inversely proportional to the square of the bearing length. A detailed derivation of these relations is given in Appendix B. Thus, small bearing length formed on the thin strip is the reason for misalignment in the joints. In the case of figure (1.1), apart from using thick channels for forming the revolute joints, the links in two opposite planes are welded together. This increases the actual

bearing length to the span between the two links.

Given that we are using bamboo strips as the links for the scissor linkage, the short bearing length is unavoidable. Further, due to short bearing length, it could get misaligned as per our impressions on reasons for misalignment. Furthermore, due to wear, clearance on the bearing surface could also increase. Therefore, we believe that the bamboo-based linkage has joints that could misalign.

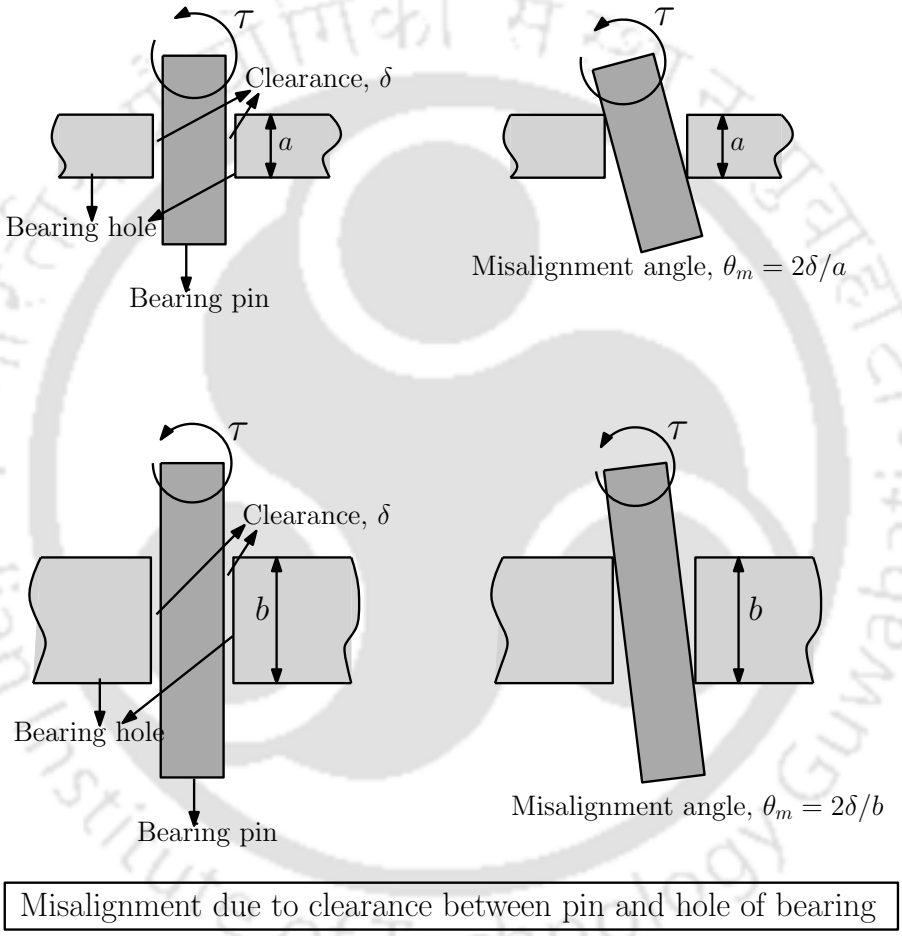

Figure 1.7: Misalignment due to clearance between pin and hole of bearing.

1.5 Linearized analytical analysis of lateral sway

Analytical analysis usually gives more insights. To circumvent the difficulty associated with non-linear equations, we linearized the non-linear equations about the

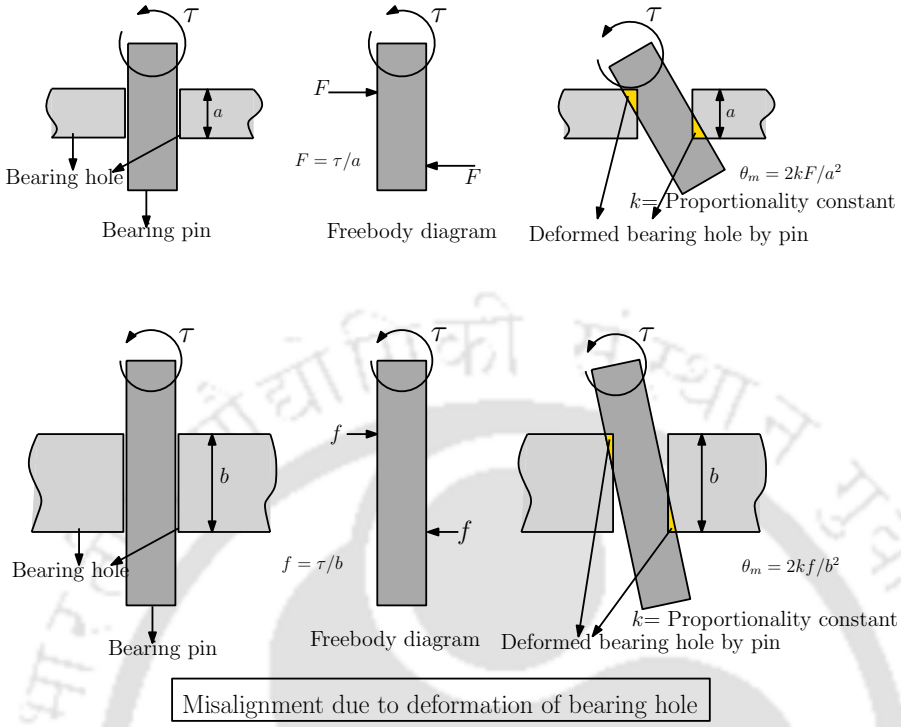

Figure 1.8: Misalignment due to deformation of the bearing hole.

ideal configuration that does not have misalignments in revolute joints. We choose angled-plane scissor linkage for the study. Since in every triangular-prism-shaped scissor linkage, an angled-plane scissor linkage is embedded, and angled-plane scissor linkage becomes parallel-plane scissor linkage when the angle between the planes becomes zero. By solving the linearized equations, we could get the analytical expression for upper and lower bound on the lateral sway for angled-plane scissor linkage and parallel-plane scissor linkage. These bounds adequately established the situations summarized in table (1.2). Furthermore, we found that

1. While lateral sway in angled-plane scissor linkage shows dependency on connector length, and there is no dependency in the case of parallel-plane scissor linkage.

2. When the number of scissor linkage units are increased, it was found that the lateral sway would tend to a finite limit in the case of angled-plane scissor linkage. In contrast, it increases almost linearly in the case of the parallel-plane scissor linkage.

Furthermore, the analytical expressions we obtain tells us the influence of different design parameters on lateral sway. Such knowledge is important for a designer while designing angled-plane scissor linkage.

1.6 Numerical analysis of lateral sway

The constrained optimization problem was non-linear. However, to do the analytical study we were forced to linearize the problem. Nevertheless, by the numerical methods, we can validate the analytical results obtained. In this context a couple of parametric studies were conducted. In one of them, the number of units in the scissor linkage was varied and the corresponding plot of lateral sway was obtained. The numerically obtained plot respected the bounds found in the analytical study.

1.7 Applications of scissor linkage made of thin strips and possibly misaligning revolute joints

Fabrication using thin strips and not much control on tolerance is easy and cheap in comparison to the fabrication of scissor linkage such as the one shown in figure (1.1) where very tight tolerances and long bearing lengths have to be maintained. However, in cases such as retraction of a projector into the roof in a large auditorium, the scissor linkage such as the one shown in figure (1.1) is an over-kill when angled-plane or triangular-prism-shaped scissor linkage could do the same job with the advantages of light weight, safety and frugal cost.

1.8 Static balance of scissor linkage

Consider the designed platform shown in figure (1.4). It also has a weight placed on the platform. The platform could be actuated by any actuator, including hands. In the presence of gravity, to pseudo-statically move the platform from one position to another, the actuator has to exert force. Static balancing is a way to fully or partially cancel this force by incorporating passive potential energy, storing elements

like springs. The video is seen in [7] shows a load of two bricks being raised up and down almost effortlessly. In the same video, one could see the amount of effort required to hold those bricks without the aid of statically balanced platforms.

A good introduction on static balancing could be found in [8]. Static balancing is typically accomplished by adding extra weights or extra springs. We restrict ourselves to only adding springs. It has been shown in literature [8] that perfect static balancing can be accomplished by adding a particular type of spring called zero-free-length springs. These special springs are typically cumbersome to realize. Thus we attempted to obtain the best possible static balance when practically available non-zero-free length springs are used. Furthermore, we realized that friction plays an important role in assessing static balance. Since there was not much theoretical work in the literature on the role of friction in static balancing, we did a simulation of the deteriorating effects of Coulomb friction on static balancing. The simulation was based on an adaptation of the friction circle that is used in graphical static analysis. Through this simulation, we also tried to see if we could rank different static balancing methods.

1.9 A few other specialities of the prototype

We realized that creating a slider joint with bamboo strips is very cumbersome. Hence, we replaced the slider joint with a straight line generating a four-bar mechanism. The mechanism could be seen in the video of [2].

1.10 Organization of thesis

Chapter 2 gives a survey of relevant literature. Chapter 3 discussed fabrication aspects of prototypes that were made. Chapter 4 discusses mathematical modelling of misalignment and linearized analytical analysis of lateral sway in parallel-plane and angled-plane scissor linkage. Chapter 5 discusses numerical simulation of parallel-plane, angled-plane scissor linkage and triangular-prism-shaped scissor linkages. Chapter 6 discusses the modelling and numerical simulation of the effects of Coulomb friction on static balancing. Chapter 7 gives scope for future work and

concludes the thesis.

Chapter 2

Literature Survey

2.1 Scissor linkage and its applications

Scissor linkage is a widely used mechanism. Its most popular application is scissor-lifts. There are several patents available on scissor-lifts [9–28]. Scissor linkage is also a simple example of a deployable mechanism. A deployable structure can be defined as a structure that can be transformed from a closed compact configuration to a predetermined, expanded form, in which they are stable and can carry loads [29]. There are several papers that dwell on deployable nature of scissor linkage [30–46].

2.1.1 Patents based on scissor linkage and its application

Charles L Larson [9] invented an extensible lift mechanism for elevating a load. More particularly, his invention relates to such a mechanism including an opposed pair of scissor mechanisms, each of which includes a pair of scissor arms pivotally connected together, where relative pivotal movement of the arms accompanies extension of the lift mechanism. The arm motion of scissors define a path of movement for the platform and upward movement of the platform is produced by actuation of some power-operated means, such as an extensible ram.

G Coad and J Carter [10] invented a scissor lift having upper and lower platforms and actuated by a cable rove so as to pull at least one set of the ends of scissors together at its extended position and also rove about a cam roller interposed between the arms and working toward the pivot connection during the portion of the motion in which the lift begins to extend.

T King and F Pearne [11] invented a work platform or cargo loader having a mobile base and a vertically translatable platform associated with the base is disclosed. Charles Traficant [12] invented a high lift mechanism for mounting on a truck chassis to move a cargo body fixed thereto between a retracted, down position and an elevated position comprising a lower frame for fixed engagement with the truck chassis, an upper frame to carry the cargo body there at the top.

Louis L Butler [13] invented a scissors-type lift mechanism that employs a reciprocating cam wedge adapted to engage cam follower rollers mounted on collapsed, transversely arranged scissor arms movable in the vertical plane. Movement of the cam in one direction forces the arms apart into a lifting movement as the rollers follow engaged cam surfaces. The movement of the cam in the opposite direction allows the scissor arms to collapse.

Duane R. Franklin and Archibald D. Evans [14] invented a scissors mechanism that supports a platform and is coupled to a sealed gas cylinder or other energy-storage device in such a way that the cylinder tends to lift the platform. Erik Knudsen [15] invented a scissor mechanism in particular for lift-tables where vertical motion is helped by a hydraulic cylinder.

Thomas A. Craig [16] invented a vehicle scissor lift, which is related to automotive service lifts of the type mounted on the floor in service garages, and more particularly to service lifts including scissor-type linkages for raising a vehicle. Jr. Angelo Leonaggeo [17] invented a hydrotherapy exercising device with a scissor lift treadmill. This apparatus can be used for exercising and massaging a human, a horse, or other animals. Ernst Langewellpott [18] invented a scissor lift table, where the lift action is done by the motor. Richard T. Rowan et al. [19] invented a scissor lift with the use of springs, which help in the motion of the table. Enoch L. Newlin [20] invented a work platform lifting machine that includes a chassis, a work platform, a scissor lift mechanism, and a telescoping electromechanical actuation arrangement.

George Lawrence Storm [21] invented a convertible lift mechanism having a scis-

sor lift linkage. This convertible lift mechanism lifts a person or an object from a first surface to a vertically displaced second surface. Donald Watkins [22] invented a scissor lift mechanism for use on the coil car with the lift having scissor legs connected to each other by a shaft. This lift is raised and lowered by a means for providing a generally vertical force to the shaft. The motion of the scissor mechanism is provided by means of a hydraulic cylinder and a bell crank mechanism.

Jean-Marie Rennetaud and Tian Zhou [23] invented an elevator with a scissor lift mechanism and a spring member serving as a virtual counterweight. This mechanism comprises an elevator car, a scissor assembly carrying the elevator car, and a drive mechanism. Barry Vaughan and Alvin Vaughan [24] invented a portable scissor-lift-assembly. This mechanism comprises a first platform provided with a top surface, a pair of opposed sides, and wheels and brackets connected to one of the sides for rotating the assembly. By using of a pair of opposed sides, lateral swaying is avoided in this mechanism, and only one vertical set of scissor mechanism is provided for vertical displacement. Michael Kaufman [25] invented a scissor lift mechanism having at least two scissor elements connected in pairs by a swivel axis. Martin Olesen [26] invented a scissor lift where the lifting action of the scissor is actuated by a hydraulic actuator. Todd Humbert and Elizabeth Humbert [28] invented a lift and tilt support apparatus that includes opposed scissor lift assemblies.

2.1.2 Articles based on scissor linkage and its application

Zhao et al. [3] presented the mechanism theory and application of deployable structures that were made of scissor-like elements (SLE). They did the mobility analysis of simple planar linkages and then explored the mechanism theory of spatial deployable units utilized in flat, cylindrical and spherical deployable structures. The theoretical results obtained in this paper have general adaptations for all kinds of deployable structures.

Tao Liu and Jian Sun [31] presented a detailed solid model and a kinematic and kinetic simulation of an actuating mechanism for scissor lifts. The actuator of the mechanism is a hydraulic cylinder. The simulation was performed in MATLAB/Simulink.

Yenal Akgün et al. [32, 33] presented a novel concept of the convertible roof.

There they used planar modified scissor-like elements. With the use of these elements, it becomes possible to change the geometry of the whole system without changing the dimensions of the struts or the span. Tian Hongyu and Zhang Ziyi [34] given a complete design and simulation of hydraulic scissor lift. They simulated the model in 3D software Pro/e. Ren Dong et al. [35] have given a dynamic study of scissor lifts. They have also suggested some way to use the scissor lifts safely. Lara Alegria Mira et al. [36] developed a transitional shelter using scissor-like elements that will be used as disaster relief shelters.

V. S. Rajashekhar et al. [37] presented a foldable stair based on a scissor mechanism. In space-constrained places, this foldable stair can be used. Lara Alegria Mira et al. [38] presented a parametric evaluation of scissor based arches. They suggested that deployable scissor structures can transform from a compact state to a fully deployed configuration. Doli Rani et al. [39] presented a scissor lift which is lifted by hydraulic arrangements. Wei Zhang et al. [40] presented a study on the static stability of scissor lift. They studied the static stability of six kinds of scissor lifts with one input force of hydraulic actuator by having the input on the lines of the nodes of the scissor lifts. Dong-Jie Zhao [41] presented a planar deployable structure with screw theory and discusses its possible applications in over-constrained lift platforms via calculating its stiffness where these platforms are all made up of a number of identical scissor-form pivoted links.

Andrea Corrado et al. [42] presented the design of a belt drive scissor lifting table to be installed on platforms, called skillet, that constitute a typical line of handling on which the operator can stay and proceed to assembly, with times established by the product manufacturing. Anupam Chaturvedi et al. [43] presented a scissor lift that is working on the basis of screw lead concepts. The use of screw lead mechanism in scissor lift mechanism makes it cost-effective.

Na Zhao et al. [44] kinematically and dynamically-characterized a novel deformable quad-rotor that is based on the scissor-like foldable mechanisms. This design is inspired by the morphological adaptation of birds during flight, and the quad-rotor allows that its volume can be varied to dynamically adapt to complex environments and spaces. The advantage of this design is that the quad-rotor can fly in different volume shapes as required. Nishant Shrivastava et al. [45] presented an embedded control system for self-adjusting scissor lift. They attached this system with the platform of the scissor lift. It measures the tilting angle of the scissor lift

and avoids fatal accidents. Yi Yang et al. [46] presented a dual scissor-like mechanism which have two translational degrees of freedom that is constructed by linking of two identical parallel scissor-like elements.

2.2 Static Balancing

A system is said to be in static balance if it can undergo quasi-static motion without any external effort when any dissipative force interactions in the system are removed. In the general motion of a system, at any configuration, inertia forces of the system, conservative and dissipative force interactions within the system and external forces acting on the system are in equilibrium [47]. Balancing can be done by three types:

1. balancing weight by the addition of counter-weight
2. balancing by the addition of springs
3. balancing by the addition of both counter-weight and springs as well

If the original weight is balanced by counter-weight, the balancing technique is called balancing by the addition of counter-weight. Similarly, if the original weight is balanced by springs, the balancing technique is called balancing by addition of springs. When any system is balanced by combining both counter-weight and springs, the balancing technique is called balancing by the addition of both counter-weight and springs. The balancing of any system by springs is advantageous because the overall weight of the system is not significantly increased.

2.2.1 Literature on balancing weight by the addition of counter-weight

Jiegao Wang and Clément Gosselin [48] have presented the static balancing of spatial three-degree-of-freedom (3-DOF) parallel mechanisms or manipulators with revolute actuators using counter-weights or springs. They derived the expressions of the position vector of the global center of mass and the potential energy of the mechanisms and used them to obtain equations of static balance.

2.2.2 Literature on balancing by addition of spring

Lucien J. B. LaCoste [49] recognized that a pendulum could be in the perfect static balance when a zero-free-length spring is attached to it. LaCoste is credited with first recognizing the role of zero-free-length springs in perfect static balancing of a gravity-loaded lever. This discovery was made in the context of devising a pendulum with a very long period of oscillation. Such a pendulum is apparently useful in seismographs. D. A. Streit and Brian Gilmore [50] presented a new equilibrator design approach based on system potential energy function. They made a thorough study of a lever under spring loads. Some of the ways to realize zero-free-length springs were also discussed. D. A. Streit et al. [51] gave a static balancing theory for planar pantograph linkages. Nathan Ulrich and Vijay Kumar [52] used a pulley of varying radius for passively compensating gravitationally-induced joint torques.

G. J. Walsh et al. [53] provided static balancing theory of a spatial two degree of freedom serial revolute jointed linkage. Ajay Gopalswamy et al. [54] gave an approximate static balancing technique where torsional springs are used as balancing elements. T. Rahman et al. [55] proposed a simple method to counter the effect of gravity in the articulated mechanism. For this scheme, they used kinematics and linear spring to produce a non-linear restoring force to oppose the gravitational moment.

Just L. Herder [56] was the first to recognize the importance of a class of problems where spring forces, which could be an approximation for more complex elastic forces, need to be compensated. The motivation for the work was to compensate for the elastic forces of the cosmetic glove of a hand prosthesis. In this work, the motion of the fingers of a hand prosthesis was modelled as the motion of the coupler link of a four-bar linkage. The elastic forces of the cosmetic glove were lumped into a zero-free-length spring attached to a point on the coupler. The work gives a perfect balancing solution for statically balancing this spring-loaded four-bar linkage. The obtained solution is based on extending the balancing of a skew lever to a skew pantograph. Thierry Laliberté et al. [57] presented static balancing of planar 3-DOF parallel mechanisms. Balancing was accomplished by counter-weights or springs or a combination of both. They did a dynamic analysis in order to illustrate the advantages and limitations of static balancing and studied the characteristics of each of the mechanisms considered. Further, Imme Ebert-Uphoff and Clément

Gosselin [58] discussed statically balanced spatial parallel platform mechanisms. Jiegao Wang and Clément Gosselin [59] presented the static balancing of four types of spatial four-degree of freedom parallel mechanisms. Both counter-weight based balancing and spring based balancing were presented.

Ion Simionescu and Liviu Ciupitu [60] presented discrete balancing and continuous balancing. They provided a new constructional solution for balancing the weights of industrial robot arms using the elastic forces of helical springs. They defined a new notion, namely efficaciousness coefficient, to study the performance of the static balancing mechanism. This coefficient is equal to the ratio of the mechanical work consumed for moving the unbalanced arm and the mechanical work consumed for moving the balanced arm.

M J French and Martin Widden [61] gave a historical account and different proofs for Anglepoise lamps. Sunil Agrawal and Abbas Fattah [62] provided an interesting method to balance a spatial gravity-loaded linkage. In the method, by adding auxiliary parallelogram linkages, a physical point that is also the center of mass of the overall system is first identified. Then, depending on the kind of motion this center of mass undergoes, springs are added to compensate for the gravity. Abhishek Agrawal and Sunil K. Agrawal [63] presented an approximate static balancing method using non-zero-free-length springs. Andrea Russo et al. [64] addressed the static balancing of the spatial parallel manipulator. They showed that prismatic-joint based parallel mechanisms cannot be statically balanced by counterweights since prismatic joints do not provide a fixed point unlike pivot of revolute joints. V. Arakelian and S. Ghazaryan [65] examined the errors in gravity balance due to the spring-mass. They presented a numerical example, which showed that the error caused by neglect of the spring-mass can be as much as 8%. R. Saravanan et al. [66] presented a new modified optimization model for finding the spring balancing mechanism of industrial robot APR 20. They presented five new design optimization methods based on conventional and evolutionary algorithms such as Newtons method, conjugate gradient method, Genetic Algorithm, Elitist Non-dominated Sorting Genetic Algorithm and differential evolution. They also presented a comprehensive user-friendly general-purpose software package to obtain the optimal parameters using different evolution algorithms.

Theeraphong Wongratanaphisan and Matthew Cole [67] presented an analysis of a gravity compensated four-bar linkage mechanism with zero-free-length linear

spring suspension. This analysis is based on the system potential energy framework. PO-Yang Lin et al. [68] presented a systematic methodology for the design of statically balanced, one-degree of freedom planar linkage with revolute joints. In this methodology, no auxiliary parallel links are required. They concluded that the design of a statically balanced, one-degree of freedom, n-link, planar linkage with (n/2) ground-adjacent links could be accomplished by fitting a ground-attached spring to each of the ground-adjacent links.

Kenan Koser [69] presented a cam-type gravity compensation mechanism for robot arms. PO-Yang Lin et al. [70] presented a novel methodology for the design of a balanced serial-type spatial manipulator. They derived the equilibrium condition for static balancing based on the potential energy. They used this methodology in spatial RSSR (revolute-spherical-spherical-revolute) linkage. Rogier Barents et al. [71] presented spring-to-spring balancing techniques for energy free adjustment in gravity equilibrators.

Giuseppe Radaelli et al. [72] presented a novel approach for static balancing of mechanisms, focusing on systems with torsional springs. This approach is based on the fact that the total potential energy of a system is constant when statically balanced.

Sangamesh Deepak and G. K. Ananthasuresh [73] presented three techniques to statically balance a four-bar linkage loaded by a zero-free-length spring attached between its coupler point and an anchor point on the ground. They motivated that these could be the starting point for the design of statically balanced systems involving inherent and possibly more complex elastic loads. They balanced a parallelogram linkage by composing the loading spring or its equivalent spring. They concluded that the number of additional links and springs required for all these techniques is less than or equal to that of the static balancing solution found in the existing literature. Sangamesh Deepak and G. K. Ananthasuresh [74] presented a perfect static balancing technique that adds only spring but not auxiliary bodies. This technique can counter-balance both spring loads and gravity loads. The technique can statically balance any planar revolute-jointed linkage having zero-free-length spring and constant load interaction between the bodies of the linkage.

PO-Yang Lin et al. [75] presented the underlying theory of weight balanced mechanism for the design of a class of spatial mobile arm support for application

in spring-assisted mobile arm support. Simon Perreault et al. [76] reported a novel method to approximate the static balancing of planar parallel cable-driven mechanisms based on the design of nonlinear spring. The main advantage of this method is to increase the level of security of parallel cable-driven mechanisms and to minimize the continuous expenditure of electrical energy from motors even when no acceleration or force is applied on the end effector.

Sanghyung Kim and Chang-Hyun Cho [77] used the space mapping method to design a gravity compensator. They used the concept of associate linkage in their design. Sushant Veer and S. Sujatha [78] presented a new method for static balancing of mechanisms with conservative loads such as gravity and spring loads using non-zero-free-length springs with childparent connections. No auxiliary links are used. The method is based on minimizing the variance of the potential energy.

2.3 Misalignment in revolute joint

C. Brutti et al. [79] discussed clearance in the kinematic joints due to deformation, wear, and manufacturing errors. The accurate modeling of these effects in multibody system analysis is a complex issue, but in many practical applications, it is mandatory to take them into account in order to understand the actual behaviour of the mechanical systems. To facilitate easy implementation in a multibody dynamic solver, a general computer-aided model of a 3D revolute joint with clearance was presented. It was demonstrated that the use of the proposed model improves the accuracy in the evaluation of the dynamic behaviour of an industrial mechanism. Zhan et al. [80] analyzed and formulated a revolute joint in terms of Hertzian-based contact force model. They presented a classical slider-crank mechanism with a clearance at the piston pin. The simulation model was developed using the analysis/design software MSC.ADAMS.

2.4 Conclusion

In the literature, we have noted that there is absolutely no work investigating the significant difference in lateral sway characteristics between angled-plane scissor linkage

and parallel-plane scissor linkage. Thus, the contribution that we are making in this thesis on the significant difference in lateral sway characteristics between angled-plane scissor linkage and parallel-plane scissor linkage is new and non-incremental.

We also note in the literature that no study on the effects of friction on static balancing has ever been carried out. Thus our contribution on finding frictional effects on static balancing is also a new line of investigation.

Chapter 3

Prototyping of bamboo-based scissor lift to avoid lateral sway

3.1 Introduction

As described in Chapter 1, with an intent to develop a lifting mechanism, we fabricate a parallel-plane scissor linkage made of bamboo strips. In the same chapter, we had also seen the problem of lateral sway. In this chapter, we describe a series of fabrication-based design explorations of the scissor linkage made of bamboo strips with the aim of minimizing the lateral sway. The design explorations are intuitive. The observations summarized in table (1.1) are the result of this fabrication based design explorations.

3.2 Design of parallel-plane scissor linkage

Figure (3.1a) shows a CAD model of parallel-plane scissor lift where point A shown in the figure is fixed to the ground and point B is constrained to move in a horizontal line passing through A. In the scissor linkages used in industries, point B is guided

along the horizontal straight line using a slider joint. The guidance of point B by a slider could also be seen in the schematic diagram of figure (1.6). However, realizing a slider using bamboo strips was found to be cumbersome. Hence, we replaced the slider with a Chebyshev mechanism that has a point that approximately follows a straight line. Similarly, points at the top of the scissor linkage, C and D, not only undergo vertical motion, but their relative horizontal distance also changes. The top platform, which is mounted on these two points C and D has to accommodate the relative change in horizontal distance between these two points. This is again accomplished by incorporating a Chebyshev mechanism on the top platform, as shown in figure (3.1b).

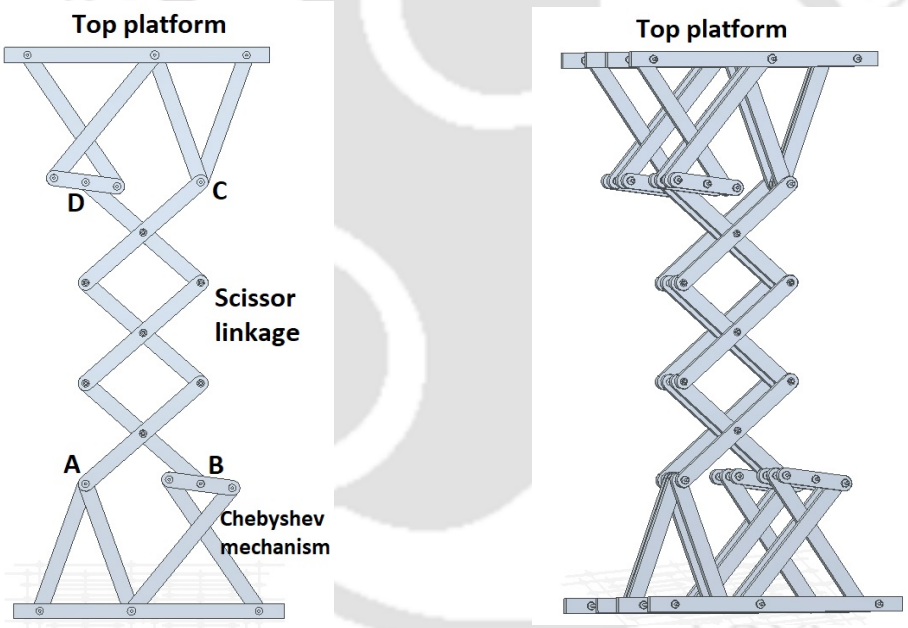

(a) Scissor linkage based vertical lift. (b) A view showing links in parallel planes.

Figure 3.1: CAD model of parallel-plane scissor linkage as shown in sub figure (a) and (b).

Similar to the popular design shown in figure (1.1), the links of linkage are placed in parallel planes, as shown in figure (3.1b). We fabricated the parallel-plane scissor linkage using bamboo strips, as shown in figure (3.2).

Figure 3.2: Parallel-plane scissor linkage made by bamboo strips.

3.2.1 The problem of lateral sway

The fabricated parallel-plane scissor linkage showed a significant lateral sway, as shown in figure (3.3). The lateral sway in figure (3.3) is due to the sway in the scissor linkage and also that of Chebyshev mechanism at the base. Another figure demonstrating the lateral sway when the linkage is oriented horizontally is shown in figure (3.4).

We attribute the lateral sway observed in parallel-plane scissor linkage to the imperfect revolute joints that are formed on bamboo strips. We find that the imperfection is due to insufficient rigidity in the bearing holes formed on the bamboo strips. Based on a few insights, we next vary the design of the scissor linkage with an intent to eliminate or decrease the lateral sway.

3.3 Triangular-prism-shaped scissor linkage

Instead of placing single-plane scissor linkage in two parallel planes, we now place it in three distinct planes in the form of the triangular prism. The geometric details of the linkage are described next.

Figure 3.3: Lateral sway in parallel-plane scissor linkage.

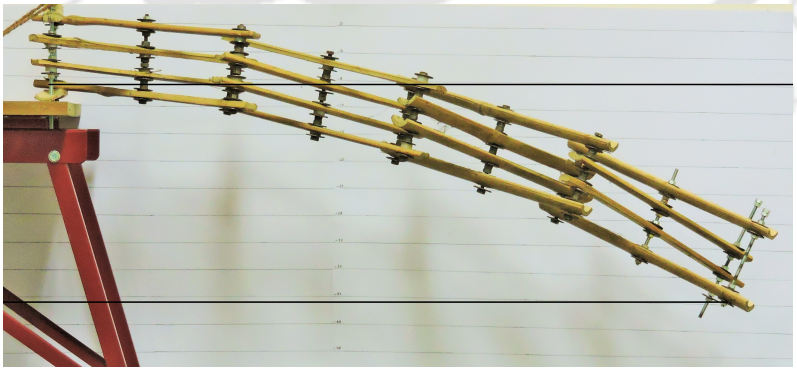

Figure 3.4: Parallel-plane scissor linkage showing lateral swaying.

3.3.1 Design of single unit of triangular-prism-shaped scissor

We now describe the steps to construct a single unit of triangular-prism-shaped scissor linkage. A single scissor-cross made of two links is first placed in a vertical plane, as shown in figure (3.5a). Further, two replicas of the scissor-cross are made and placed in two different vertical planes such that the three planes form the faces of an equilateral triangle as shown in figure (3.5b). The three scissor-crosses are secured to each other through connectors, as shown in figure (3.5c). Because of the connectors, the angles of the three scissor-crosses are synchronized to be equal to each other. The detailed geometry of the connectors is shown in figure (3.5d). The main feature of the connector is that it provides two bearing surfaces whose axes are inclined at an angle of 120° to each other. The triangular-prism-shaped scissor linkage so formed is an over-constrained linkage, and it has ideally a single degree of freedom. The degree of freedom corresponds to the change in the angle of the crosses. Several units of triangular-prism-shaped scissor linkage can be stacked one over the other to form multi-unit scissor linkage as seen in figure (3.6).

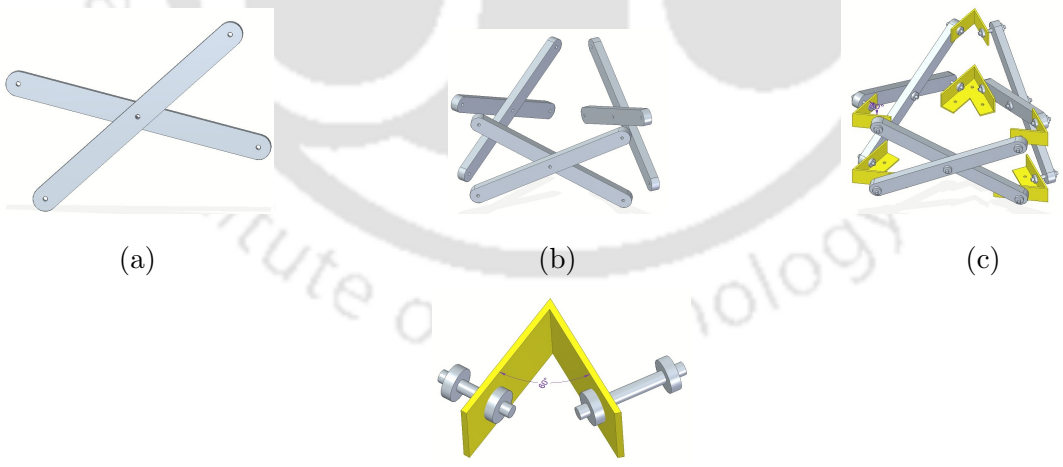

(a) (b) (c)

(d)

Figure 3.5: Construction of a single unit of triangular-prism-shaped scissor linkage.

3.3.2 Multiple-unit triangular-prism-shaped scissor linkage and its reduced lateral sway

The single unit of triangular-prism-shaped scissor linkage is stacked one after the other to get multiple-unit scissor linkage. A fabricated multi-unit triangular-prism-shaped scissor linkage is shown in figure (3.6). When compared with the lateral sway of parallel-plane scissor linkage shown in figure (3.4), the fabricated triangular-prism-shaped scissor linkage has a much smaller lateral sway. Hence, we will choose this linkage as a means to reduce the lateral sway.

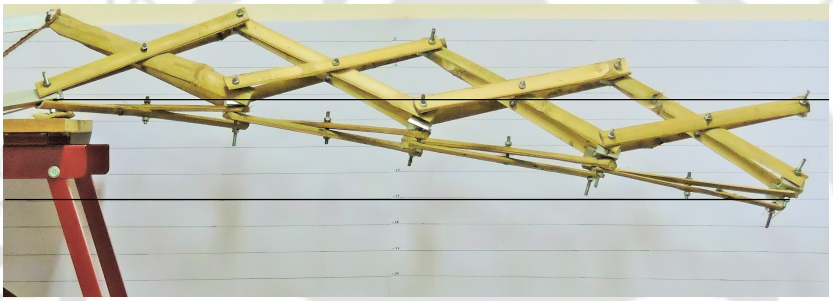

Figure 3.6: Triangular-prism-shaped scissor linkage showing lateral swaying.

3.3.3 Design of base of triangular-prism-shaped scissor linkage

After confirming the smaller lateral sway property of triangular-prism-shaped scissor linkage, we redesigned the base of the scissor linkage as well as the top platform of the scissor linkage to conform to triangular-prism-shaped scissor linkage. The base of the linkage is a crucial part of any linkage. We tried two types of base supports:

1. strengthened slider-joint-base

2. strengthened Chebyshev- mechanism-base

3.3.4 Slider support base

Figure (3.7) shows the CAD model and figure (3.8) shows the fabricated base containing sliders that act as support for triangular-prism-shaped scissor linkage. In the base six sliders are used. In between six sliders, two are used to provide direct support to the triangular-prism-shaped scissor linkage, and others are intended to increase the rigidity of the base.

3.3.5 Strengthened Chebyshev mechanism

We have already seen Chebyshev mechanism being used for the base of the parallel-plane scissor linkage. Similarly, here we introduce Chebyshev mechanism in two planes to support two planes of the triangular-prism-shaped scissor linkage. The third plane is unsupported. Just as parallel-plane scissor linkage undergoes lateral sway, Chebyshev mechanism also undergoes lateral sway. To overcome the swaying of the mechanism, we added aluminium strips to increase the bearing length of the joints of the Chebyshev mechanism. Figure (3.9) shows the strengthened Chebyshev mechanism, which supports the triangular-prism-shaped scissor linkage.

3.3.6 Design of top platform of triangular-prism-shaped scissor linkage

As seen in figure (3.1a), the upper platform of the parallel-plane scissor linkage was supported on Chebyshev mechanism. In the case of triangular-prism-shaped scissor linkage, we choose to support the upper-platform through Roberts straight-line mechanism. Figures (3.10) and (3.11) show the CAD model of upper platform design, which is supported by Roberts mechanism. Figure (3.11) shows the single plane view of Roberts mechanism, which supports the top platform/upper platform. Roberts mechanism helps the upper platform to maintain a horizontal position while the scissor linkage moves up and down.

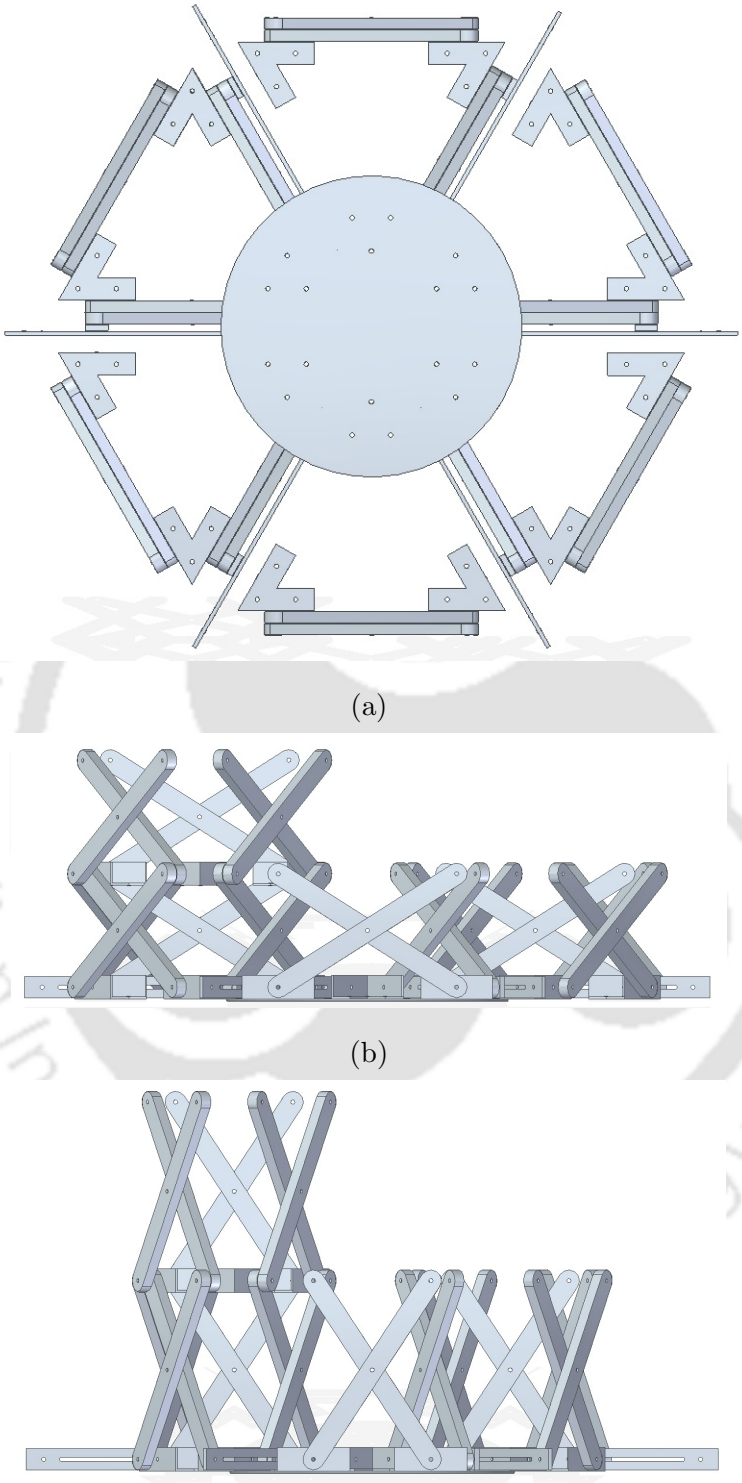

(a)

(b)

(c)

Figure 3.7: CAD model of different isometric view of triangular-prism-shaped scissor linkage that is supported by slider-jointed base.

Figure 3.8: Triangular-prism-shaped scissor linkage which is supported by slider-jointed base.

Figure 3.9: Prototype of strengthened Chebyshev mechanism.

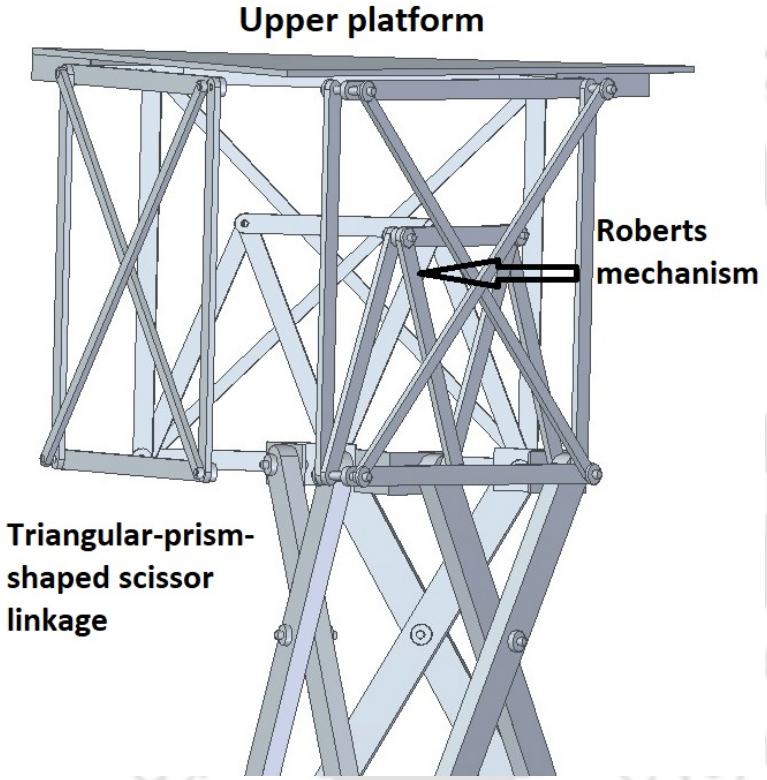

Figure 3.10: CAD model of upper platform supported by Roberts mechanism.

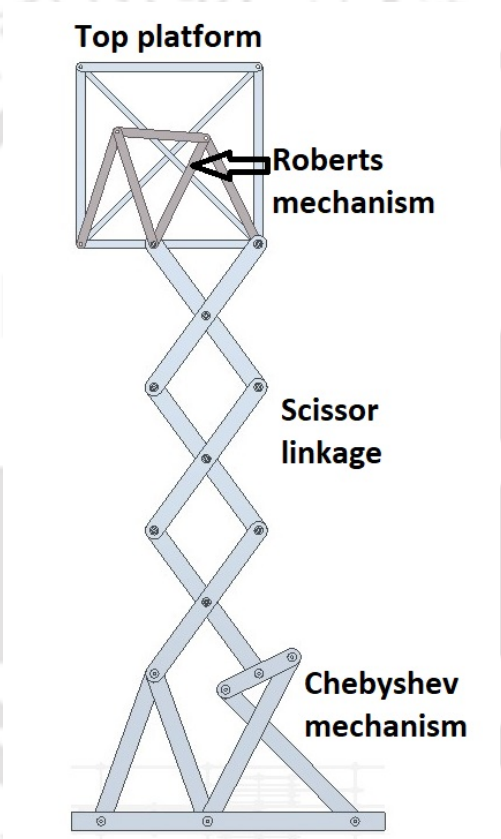

Figure 3.11: Working details of Roberts mechanism in single plane view.

3.3.7 The final prototype

The slider-jointed base for triangular-prism-shaped scissor linkage was unsatisfactory due to insufficient ground-clearance, high friction at the slider-joint, and the tendency of slider joints to misalign. Hence, we choose to persist with the Chebyshev mechanism base for the triangular-prism-shaped scissor linkage. The CAD model of the final prototype is shown in figure (3.12a), and the fabricated prototype is shown in figure (3.12b).

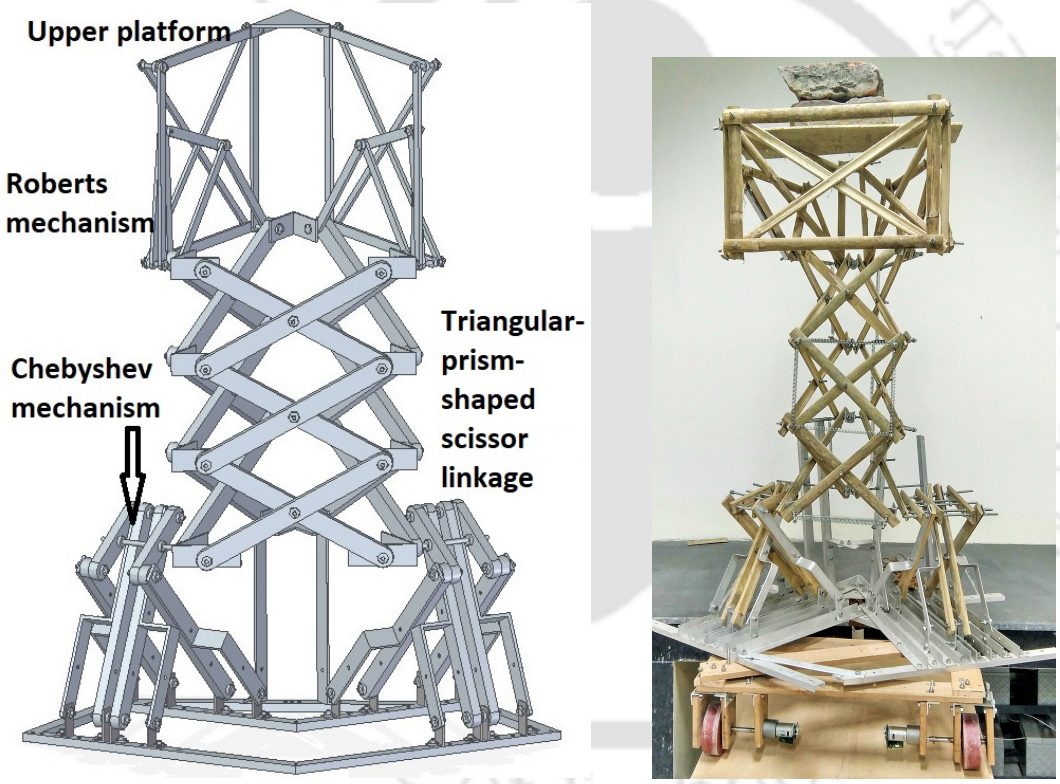

(a) CAD model of triangular-prism-shaped scissor linkage with upper platform and Chebyshev mechanism in the base.

(b) Triangular-prism-shaped scissor linkage fabricated with bamboo sticks.

Figure 3.12: CAD model and fabricated model of triangular-prism-shaped scissor linkage.

3.4 Results and novelties

The results and novelties of the chapter are listed below:

1. triangular-prism-shaped scissor linkage has significantly smaller lateral sway in comparison to parallel-plane scissor linkage as shown in figure (3.6),
2. the usual slider-jointed base and upper-platform in scissor linkage were replaced by straight-line generating Chebyshev mechanism and Roberts mechanism to overcome difficulties associated with making slider joints on bamboos.

Chapter 4

Analytical reason for smaller lateral sway in angled-plane scissor linkage

4.1 Introduction

The context for this chapter was well set in Section 1.2. Given a scissor linkage having misaligning joints but otherwise ideal (links are rigid, there is no offset in joints), we are required to deduce analytically through the equations of mechanics the significantly different lateral sway characteristics between parallel-plane scissor linkage and angled-plane scissor linkage. Given that, so far in literature the different lateral sway characteristics have never been demonstrated through equations of mechanics. To facilitate thinking, we find it prudent to make choices in modelling so that the number of variables in the mathematical model is small.

The scissor linkage is essentially a multibody system consisting of multiple rigid bodies connected by joints. This chapter follows the modelling of the multibody system as presented in books such as [5, 81, 82]. The coordinates capable of inde-

pendently describing translation and orientation of each of the rigid-bodies in the scissor linkage form the variables. The revolute joints of the linkage result in equality constraints between the variables. These equality constraints are modified by introducing slack variables to model misalignment. Inequality constraints are also introduced to limit slack variables, which represent misalignment between a lower and an upper bound. A function that represents lateral sway is also defined. We are interested in maximizing the lateral sway function. Thus, constrained optimization is the underlying mathematical problem of this chapter.

In order to understand the properties of the solution to the optimization problem, we linearise the constraint equations to obtain a simpler linear programming problem. We solve the equality equations to express all the variables in terms of only a few variables. Further, from inequality constraints, we make a series of deductions that show different lateral sway characteristics between angled-plane scissor linkage and parallel-plane scissor linkage. In particular, we can also see how design parameters of the scissor linkage, such as length of scissor links and length of connector, affects the lateral sway. Such an understanding is important for designing practical scissor linkages made of thin strips.

4.2 Description of scissor linkages

4.2.1 Single-plane scissor linkage

Figure (4.1) shows a single-plane scissor linkage. At its base are links $(1,0)$ and $(2,0)$, which are connected by a prismatic joint. One end of the scissor linkage connects to bodies $(1,0)$ and $(2,0)$ with revolute joints at points $A_{(2,1)}$ and $A_{(1,1)}$ respectively. Link $(1,0)$ is connected to the ground with a revolute joint at $A_{(2,1)}$. Point $A_{(1,1)}$ on link $(2,0)$ is guided such that its y coordinate is constrained to be the same as that of $A_{(2,1)}$. The axes of all the revolute joints are along z-axis. This linkage has a single degree of freedom, and the variable θ shown in figure (4.1) describes the configuration of the linkage. Within the scissor linkage, several units are identified in figure (4.1). A unit can be treated as a building block that can be repeatedly connected in series to form the scissor linkage. Each unit is serially numbered, starting from the unit that is connected to the ground. An i^{th} unit has

two links labelled as $(1, i)$ and $(2, i)$. On link $(1, i)$, there are two revolute joints at points $A_{(1,i)}$ and $O_{(1,i)}$ while on link $(2, i)$, the joints are at points $A_{(2,i)}$ and $O_{(2,i)}$.

In the analysis that we carry out further, we keep θ unchanged. Hence, in order to simplify, for the purpose of analysis, we consider scissor linkage to directly connect to the ground at $A_{(2,1)}$ and $A_{(1,1)}$. We neglect bodies $(1, 0)$ and $(2, 0)$. The distance between $A_{(2,1)}$ and $A_{(1,1)}$ is dependent on θ that is considered for the analysis.

4.2.2 Angled-plane scissor linkage and parallel-plane scissor linkage

Angled-plane scissor linkage is the same as single plane scissor linkage except that there are two planes of scissor linkage with a connector to synchronize the motion between the two planes as seen in figure (4.2). When the angle between the two planes of the angled-plane scissor linkage becomes zero, it becomes parallel-plane scissor linkage as shown in figure (4.3).

4.3 Modelling of misalignment

A scissor linkage is a multibody system. In the prototype made, we could not observe any perceptible deformation of the links even though the misalignment in the joints was perceptible. Hence, we treat the links in the scissor linkage to be rigid. As is the norm in multibody dynamics, a local Cartesian frame of reference is rigidly fixed to everybody. If i is the label assigned to the body, then the origin of the local frame body is represented as O_i and x, y and z axes as x_i, y_i, z_i, respectively.

4.3.1 Local coordinate frame and coordinate transformation

Column matrix $\boldsymbol{a}^{(i)}$ represents vector $\boldsymbol{a}$ that is expressed component wise as a column vector in the local coordinate frame of body i. Vector $\boldsymbol{r}_{A/B}$ represents position vector of A with respect to B. The well know coordinate transformation between two coordinate frames i and j is

$$\boldsymbol{r}^i_{A/O_i} = \boldsymbol{r}^i_{O_j/O_i} + \boldsymbol{R}^i_j \boldsymbol{r}^{(j)}_{A/O_j} \tag{4.1}$$

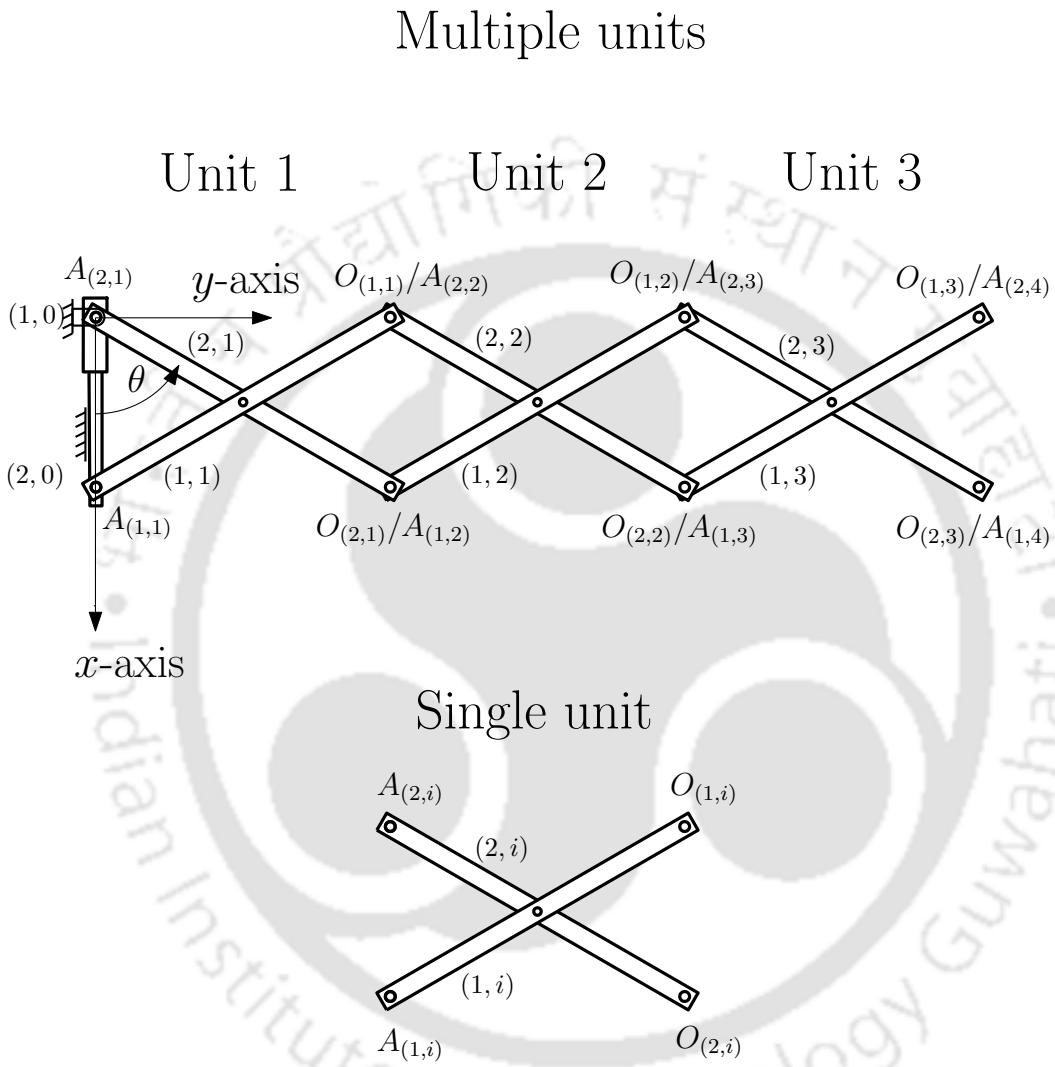

Figure 4.1: Single-plane scissor linkage.

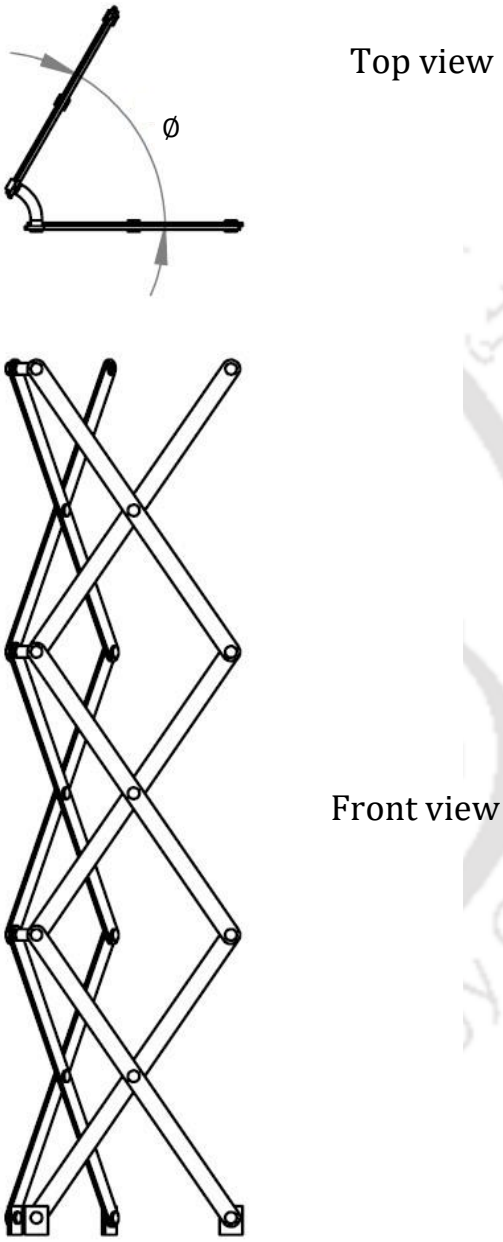

Figure 4.2: Angled-plane scissor linkage.

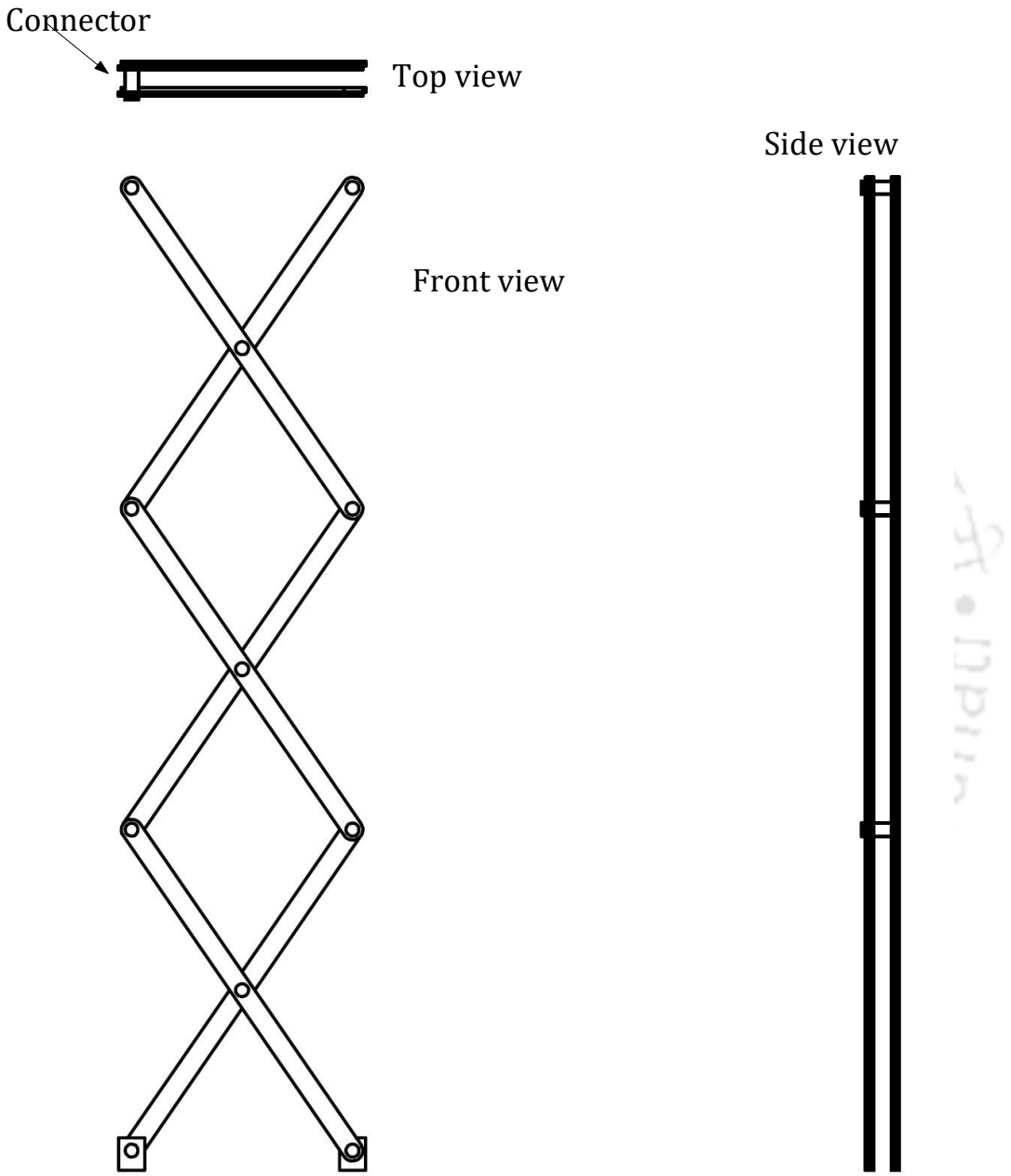

Figure 4.3: Parallel-plane scissor linkage.

where $\boldsymbol{r}^i_{A/O_i}$ is coordinate of point A in frame i as shown in figures (4.4) and (4.5), and $\boldsymbol{r}^j_{A/O_j}$ is the coordinate of the same point in frame j. Further, $\boldsymbol{R}^i_j$ represents rotation matrix of frame j with respect to frame i.

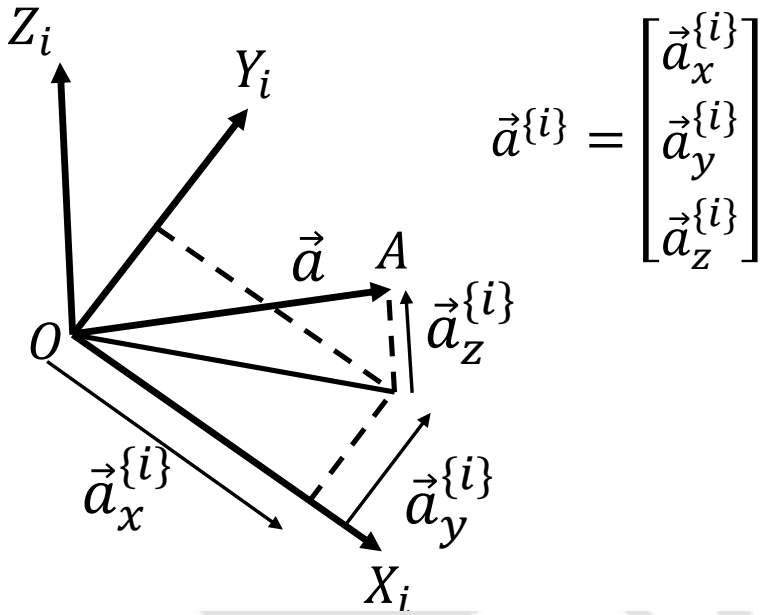

Figure 4.4: Vector r^i_{A/O_i}.

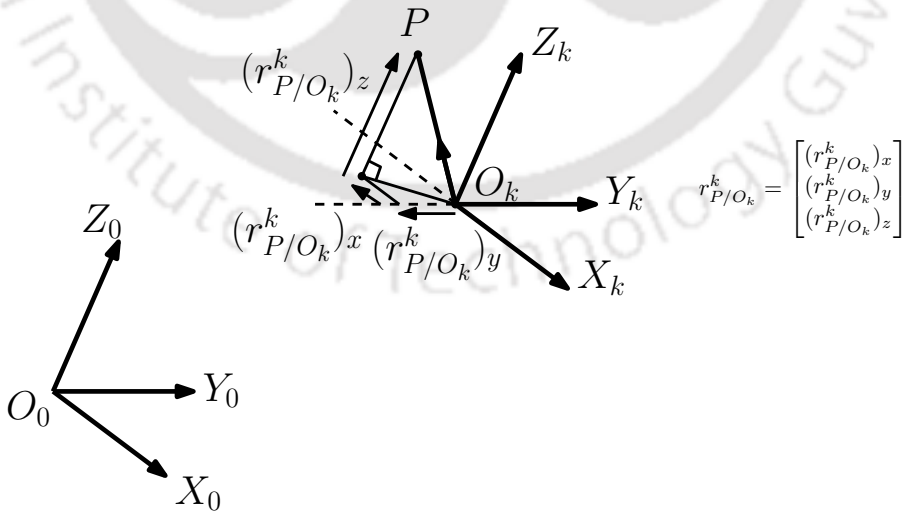

Figure 4.5: Local coordinate of $\boldsymbol{P}$ in coordinate frame k.

4.3.2 Constraint equation for revolute joints

In order to say that there is revolute joint between two bodies, any of the following equivalent conditions have to be satisfied.

4.3.2.1 Revolute Joint Condition 1

There exists on each of the two bodies a revolute surface fixed to the body such that the revolute surfaces of the two bodies mate with each other.

4.3.2.2 Revolute Joint Condition 2

On each of the bodies, there exists an axis such that the two axes are coincident and do not slide with respect to each other.

4.3.2.3 Revolute Joint Condition 3

Fixed to one body, there exists vectors $\boldsymbol{u}$ and $\boldsymbol{v}$ and a point P_h and fixed to the other body there exists vector $\boldsymbol{w}$ and point P_s such that

$$\boldsymbol{u} \cdot \boldsymbol{w} = 0 \tag{4.2}$$

$$\boldsymbol{v} \cdot \boldsymbol{w} = 0 \tag{4.3}$$

$$P_h \equiv P_s \tag{4.4}$$

4.3.2.4 Relation between Revolute Joint Condition 1 in Section 4.3.2.1 and Revolute Joint Condition 2 in Section 4.3.2.2

Any revolute surface has an axis. In fact, the revolute surface can be considered as a surface of revolution about the axis. The axes referred to in Section 4.3.2.2 are actually the axes of the two revolute surfaces stated in Section 4.3.2.1.

4.3.2.5 Relation between Revolute Joint Condition 2 of Section 4.3.2.2 and Revolute Joint Condition 3 of Section 4.3.2.3

Any axis can be referred by a vector that is parallel to it and a point through which the axis passes. For convenience, let us label the two bodies as the first body and the second body. In Section 4.3.2.2, the axis fixed to the first body is mathematically stated in Section 4.3.2.3 as an axis that is parallel to vector $\boldsymbol{u} \times \boldsymbol{v}$ and passing through point P_h. Similarly, in Section 4.3.2.2, the axis fixed to the second body is mathematically stated as an axis that is parallel to $\boldsymbol{w}$ and passing through P_s in Section 4.3.2.3.

An illustration of the two bodies along with the vectors and the points fixed to them is given in figure (4.6). However, in the figure, it is evident that the vectors and the points are not satisfying equation (4.2), equation (4.3) and equation (4.4). A configuration where equation (4.2), equation (4.3) and equation (4.4) are satisfied is shown in figure (4.7).

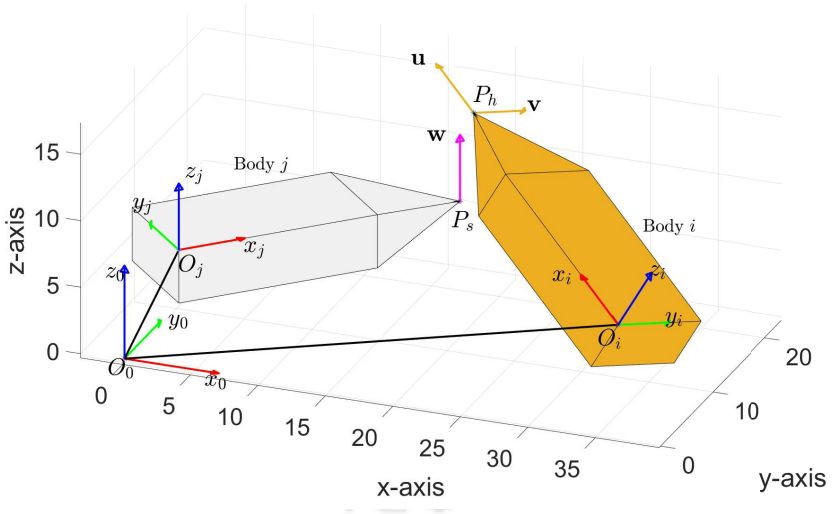

Figure 4.6: Points and vectors required to mathematically define a revolute joint.

Let the bodies between which there is revolute joint be labeled as body i and body j. Let the same labels be used for a Cartesian local coordinate frame of reference on the respective bodies. Consider a ground fixed global Cartesian coordinate frame of reference and let it be labelled as frame 0. In terms of the components of the vectors and the position vectors in the Cartesian Coordinate frames, we can rewrite

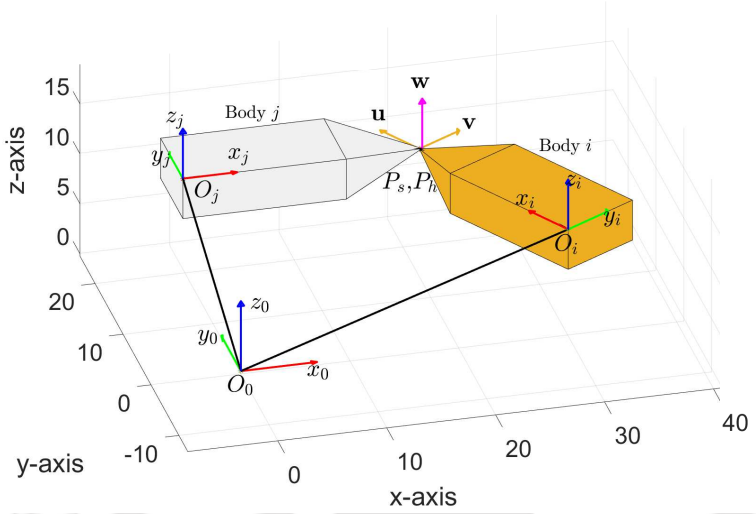

Figure 4.7: P_h, $\boldsymbol{u}$, $\boldsymbol{v}$, P_s, $\boldsymbol{w}$ when the constraints of revolute joint are perfectly satisfied.

equation (4.2), equation (4.3) and equation (4.4) as

$$\left[\boldsymbol{R}_i^0 \boldsymbol{u}^{(i)}\right]^T \boldsymbol{R}_j^0 \boldsymbol{w}^{(j)} = 0 \tag{4.5}$$

$$\left[\boldsymbol{R}_i^0 \boldsymbol{v}^{(i)}\right]^T \boldsymbol{R}_j^0 \boldsymbol{w}^{(j)} = 0 \tag{4.6}$$

$$\left[\boldsymbol{r}^0_{O_i/O_0} + \boldsymbol{R}_i^0 \boldsymbol{r}^{(i)}_{P_h/O_i}\right] - \left[\boldsymbol{r}^0_{O_j/O_0} + \boldsymbol{R}_j^0 \boldsymbol{r}^{(j)}_{P_s/O_j}\right] = \boldsymbol{0} \tag{4.7}$$

4.3.3 Mathematical model of misalignment

The following statements are equivalent definitions of misalignment.

4.3.3.1 Misalignment Definition 1

In a revolute joint, misalignment means the axis on each of the two bodies make a non-zero angle with each other instead of being parallel.

4.3.3.2 Misalignment Definition 2

With reference to parameters stated in Section 4.3.2.3, misalignment means

$$\boldsymbol{u} \cdot \boldsymbol{w} \neq 0 \tag{4.8}$$

$$\boldsymbol{v} \cdot \boldsymbol{w} \neq 0 \tag{4.9}$$

4.3.3.3 A measure of misalignment

It could be noted that

1. a) Misalignment is zero if and only if the axis fixed to each of the bodies in the revolute joint make the zero angle between each other.
   b) Misalignment is zero if and only if

$$\begin{bmatrix} \boldsymbol{u} \cdot \boldsymbol{w} \\ \boldsymbol{v} \cdot \boldsymbol{w} \end{bmatrix} = \begin{bmatrix} 0 \\ 0 \end{bmatrix} \tag{4.10}$$

2. a) Misalignment is *non-zero* if and only if the axis fixed to each of the bodies in the revolute joint make a *non-zero* angle between each other.
   b) Misalignment is *non-zero* if and only if

$$\begin{bmatrix} \boldsymbol{u} \cdot \boldsymbol{w} \\ \boldsymbol{v} \cdot \boldsymbol{w} \end{bmatrix} \neq \begin{bmatrix} 0 \\ 0 \end{bmatrix} \tag{4.11}$$

Based on what is noted so far in this sub-sub-section,

$$\begin{bmatrix} \boldsymbol{u} \cdot \boldsymbol{w} \\ \boldsymbol{v} \cdot \boldsymbol{w} \end{bmatrix} \tag{4.12}$$

qualifies as a measure of misalignment. Hence, we formalize the mathematical expression of misalignment as the expression numbered (4.12).

4.3.4 Limits on misalignment

In the scissor linkage we consider, revolute joints don't have arbitrarily large misalignment. The misalignment is typically small. The misalignment is dictated by factors such as the clearance, the material used and the load on the linkage. We

don't want to increase the number of variables by including the effects of material deformation and unilateral contacts. Instead, what we say is that misalignment cannot exceed a small value ϵ and ϵ is given to us. We don't focus on how that value was arrived. As we will later see, that there is misalignment which cannot exceed a particular value is good enough to demonstrate the contrasting characteristics of lateral sway between angled-plane and parallel-plane scissor linkage. That the misalignment cannot exceed ϵ, is mathematically modelled as

$$|\boldsymbol{u} \cdot \boldsymbol{w}| \leq \epsilon \tag{4.13}$$

$$|\boldsymbol{v} \cdot \boldsymbol{w}| \leq \epsilon \tag{4.14}$$

$$\epsilon \in \mathbb{R}, \qquad \epsilon > 0 \tag{4.15}$$

where we assume that ϵ is already given to us.

4.3.5 A column matrix of two variables representing misalignment

In expression (4.12), misalignment is represented as a column matrix of two expressions involving multiple variables. Suppose that we are interested in expressing misalignment as a column matrix of two scalar variables. This can be accomplished as shown below.

$$\begin{bmatrix} \boldsymbol{u} \cdot \boldsymbol{w} \\ \boldsymbol{v} \cdot \boldsymbol{w} \end{bmatrix} + \begin{bmatrix} s_1 \\ s_2 \end{bmatrix} = \begin{bmatrix} 0 \\ 0 \end{bmatrix} \tag{4.16}$$

Thus, under constraint equation (4.16) and mathematical expression for misalignment given in expression (4.12),

$$\begin{bmatrix} s_1 \\ s_2 \end{bmatrix} \tag{4.17}$$

is a column matrix of two scalars representing misalignment (with opposite sign).

4.3.5.1 New form of limits on misalignment

Because of equation (4.16) and the limits on misalignment stated in expression (4.13) and expression (4.14) can now be written as

$$|s_1| < \epsilon \tag{4.18}$$

$$|s_2| < \epsilon \tag{4.19}$$

4.3.6 Slack variables

In an optimization problem, if we have an inequality constraint $f(\boldsymbol{x}) < a$ where $\boldsymbol{x}$ is a column matrix of variables, f is a scalar function of the variables and a is constant, it is typically tranformed into following form

$$f((x)) + s = 0 \tag{4.20}$$

$$s < a \tag{4.21}$$

and s is called as slack variable. In our case too, expression (4.13) and expression (4.14) corresponds to $f(\boldsymbol{x}) < a$, equation (4.16) corresponds to $f((x)) + s = 0$ and $s < a$ correspond to expression (4.18) and expression (4.19). Further, expression (4.13) and expression (4.14) would become constraints of an optimization problem. Hence, s_1 and s_2 could justifiably called as slack variables.

4.3.7 Component form of constraints in a misaligning revolute joint

Equation (4.16) and inequalities numbered (4.18) and (4.19) when written in the components form, we get

$$\left[\boldsymbol{R}_i^0 \boldsymbol{u}^{(i)}\right]^T \boldsymbol{R}_j^0 \boldsymbol{w}^{(j)} + s_1 = 0 \tag{4.22}$$

$$\left[\boldsymbol{R}_i^0 \boldsymbol{v}^{(i)}\right]^T \boldsymbol{R}_j^0 \boldsymbol{w}^{(j)} + s_2 = 0 \tag{4.23}$$

$$|s_1| \leq \epsilon, \quad \text{and} \quad |s_2| \leq \epsilon \tag{4.24}$$

4.3.8 Why linearization?

The core idea of the chapter is to

1. collect the constraint equations (4.7), (4.22), (4.23) and (4.24) for all the revolute joints in scissor linkage,
2. solve for motion variables,
3. deduce the properties of scissor linkage based on the solution.

The constraint equations (4.7), (4.22), (4.23) and (4.24) are non-linear in motion variables such as $\boldsymbol{R}_i^0$. The non-linearity makes it difficult to solve for motion variables. Hence, we instead choose to linearize the constraint equation about the ideal configuration. The linearization is described next.

4.3.9 Linearization of constraint equations

In the constraint equations, the variables whose change represent motion are $\boldsymbol{r}^0_{O_i/O_0}$, $\boldsymbol{r}^0_{O_j/O_0}$, $\boldsymbol{R}_i^0$, $\boldsymbol{R}_j^0$. When we linearize, the variables are replaced by $\boldsymbol{r}^0_{O_i/O_0} + \boldsymbol{\delta r}^0_{O_i/O_0}$, $\boldsymbol{r}^0_{O_j/O_0} + \boldsymbol{\delta r}^0_{O_j/O_0}$, $\boldsymbol{R}_i^0 + \boldsymbol{\delta R}_i^0$, $\boldsymbol{R}_j^0 + \boldsymbol{\delta R}_j^0$. In the linearized case, $\boldsymbol{r}^0_{O_i/O_0}$, $\boldsymbol{r}^0_{O_j/O_0}$, $\boldsymbol{R}_i^0$, $\boldsymbol{R}_j^0$ are constants representing position and orientation of reference configuration while $\boldsymbol{\delta r}^0_{O_i/O_0}$, $\boldsymbol{\delta r}^0_{O_j/O_0}$, $\boldsymbol{\delta R}_i^0$, $\boldsymbol{\delta R}_j^0$ are variables representing motion from reference configuration of the bodies.

It is well known that nine numbers that constitute the rotation matrix are not independent. They have to obey the constraints of normality and orthogonality between the columns of the matrix. The perturbations $\boldsymbol{\delta R}_i^0$ and $\boldsymbol{\delta R}_j^0$ also should be consistent with it. One way to ensure this is to write

$$\boldsymbol{\delta R}_i^0 = \boldsymbol{R}_i^0 \tilde{\boldsymbol{\gamma}}^{\boldsymbol{i}}_{\boldsymbol{i/0}} \tag{4.25}$$

where $\boldsymbol{\gamma}_{i/0}$ represent a unit vector along the axis of small rotation that is multiplied by the magnitude of small rotation. Further,

$$\tilde{\boldsymbol{\gamma}}^i_{i/0} = \begin{bmatrix} 0 & -\gamma^i_{z,i/0} & \gamma^i_{y,i/0} \\ \gamma^i_{z,i/0} & 0 & -\gamma^i_{x,i/0} \\ -\gamma^i_{y,i/0} & \gamma^i_{x,i/0} & 0 \end{bmatrix} \tag{4.26}$$

More details on skew symmetric matrix representation of small rotation or angular velocity could be found in [83] on page 144 and 145.

Let us choose a reference configuration which satisfies the constraints of revolute joint (equations (4.7), (4.22) and (4.23)) without any misalignment, i.e., $s_1 = s_2 = 0$. When the constraint equations (4.7), (4.22) and (4.23) are linearized about such a reference configuration, the linearized constraint equations become

$$\left[\boldsymbol{\delta r}^0_{O_i/O_0} + \boldsymbol{R}^0_i \tilde{\boldsymbol{\gamma}}^i_{i/0} \boldsymbol{r}^{(i)}_{P_h/O_i}\right] - \left[\boldsymbol{\delta r}^0_{O_j/O_0} + \boldsymbol{R}^0_j \tilde{\boldsymbol{\gamma}}^j_{j/0} \boldsymbol{r}^{(j)}_{Pv/O_j}\right] = \mathbf{0} \tag{4.27}$$

$$\left[\boldsymbol{R}^0_i \boldsymbol{u}^{(i)}\right]^T \boldsymbol{R}^0_j \tilde{\boldsymbol{\gamma}}^j_{j/0} \boldsymbol{w}^{(j)} + \left[\boldsymbol{R}^0_i \tilde{\boldsymbol{\gamma}}^i_{i/0} \boldsymbol{u}^{(i)}\right]^T \boldsymbol{R}^0_j \boldsymbol{w}^{(j)} + \delta s_1 = 0 \tag{4.28}$$

$$\left[\boldsymbol{R}^0_i \boldsymbol{v}^{(i)}\right]^T \boldsymbol{R}^0_j \tilde{\boldsymbol{\gamma}}^j_{j/0} \boldsymbol{w}^{(j)} + \left[\boldsymbol{R}^0_i \tilde{\boldsymbol{\gamma}}^i_{i/0} \boldsymbol{v}^{(i)}\right]^T \boldsymbol{R}^0_j \boldsymbol{w}^{(j)} + \delta s_2 = 0 \tag{4.29}$$

$$|\delta s_1| \leq \epsilon, \quad \text{and} \quad |\delta s_2| \leq \epsilon \tag{4.30}$$

4.4 Deductions from constraint equations of a unit of angled-plane scissor linkage

In this section, we write down the linearised constraint equations (4.27), (4.28), (4.29) and (4.30) for all the joint in a unit of angled-plane scissor linkage. It is from the solution of these equations that we deduce the distinguishing properties of angled-plane scissor linkage and parallel-plane scissor linkage.

4.4.1 Description of links and joints

Consider figure (4.8), which shows the i^{th} unit of angled-plane scissor linkage in three views: front view, top view and auxiliary view under ideal conditions, i.e., when the misalignment is zero for all joints. The ideal configuration also serves as a reference configuration for linearization. A ground fixed frame x_0-y_0-z_0 has been assigned not shown in the figure. The plane x_0-z_0 would constitute the horizontal plane. The angle ϕ between the planes of the scissor linkage is evident in the top view. The length of these links is denoted as l. In each of the two planes, the scissor links make an angle of θ with the horizontal plane as shown in figure (4.8).

In figure (4.8), $(5, i)$ is the connecting link that synchronizes the motion between scissor linkages of two planes. The geometry of the connecting link is characterized by the parameter ϕ, and c as could be seen in the enlarged picture of connecting link.

Links $(1, i-1)$, $(2, i-1)$, $(3, i-1)$ and $(4, i-1)$ support links $(2, i)$, $(1, i)$, $(4, i)$ and $(3, i)$ through revolute joints at $O_{(1,i-1)}$, $O_{(2,i-1)}$, $O_{(3,i-1)}$ and $O_{(4,i-1)}$ respectively. It may be noted that with this connection between unit i and $i-1$, $O_{(1,i-1)}$, $O_{(2,i-1)}$, $O_{(3,i-1)}$ and $O_{(4,i-1)}$ became coincident with $A_{(2,i)}$, $A_{(1,i)}$, $A_{(4,i)}$ and $A_{(3,i)}$

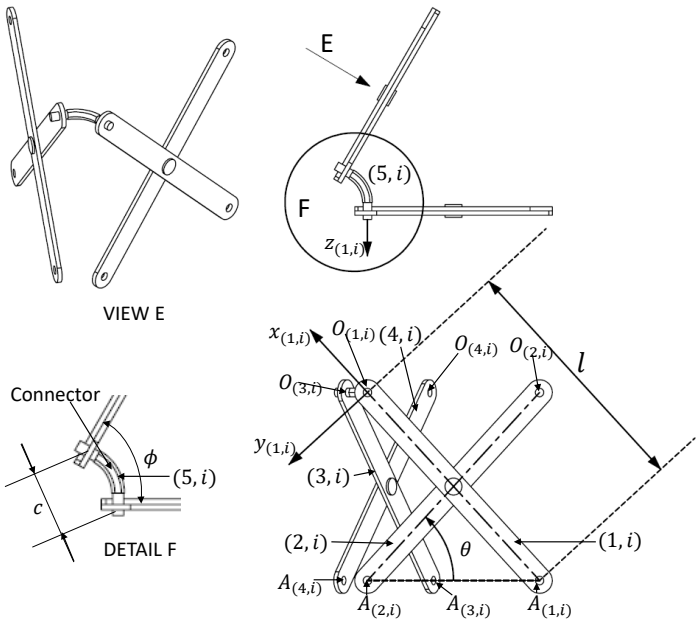

Figure 4.8: Notations used to describe a single unit of angled-plane scissor linkage.

respectively. As said previously, i represents the unit number. The unit closest ground of fixed frame is numbered as 1. Subsequent units are serially numbered until the last unit. Because of revolute joints, $O_{(1,i-1)}$, $O_{(2,i-1)}$, $O_{(3,i-1)}$ and $O_{(4,i-1)}$ became coincident with $A_{(2,i)}$, $A_{(1,i)}$, $A_{(4,i)}$ and $A_{(3,i)}$ respectively. For the first unit links $(2,1)$, $(1,1)$, $(4,1)$ and $(3,1)$ connect to the ground at points $A_{(2,1)}$, $A_{(1,1)}$, $A_{(4,1)}$ and $A_{(3,1)}$ respectively. These four joints constitute boundary conditions.

At the other extreme, if N is the number of units, then N^{th} unit connects to the load carrying platform at $O_{(1,N)}$, $O_{(2,N)}$, $O_{(3,N)}$ and $O_{(4,N)}$ through revolute joints. The top platform is not shown in figure (4.8). However it could be seen in figures (1.1) and (1.4).

For all the links, local coordinate frames are assigned. Local coordinate frame for the link $(1,i)$ is shown in figure (4.8). As given next, the remaining local coordinate frames of other links are described by rotation matrices and the position vector of origins.

Let $\boldsymbol{\mathcal{R}}_z(\beta)$ be the rotation matrix representing the coordinate frame that is rotated by angle β about z axis from a coordinate reference frame. $\boldsymbol{\mathcal{R}}_y(\beta)$ and $\boldsymbol{\mathcal{R}}_x(\beta)$ have similar meaning. With this, the rotation matrices for the local coordinate frame

of the links in a typical i^{th} unit are given next.

$$\begin{aligned}
\boldsymbol{R}^0_{1,i} &= \boldsymbol{\mathcal{R}}_z\left(\pi-\theta\right)\\
\boldsymbol{R}^0_{2,i} &= \boldsymbol{\mathcal{R}}_z\left(\theta\right)\\
\boldsymbol{R}^0_{3,i} &= \boldsymbol{\mathcal{R}}_y\left(\phi\right)\boldsymbol{R}^0_{1,i}\\
\boldsymbol{R}^0_{4,i} &= \boldsymbol{\mathcal{R}}_y\left(\phi\right)\boldsymbol{R}^0_{2,i}\\
\boldsymbol{R}^0_{5,i} &= \boldsymbol{\mathcal{R}}_y\left(\frac{\pi}{2}+\frac{\phi}{2}\right)
\end{aligned} \tag{4.31}$$

Further the position vector of the origin of local coordinate frames are

$$\begin{aligned}
\boldsymbol{r}^0_{1,i} &= \begin{bmatrix}0 & il\sin\theta & 0\end{bmatrix}^T\\
\boldsymbol{r}^0_{2,i} &= \boldsymbol{r}^0_{1,i} + \begin{bmatrix}l\cos\theta & 0 & 0\end{bmatrix}^T\\
\boldsymbol{r}^0_{3,i} &= \boldsymbol{r}^0_{1,i} + \boldsymbol{R}^0_{5,i}\begin{bmatrix}c & 0 & 0\end{bmatrix}^T\\
\boldsymbol{r}^0_{4,i} &= \boldsymbol{r}^0_{3,i} + \begin{bmatrix}l\cos\theta & 0 & 0\end{bmatrix}^T\\
\boldsymbol{r}^0_{5,i} &= \boldsymbol{r}^0_{1,i}
\end{aligned} \tag{4.32}$$

We now provide details of each revolute joint.

The small perturbations in position vector and orientation of k^{th} link in i^{th} unit are $\boldsymbol{\delta r}_{(k,i)} = \begin{bmatrix}\delta r_{x,(k,i)}\\ \delta r_{y,(k,i)}\\ \delta r_{z,(k,i)}\end{bmatrix}$ and $\boldsymbol{\gamma}_{(k,i)} = \begin{bmatrix}\gamma_{x,(k,i)}\\ \gamma_{y,(k,i)}\\ \gamma_{z,(k,i)}\end{bmatrix}$ respectively. Further, slack variables δs_1 and δs_2 (see equations (4.28) and (4.29)) for k^{th} joint in i^{th} unit are represented as $\delta s_{1,(k,i)}$ and $\delta s_{2,(k,i)}$, respectively. These variables are also shown in table (4.1).

4.4.2 System of equations from all revolute joints

Suppose that there are N units in an angled-plane scissor linkage. The link details and joint details of i^{th} unit ($1 \le i \le N$) are as per Section 4.4.1. The first four revolute joints in the first unit would join the first four links in the first unit with the first four links in the zeroth unit. The rotation matrices and position vector of origin of local coordinate frame of these four links of the zeroth unit, $(1,0)$, $(2,0)$, $(3,0)$ and $(4,0)$, are again as per equations (4.31) and (4.32). However, these links are treated as fixed to the ground. Hence we take

$$\begin{aligned}
\boldsymbol{\delta r}_{(1,0)} = \boldsymbol{\delta r}_{(2,0)} = \boldsymbol{\delta r}_{(3,0)} = \boldsymbol{\delta r}_{(4,0)} &= \begin{bmatrix}0 & 0 & 0\end{bmatrix}^T\\
\boldsymbol{\gamma}_{(1,0)} = \boldsymbol{\gamma}_{(2,0)} = \boldsymbol{\gamma}_{(3,0)} = \boldsymbol{\gamma}_{(4,0)} &= \begin{bmatrix}0 & 0 & 0\end{bmatrix}^T
\end{aligned}$$

Table 4.1: Details of revolute joints in a unit indexed with i, i.e., i^{th} unit.

Joint No.	i	j	$\boldsymbol{r}^i_{P_h/O_i}$	$\boldsymbol{r}^j_{P_s/O_j}$	$\boldsymbol{u}^i$	$\boldsymbol{v}^i$	$\boldsymbol{w}^j$	δs_1, δs_2
(1,i)	$(1, i-1)$	$(2, i)$	$\begin{bmatrix}0\\0\\0\end{bmatrix}$	$\begin{bmatrix}-l\\0\\0\end{bmatrix}$	$\begin{bmatrix}1\\0\\0\end{bmatrix}$	$\begin{bmatrix}0\\1\\0\end{bmatrix}$	$\begin{bmatrix}0\\0\\1\end{bmatrix}$	$\delta s_{1,(1,i)}$, $\delta s_{2,(1,i)}$
(2,i)	$(2, i-1)$	$(1, i)$	$\begin{bmatrix}0\\0\\0\end{bmatrix}$	$\begin{bmatrix}-l\\0\\0\end{bmatrix}$	$\begin{bmatrix}1\\0\\0\end{bmatrix}$	$\begin{bmatrix}0\\1\\0\end{bmatrix}$	$\begin{bmatrix}0\\0\\1\end{bmatrix}$	$\delta s_{1,(2,i)}$, $\delta s_{2,(2,i)}$
(3,i)	$(3, i-1)$	$(4, i)$	$\begin{bmatrix}0\\0\\0\end{bmatrix}$	$\begin{bmatrix}-l\\0\\0\end{bmatrix}$	$\begin{bmatrix}1\\0\\0\end{bmatrix}$	$\begin{bmatrix}0\\1\\0\end{bmatrix}$	$\begin{bmatrix}0\\0\\1\end{bmatrix}$	$\delta s_{1,(3,i)}$, $\delta s_{2,(3,i)}$
(4,i)	$(4, i-1)$	$(3, i)$	$\begin{bmatrix}0\\0\\0\end{bmatrix}$	$\begin{bmatrix}-l\\0\\0\end{bmatrix}$	$\begin{bmatrix}1\\0\\0\end{bmatrix}$	$\begin{bmatrix}0\\1\\0\end{bmatrix}$	$\begin{bmatrix}0\\0\\1\end{bmatrix}$	$\delta s_{1,(4,i)}$, $\delta s_{2,(4,i)}$
(5,i)	$(1, i)$	$(2, i)$	$\begin{bmatrix}-\frac{l}{2}\\0\\0\end{bmatrix}$	$\begin{bmatrix}-\frac{l}{2}\\0\\0\end{bmatrix}$	$\begin{bmatrix}1\\0\\0\end{bmatrix}$	$\begin{bmatrix}0\\1\\0\end{bmatrix}$	$\begin{bmatrix}0\\0\\1\end{bmatrix}$	$\delta s_{1,(5,i)}$, $\delta s_{2,(5,i)}$
(6,i)	$(3, i)$	$(4, i)$	$\begin{bmatrix}-\frac{l}{2}\\0\\0\end{bmatrix}$	$\begin{bmatrix}-\frac{l}{2}\\0\\0\end{bmatrix}$	$\begin{bmatrix}1\\0\\0\end{bmatrix}$	$\begin{bmatrix}0\\1\\0\end{bmatrix}$	$\begin{bmatrix}0\\0\\1\end{bmatrix}$	$\delta s_{1,(6,i)}$, $\delta s_{2,(6,i)}$
(7,i)	$(1, i)$	$(5, i)$	$\begin{bmatrix}0\\0\\0\end{bmatrix}$	$\begin{bmatrix}0\\0\\0\end{bmatrix}$	$\begin{bmatrix}1\\0\\0\end{bmatrix}$	$\begin{bmatrix}0\\1\\0\end{bmatrix}$	$\begin{bmatrix}-\cos\frac{\phi}{2}\\0\\-\sin\frac{\phi}{2}\end{bmatrix}$	$\delta s_{1,(7,i)}$, $\delta s_{2,(7,i)}$
(8,i)	$(3, i)$	$(5, i)$	$\begin{bmatrix}0\\0\\0\end{bmatrix}$	$\begin{bmatrix}c\\0\\0\end{bmatrix}$	$\begin{bmatrix}1\\0\\0\end{bmatrix}$	$\begin{bmatrix}0\\1\\0\end{bmatrix}$	$\begin{bmatrix}-\cos\frac{\phi}{2}\\0\\\sin\frac{\phi}{2}\end{bmatrix}$	$\delta s_{1,(8,i)}$, $\delta s_{2,(8,i)}$

Let us collect equations (4.27), (4.28) and (4.29) associated with all the joints in all the units starting from one to N. In this system of equations, the variables are

1. $\boldsymbol{\delta r}_{k,i}$, $k = 1, \cdots, 5$ and $i = 1, \cdots, N$.

2. $\boldsymbol{\gamma}_{k,i}$, $k = 1, \cdots, 5$ and $i = 1, \cdots, N$.

3. $\delta s_{1,(k,i)}$, $k = 1, \cdots, 8$ and $i = 1, \cdots, N$.

4. $\delta s_{2,(k,i)}$, $k = 1, \cdots, 8$ and $i = 1, \cdots, N$.

4.4.3 Solution to variables from the system of equations

When the system of equations obtained in Subsection 4.4.2 is solved for variables, the solution obtained for variables associated with i^{th} unit is

$$\delta s_{1,(1,i)} = (\sin 2\theta)\gamma_{x,(2,i)} + \gamma_{y,(3,i-1)} + (\cos 2\theta)\gamma_{y,(3,i)} \tag{4.33}$$

$$\delta s_{1,(2,i)} = -(\sin 2\theta)\gamma_{x,(1,i)} + \gamma_{y,(3,i-1)} + (\cos 2\theta)\gamma_{y,(3,i)} \tag{4.34}$$

$$\delta s_{1,(3,i)} = (\sin 2\theta)\gamma_{x,(4,i)} + \gamma_{y,(3,i-1)} + (\cos 2\theta)\gamma_{y,(3,i)} \tag{4.35}$$

$$\delta s_{1,(4,i)} = -(\sin 2\theta)\gamma_{x,(3,i)} + \gamma_{y,(3,i-1)} + (\cos 2\theta)\gamma_{y,(3,i)} \tag{4.36}$$

$$\delta s_{1,(5,i)} = 2\cos\theta\left((\sin\theta)\gamma_{x,(2,i)} + (\cos\theta)\gamma_{y,(3,i)}\right) \tag{4.37}$$

$$\delta s_{1,(6,i)} = 2\cos\theta\left((\sin\theta)\gamma_{x,(4,i)} + (\cos\theta)\gamma_{y,(3,i)}\right) \tag{4.38}$$

$$\delta s_{1,(7,i)} = \gamma_{y,(3,i)} + \frac{\sin\left(\frac{\phi}{2}\right)\left(2l\cos\theta\left(\gamma_{y,(3,1)} + \cdots + \gamma_{y,(3,i-1)} + \gamma_{y,(3,i)}\right) - (c\sin\theta)\gamma_{x,(5,i)}\right)}{c} \tag{4.39}$$

$$\delta s_{1,(8,i)} = \gamma_{y,(3,i)} + \frac{\sin\frac{\phi}{2}\left((c\sin\theta)\gamma_{x,(5,i)} + (2l\cos\theta)\left(\gamma_{y,(3,1)} + \cdots + \gamma_{y,(3,i-1)} + \gamma_{y,(3,i)}\right)\right)}{c} \tag{4.40}$$

$$\delta s_{2,(1,i)} = -\gamma_{x,(1,i-1)} - (\cos 2\theta)\gamma_{x,(2,i)} + (\sin 2\theta)\gamma_{y,(3,i)} \tag{4.41}$$

$$\delta s_{2,(2,i)} = -(\cos 2\theta)\gamma_{x,(1,i)} - \gamma_{x,(2,i-1)} - (\sin 2\theta)\gamma_{y,(3,i)} \tag{4.42}$$

$$\delta s_{2,(3,i)} = -\gamma_{x,(3,i-1)} - (\cos 2\theta)\gamma_{x,(4,i)} + (\sin 2\theta)\gamma_{y,(3,i)} \tag{4.43}$$

$$\delta s_{2,(4,i)} = -(\cos 2\theta)\gamma_{x,(3,i)} - \gamma_{x,(4,i-1)} - (\sin 2\theta)\gamma_{y,(3,i)} \tag{4.44}$$

$$\delta s_{2,(5,i)} = -\gamma_{x,(1,i)} - (\cos 2\theta)\gamma_{x,(2,i)} + (\sin 2\theta)\gamma_{y,(3,i)} \tag{4.45}$$

$$\delta s_{2,(6,i)} = -\gamma_{x,(3,i)} - (\cos 2\theta)\gamma_{x,(4,i)} + (\sin 2\theta)\gamma_{y,(3,i)} \tag{4.46}$$

$$\delta s_{2,(7,i)} = \frac{\sin\frac{\phi}{2}\left((c\cos\theta)\gamma_{x,(5,i)} + 2l\sin\theta\left(\gamma_{y,(3,1)} + \cdots + \gamma_{y,(3,i-1)} + \gamma_{y,(3,i)}\right)\right)}{c} - \gamma_{x,(1,i)} \tag{4.47}$$

$$\delta s_{2,(8,i)} = \frac{\sin\frac{\phi}{2}\left(2l\sin\theta\left(\gamma_{y,(3,1)} + \cdots + \gamma_{y,(3,i-1)} + \gamma_{y,(3,i)}\right) - (c\cos\theta)\gamma_{x,(5,i)}\right)}{c} - \gamma_{x,(3,i)} \tag{4.48}$$

Furthermore, the deflections of top points of unit i which are also the deflection of origin of local coordinates of links $(1,i)$, $(2,i)$, $(3,i)$ and $(4,i)$ turnout to be

$$\boldsymbol{\delta r}_{(1,i)} = \left[0, 0, -l\left(\gamma_{y,3,1} + \cdots + \gamma_{y,3,i-1} + \gamma_{y,3,i}\right)\right]^T \tag{4.49}$$

$$\boldsymbol{\delta r}_{(2,i)} = \left[0, 0, -l\left(\gamma_{y,3,1} + \cdots + \gamma_{y,3,i-1} + \gamma_{y,3,i}\right)\right]^T \tag{4.50}$$

$$\boldsymbol{\delta r}_{(3,i)} = \left[-l\sin\phi\left(\gamma_{y,3,1} + \cdots + \gamma_{y,3,i-1} + \gamma_{y,3,i}\right), 0, -l\cos\phi\left(\gamma_{y,3,1} + \cdots + \gamma_{y,3,i-1} + \gamma_{y,3,i}\right)\right]^T \tag{4.51}$$

$$\boldsymbol{\delta r}_{(4,i)} = \left[-l\sin\phi\left(\gamma_{y,3,1} + \cdots + \gamma_{y,3,i-1} + \gamma_{y,3,i}\right), 0, -l\cos\phi\left(\gamma_{y,3,1} + \cdots + \gamma_{y,3,i-1} + \gamma_{y,3,i}\right)\right]^T \tag{4.52}$$

4.4.4 Inequalities

Apart from equations (4.27), (4.28) and (4.29), as seen in expression (4.30), there are also inequalities modelling the misalignment in revolute joints. If we apply the inequalities in particular to $\delta s_{1,(7,i)}$ and $\delta s_{1,(8,i)}$ and use equations (4.39) and (4.40), we get

$$\left|\gamma_{y,(3,i)} + \frac{\sin\frac{\phi}{2}\left(2l\cos\theta\left(\gamma_{y,(3,1)} + \cdots + \gamma_{y,(3,i-1)} + \gamma_{y,(3,i)}\right) - (c\sin\theta)\gamma_{x,(5,i)}\right)}{c}\right| \leq \epsilon \tag{4.53}$$

$$\left|\gamma_{y,(3,i)} + \frac{\sin\frac{\phi}{2}\left((c\sin\theta)\gamma_{x,(5,i)} + 2l\cos\theta\left(\gamma_{y,(3,1)} + \cdots + \gamma_{y,(3,i-1)} + \gamma_{y,(3,i)}\right)\right)}{c}\right| \leq \epsilon \tag{4.54}$$

Adding inequalities, (4.53) and (4.54), and dividing them by two, we get

$$\left|\gamma_{y,(3,i)} + \frac{2l\sin\frac{\phi}{2}\cos\theta\left(\gamma_{y,(3,1)} + \cdots + \gamma_{y,(3,i-1)} + \gamma_{y,(3,i)}\right)}{c}\right| \leq \epsilon \tag{4.55}$$

For the first unit, inequality (4.55) becomes

$$\left|\left(1 + 2\frac{l}{c}\sin\frac{\phi}{2}\cos\theta\right)\gamma_{y,(3,1)}\right| \leq \epsilon \tag{4.56}$$

$l > 0$, $c > 0$ and θ and ϕ are such that $\sin\frac{\phi}{2}$ and $\cos\theta$ are positive. Hence we may simplify inequality (4.56) as

$$\left|\gamma_{y,(3,1)}\right| \leq \frac{\epsilon}{\left(1 + 2\frac{l}{c}\sin\frac{\phi}{2}\cos\theta\right)} \tag{4.57}$$

Furthermore, for the second unit, inequality (4.55) becomes

$$\left|\left(1 + 2\frac{l}{c}\sin\frac{\phi}{2}\cos\theta\right)\gamma_{y,(3,2)} + \left(2\frac{l}{c}\sin\frac{\phi}{2}\cos\theta\right)\gamma_{y,(3,1)}\right| \leq \epsilon \tag{4.58}$$

Adding equation (4.57) and (4.58) with simplification gives

$$\begin{aligned} \left|\gamma_{y,(3,2)} + \gamma_{y,(3,1)}\right| &\leq \epsilon\left(r + r^2\right) \\ \text{where } r &= \frac{1}{\left(1 + 2\frac{l}{c}\sin\frac{\phi}{2}\cos\theta\right)} \end{aligned} \tag{4.59}$$

We can see that there is a pattern in equation (4.59) which can be generalized as

$$\left|\sum_{k=1}^{k=i} \gamma_{y,(3,k)}\right| \leq \epsilon \sum_{k=1}^{k=i} r^k \tag{4.60}$$

4.4.5 A measure of lateral sway

Consider equations (4.49) to (4.52). $\boldsymbol{\delta r}_{(1,i)}$, $\boldsymbol{\delta r}_{(2,i)}$, $\boldsymbol{\delta r}_{(3,i)}$, and $\boldsymbol{\delta r}_{(4,i)}$ are the perturbations in the position of origin of the local frames of bodies $(1,i)$, $(2,i)$, $(3,i)$ and $(4,i)$. We had placed the origin of local frames of these bodies at their top ends along the positive side of the y-axis. The x-axis and y-axis along with the origin for the local frame of the body $(1,i)$ is illustrated in figure (4.8). Further observation of equations (4.49) to (4.52) reveals that the proportion between x, y and z components of the perturbation vectors are constant. In particular, we can rewrite equation (4.49) to (4.52) as

$$\boldsymbol{\delta r}_{(1,i)} = [0,0,-1]^T\, l\,(\gamma_{y,3,1} + \cdots + \gamma_{y,3,i-1} + \gamma_{y,3,i}) \tag{4.61}$$

$$\boldsymbol{\delta r}_{(2,i)} = [0,0,-1]^T\, l\,(\gamma_{y,3,1} + \cdots + \gamma_{y,3,i-1} + \gamma_{y,3,i}) \tag{4.62}$$

$$\boldsymbol{\delta r}_{(3,i)} = [-\sin\phi, 0, -\cos\phi]^T\, l\,(\gamma_{y,3,1} + \cdots + \gamma_{y,3,i-1} + \gamma_{y,3,i}) \tag{4.63}$$

$$\boldsymbol{\delta r}_{(4,i)} = [-\sin\phi, 0, -\cos\phi]^T\, l\,(\gamma_{y,3,1} + \cdots + \gamma_{y,3,i-1} + \gamma_{y,3,i}) \tag{4.64}$$

where the perturbations are written as a vector times a scalar. These respective vectors represent the directions along which lateral sway of the four points occur. The average of displacement of these points along the respective directions of sway could be considered as a measure of lateral sway. If we represent the average by $\mathcal{C}_i$, then

$$\mathcal{C}_i = \frac{1}{4}\left(\begin{bmatrix}0 & 0 & -1\end{bmatrix}^T \left(\boldsymbol{\delta r}_{(1,i)} + \boldsymbol{\delta r}_{(2,i)}\right)\right) + \frac{1}{4}\left(\begin{bmatrix}-\sin\theta & 0 & -\cos\theta\end{bmatrix}^T \left(\boldsymbol{\delta r}_{(3,i)} + \boldsymbol{\delta r}_{(4,i)}\right)\right) \tag{4.65}$$

Simplification of equation (4.65) using equations (4.49)-(4.52) gives

$$\mathcal{C}_i = l \sum_{k=1}^{i} \gamma_{y,(3,k)} \tag{4.66}$$

Given that l is positive, using inequality (4.60) and equation (4.66), we get

$$|\mathcal{C}_i| \leq l\epsilon \sum_{k=1}^{k=i} r^k \tag{4.67}$$

4.4.6 Bounds on the magnitude of maximum lateral sway

Let $l = 0.3\,m$, $c = .04\,m$, $\epsilon = 0.01$ and $\theta \leq 80°$. Let us further investigate under the following two cases:

4.4.6.1 Case 1: Angled scissor linkage i.e., $\phi \neq 0$

To understand the implications of angled-plane scissor, let $\phi = \frac{\pi}{3}$. With these numerical values, the maximum value of r as given equation in (4.59) is 0.434. Since $r < 1$, the upper and lower bounds as given in inequality (4.67) is a geometric series. Thus, using the formula for sum of geometric series, we can rewrite inequality (4.67) as

$$|\mathcal{C}_i| \leq l\epsilon r \frac{1 - r^i}{1 - r} \tag{4.68}$$

If $\mathcal{C}_{i,max}$ is the maximum of feasible $\mathcal{C}_i$, then $l\epsilon r \dfrac{1 - r^i}{1 - r}$ is an upper bound on $\mathcal{C}_{i,max}$. This upper bound is plotted as the curve that is labelled as "upper bound of angled-plane scissor linkage" in figure (4.9). Based on deliberations so far, the magnitude of $\mathcal{C}_{i,max}$ can be anywhere in the region shaded in light-grey.

4.4.6.2 Case 2: Parallel-plane scissor linkage $\phi = 0$

When $\phi = 0$, the value of r as given equation in (4.59) is 1. Since $r = 1$, the upper and lower bounds as given in inequality (4.67) is an arithmetic progression and similar to inequality (4.68), we can write

$$|\mathcal{C}_i| \leq l\epsilon i \tag{4.69}$$

Similar to previous case, $l\epsilon i$ is an upperbound on $\mathcal{C}_{i,max}$. The bound is shown as a curve that is labelled as "upper bound of parallel-plane scissor linkage" in fig-

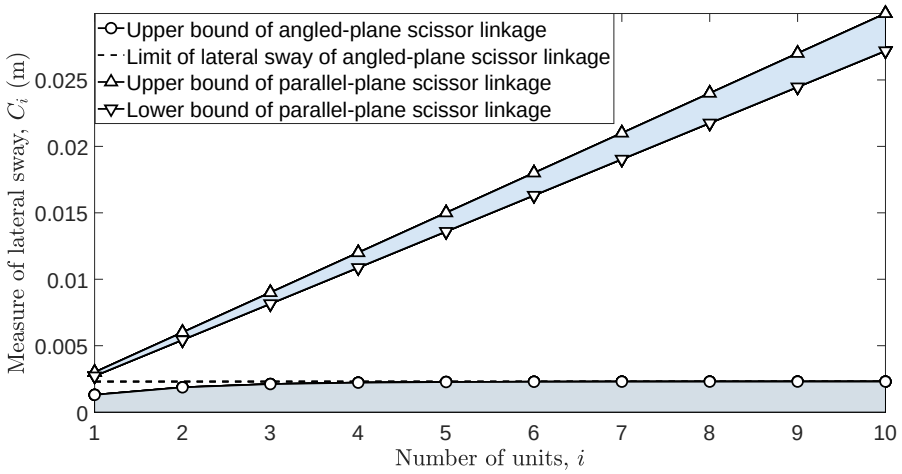

Figure 4.9: The gulf between maximum lateral sway of parallel-plane scissor and angled-plane scissor linkage.

ure (4.9). In order to establish a wide gulf between lateral deflection, $\mathcal{C}_i$, of parallel-plane scissor linkage and angled-plane scissor linkage, we will present another bound for $\mathcal{C}_{i,max}$.

Let us take stock of the situation so far. Consider i^{th} unit of scissor linkage. Assume that all the variables related to all the units prior to i^{th} unit are known. To begin with, this is definitely true if $i = 1$. Also, for the moment, we will ignore any units after i^{th} unit. In this context, i^{th} unit has five bodies (see figure (4.8)). Each body has six variables corresponding to $\delta\boldsymbol{r}$ and $\boldsymbol{\gamma}$. Further, the unit has eight revolute joints (see figure (4.8)). Associated with every revolute joint, we have two slack variables. Thus, per unit, we have 46 variables. Further, every revolute joint leads to five constraint equations (see equations (4.27)-(4.29)). Hence, in total, we have 40 equality constraints. Clearly, the number of equality constraints are less than the number of variables, and we have an underdetermined system of linear equations. We would not get unique solutions, but all the variables could be expressed in terms of just $46 - 40 = 6$ of them. This is evident in equations (4.33)-(4.52) where all the variables are expressed in terms of just $\gamma_{x,(1,i)}$, $\gamma_{x,(2,i)}$, $\gamma_{x,(3,i)}$, $\gamma_{x,(4,i)}$, $\gamma_{x,(5,i)}$ and $\gamma_{y,(3,i)}$. Let us call them as free variables associated with unit i.

For the first unit, there are no units prior to it, and we can choose the six variables corresponding to the unit. Once they are chosen, for the second unit, the free variables of the unit prior to it is already chosen, and we can choose its own

free variables. In this way, we can make the choice of free variables of all the units recursively.

The choice of free variables is called feasible if the slack variables resulting from the choice satisfy its own $\pm\epsilon$ bounds. Since we are investigating maximum possible lateral sway, our interest is to find feasible free variables that would maximize $\mathcal{C}_N$ where N is the last unit number. Finding such feasible free variables would constitute a linear optimization problem. We found solving the problem analytically daunting. Computer Algebra Systems like MATHEMATICA also could not help. Hence, in this analytical study, we have focussed on only establishing bounds on $\mathcal{C}_{i,max}$, the maximum possible lateral sway at unit i. Magnitude wise, the bounds that we obtained in equations (4.68) and (4.69) are the upper bounds on $\mathcal{C}_{i,max}$

There is an interesting way of obtaining lower bound on $\mathcal{C}_{i,max}$. If we find $\mathcal{C}_i$ for one feasible solution, it would automatically become a lower bound on $\mathcal{C}_{i,max}$. We are now presenting one such feasible solution for the case of parallel-plane scissor linkage.

If, $\forall j = 1, 2 \cdots i$,

$$\gamma_{x,k,j} = \begin{cases} \epsilon \cos\theta & \text{if } k = 1 \text{ or } 3 \\ -\epsilon \cos\theta & \text{if } k = 2 \text{ or } 4 \\ 0 & \text{if } k = 5 \end{cases} \tag{4.70}$$

$$\gamma_{y,k,j} = \begin{cases} \epsilon \sin\theta & \text{if } k = 1 \text{ or } 2 \text{ or } 3 \text{ or } 4 \\ 0 & \text{if } k = 5 \end{cases} \tag{4.71}$$

$$\gamma_{z,k,j} = 0 \quad \forall k = 1, 2, 3, 4, 5 \tag{4.72}$$

then the slack variables become

$$\delta s_{p,q,r} = \begin{cases} -\epsilon \sin\theta & \text{if } p \in \{1\},\ q \in \{1,2,3,4\},\ r \in \{1\} \\ +\epsilon \cos\theta & \text{if } p \in \{2\},\ q \in \{1,3,\},\ r \in \{1\} \\ -\epsilon \cos\theta & 7 \text{ if } p \in \{2\},\ q \in \{2,4,\},\ r \in \{1\} \\ +\epsilon \sin\theta & \text{if } p \in \{1\},\ q \in \{7,8\},\ r \in \{1, \cdots i\} \\ -\epsilon \cos\theta & \text{if } p \in \{2\},\ q \in \{7,8\},\ r \in \{1, \cdots i\} \\ 0 & \text{otherwise} \end{cases} \tag{4.73}$$

It is to be noted that all the slack variables are within the bounds of $\pm\epsilon$ and hence angular perturbations given in equations (4.70)-(4.72) are feasible perturbations. Further, from equations (4.71) and (4.66), we get

$$\mathcal{C}_i = i\epsilon l \sin\theta \tag{4.74}$$

The implication of equation (4.74) is that $\mathcal{C}_{i,max}$ is either equal to or greater than $i\epsilon l \sin\theta$. Thus, we may treat $i\epsilon \sin\theta$ as the lower bound for $\mathcal{C}_{i,max}$. The curve corresponding to this lower bound is the curve that is labelled as "lower bound of parallel-plane scissor linkage" in figure (4.9).

4.5 Results, practical utility and conclusion

We now list out the contrasting features of parallel-plane scissor linkage and angled-plane scissor linkage.

4.5.1 Dependency on connector length c.

The lateral sway given in equation (4.66) is independent of connector length c. Nevertheless, as seen in equations (4.33)-(4.48), slack variables, in particular $\delta s_{1,7,i}$, $\delta s_{1,8,i}$, $\delta s_{1,7,i}$ and $\delta s_{2,8,i}$, do depend on connector length c. These slack variables in turn impose bounds on lateral sway, $\mathcal{C}_i$, as exemplified in equation (4.67).

By expanding the expressions for $\delta s_{1,7,i}$, $\delta s_{1,8,i}$, $\delta s_{2,7,i}$ and $\delta s_{2,8,i}$ in equations (4.39), (4.40), (4.47) and (4.48), we see that among the terms in each of the four expressions, c if present is in denominator along with $\sin\phi$ in numerator. Due to the presence of $\sin\phi$ in the numerator, the dependency on c would vanish in the case of $\sin\phi = 0$, i.e., in the case of parallel-plane scissor linkage. **Since slack variables in parallel-plane scissor linkage do not depend on c, the maximum lateral sway $\mathcal{C}_{i,max}$ is in no way influenced by connector length c, unlike angled-plane scissor linkage.**

4.5.2 Bounds on maximum lateral sway

As is evident in figure (4.9), the maximum magnitude of lateral sway, $\mathcal{C}_{i,max}$ in the case of angled-plane scissor linkage is bounded between zero and a geometric series in i. The feasible region is indicated in light grey color in figure (4.9). For practically reasonable values of l and c, the geometric series is convergent. In contrast, as is evident from curve that is labelled as "upper bound of parallel-plane scissor linkage" and curve that is labelled as "lower bound of parallel-plane scissor linkage"

in figure (4.9), the maximum lateral sway, $\mathcal{C}_{i,max}$ is bounded between two arithmetic progressions in i. **Thus we can say that as the number of units increases, the maximum lateral sway increases without convergence in parallel-plane scissor linkage whereas it gets restricted by a constant limit in the case of angled-plane scissor linkage.**

4.5.3 Practical utility of the results

The argument on smaller lateral sway in angled-plane scissor linkage was based on the bounds given in inequality (4.68). The bounds in this inequality are dependent on common ratio r whose expression is given in equation (4.59). The expression shows the dependency of common ratio r on the design parameters such as connector length c, length of links l, and the angle between the planes ϕ. This expression would help a designer to understand the impact of design choices for c, l and ϕ on lateral sway. It leads to better designs. A possible design process involving the results of this chapter is given in Appendix C.

4.5.4 Summary

The chapter aimed to demonstrate through equations of mechanics the large lateral sway in parallel-plane scissor linkage and a significantly smaller lateral sway in angled-plane scissor linkage when the revolute joint of the linkage could misalign but the linkage is otherwise ideal. Using well-known modelling techniques in multibody mechanics, constraint equations corresponding to revolute joints were written in terms of state variables of each rigid body. Slack variables were introduced to model misalignment. For simplicity, a constant upper and lower bounds were chosen for all slack variables. The resulting model was a nonlinear optimization problem. To further simplify, the nonlinear equations were linearised. By solving linearised equations along with a few mathematical manipulations, the following contrasting properties were deduced:

1. The connector length does not influence lateral deflection of parallel-plane scissor linkage, but it does influence lateral sway of angled-plane scissor linkage.

2. For practically reasonable values of the parameters of the scissor linkage, the

maximum lateral sway is bounded by a converging geometric series for angled-plane scissor linkage and sandwiched between two arithmetic progressions for parallel-plane scissor linkage. The index of both the arithmetic progressions and the geometric series is the number of repeating units in the scissor linkage. When the sequences of numbers were plotted against the number of repeating units, a wide gulf was seen between the lateral sway bounds of parallel plane scissor linkage and angled-plane scissor linkage. This wide gulf signified the significantly different characteristics of lateral sway.

The above two properties adequately bring out contrasting characteristics of lateral sway. The expressions derived for the bounds of lateral sway helps a designer to make appropriate design choices on the parameter of the scissor linkage.

Chapter 5

Numerical analysis of lateral sway

5.1 Introduction

There are multiple reasons for the numerical determination of maximum possible sway. First, it serves as a validation of the results obtained in Section 4.5. Secondly, the non-linearities in the constraints discussed in Section 4.3.2 can be handled without linearization in the case of numerical methods.

We apply the numerical method to the following linkages:

1. Angled-plane scissor linkage
2. Parallel-plane scissor linkage
3. Triangular-prism-shaped scissor linkage

The geometric details of angled-plane scissor linkage was described in figures (4.2) and (4.8). In Chapter 4, the parallel-plane scissor linkage was treated as an angled-plane scissor linkage when the angle between planes become zero, as illustrated in figure (4.3). However, in this chapter, the parallel-plane scissor linkage would have additional connectors. The details of both parallel-plane scissor linkage and triangular-prism-shaped scissor linkage are described next.

5.2 Description of scissor linkages

5.2.1 Parallel-plane scissor linkage

The parallel-plane scissor linkage used in this chapter is slightly different from the parallel-plane scissor linkage used in Chapter 4. Figure (4.8) with ϕ taken as zero shows the repeating unit of parallel-plane scissor linkage used in Chapter 4 whereas the repeating unit of parallel-plane scissor linkage that is used in this chapter is shown in figure (5.1). Figure (5.1) differs from figure (4.8) by the existence of two extra links which are labelled as $(6, i)$ and $(7, i)$ as shown in figure (5.1). These links $(6, i)$ and $(7, i)$ connect to the scissor linkage with revolute joints.

5.2.1.1 Boundary conditions

The links $(1, i-1)$, $(2, i-1)$, $(3, i-1)$ and $(4, i-1)$ support the links $(2, i)$, $(1, i)$, $(4, i)$ and $(3, i)$ through revolute joints which make $O_{(1,i-1)}$ coincident with $A_{(2,i)}$, $O_{(2,i-1)}$ coincident with $A_{(1,i)}$, $O_{(3,i-1)}$ coincident with $A_{(4,i)}$, and $O_{(4,i-1)}$ coincident with $A_{(3,i)}$. Further, for the first unit, at $A_{(1,1)}$, $A_{(2,1)}$, $A_{(3,1)}$ and $A_{(4,1)}$, links $(1, 1)$,$(2, 1)$,$(3, 1)$ and $(4, 1)$ respectively connect to the ground through revolute joints. At the other extreme, if N represents last unit number, then at points $O_{(1,N)}$, $O_{(2,N)}$, $O_{(3,N)}$ and $O_{(4,N)}$ of links $(1, N)$,$(2, N)$,$(3, N)$ and $(4, N)$ there are connections to a platform where loads can be placed. These conditions are exactly the same as in the case of parallel-plane scissor linkage of Chapter 4. Hence, the parallel-plane scissor linkage of this chapter is the over-constrained parallel-plane scissor linkage of the previous chapter. Hence, if the misalignment limit is the same in both cases, the lateral sway for parallel-plane scissor linkage of this chapter cannot exceed the lateral sway of parallel-plane scissor linkage of the previous chapter.

5.2.2 Triangular-prism-shaped scissor linkage

The repeating unit of triangular-prism-shaped scissor linkage is shown in figure (5.2). It is worth comparing this repeating unit with the repeating unit of angled-plane scissor linkage shown in figure (4.8). The difference is in the presence of additional links which are labelled as $(5, i)$, $(6, i)$, $(8, i)$ and $(9, i)$ in figure (5.2). The associated

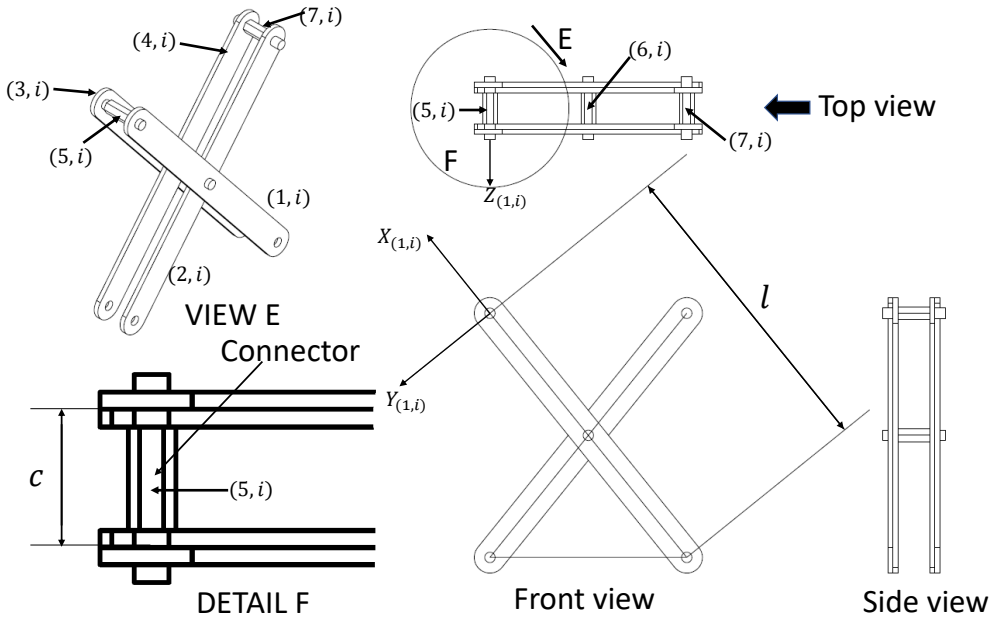

Figure 5.1: Multiple view of single unit of parallel-plane scissor linkage.

additional revolute joints are between bodies $(2,i)-(8,i)$, $(6,i)-(8,i)$, $(5,i)-(6,i)$, $(9,i)-(4,i)$ and $(9,i)-(5,i)$.

Further, boundary conditions are also the same. In the first unit links $(1,1)$, $(2,1)$, $(3,1)$ and $(4,1)$ connect through revolute joints at $A_{(1,1)}$, $A_{(2,1)}$, $A_{(3,1)}$ and $A_{(4,1)}$ respectively. Note that links $(5,1)$ and $(6,1)$ do not connected to the ground at $A_{(5,1)}$ and $A_{(6,1)}$. At the other extreme also, if N represents number of last unit, loading platform connects with revolute joint only at $O_{(1,N)}$, $O_{(2,N)}$, $O_{(3,N)}$ and $O_{(4,N)}$. There is no connection of links $(5,N)$ and $(6,N)$ with loading platform. Hence the triangular-prism-shaped scissor linkage may be treated as an over-constrained angled-plane scissor linkage. If misalignment limits are the same, the maximum displacement from the ideal conditions of the points that are connecting to the loading platform cannot exceed that of angled-plane scissor linkage.

5.3 Validation by numerical simulation

The constraint equations (4.7)-(4.23) were linearized in equations (4.27)-(4.29) to facilitate analytical study. However, if we perform a numerical study, we can di-

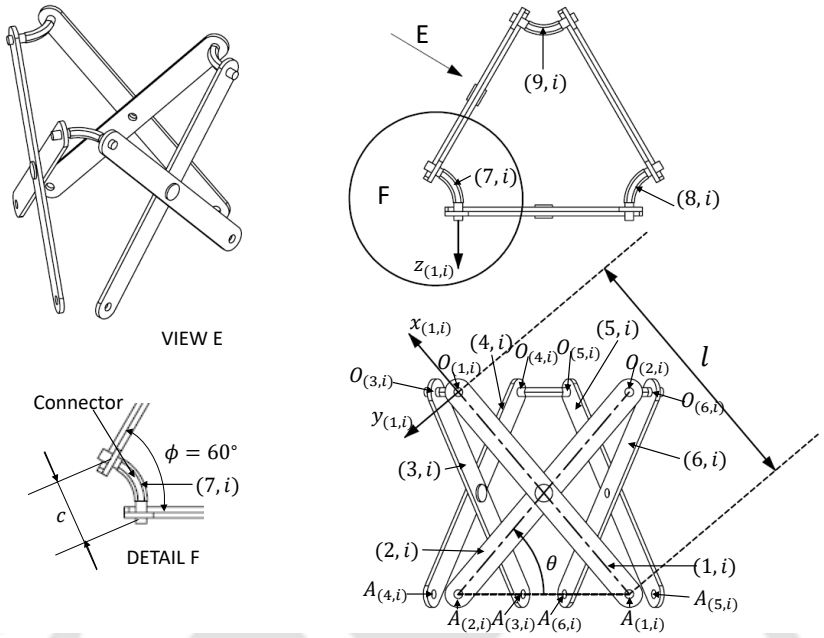

Figure 5.2: Notations used to describe a single unit of triangular-prism-shaped scissor linkage.

rectly deal with the non-linear equations (4.7)-(4.23). Furthermore, when a nonlinear rigid-body analysis is carried out, orientation is typically represented by Euler parameters [81]. The reason to use the Euler parameters over the Euler angles is presented in Appendix E. Hence, we carried out a numerical analysis whose variables, constraints and the objective function are listed below.

1. The variables of the analysis are:
   (a) $\boldsymbol{r}_i$, $i = 1, \cdots, N$,
   (b) $\boldsymbol{q}_i$, $i = 1, \cdots, N$, $\boldsymbol{q}_i$ is the column matrix of Euler parameters representing $\boldsymbol{R}_i^0$,
   (c) $s_{(1,i)}$, $i = 1, \cdots, N$, and
   (d) $s_{(2,i)}$, $i = 1, \cdots, N$.
2. The equality constraints in the analysis are:
   (a) constraints of revolute joint (4.7)-(4.23) for every revolute joint where rotation matrices are expressed in terms of Euler parameters,

(b) the constraint that the sum of squares of Euler parameters associated with each body is 1.

3.

4. Inequality constraints are upper and lower bounds on the slack variables,

5. The objective function is the measure of lateral sway of the top most points of the linkage as it is detailed in Subsection 5.3.1.

5.3.1 Objective function

All the scissor linkage that we have considered in the numerical study are essentially the one shown in figure (4.8) but with some additional links and joints. Hence some of the properties of scissor linkage of figure (4.8) that was deduced in Chapter 4 is applicable to all the types of scissor linkages considered in this chapter. In particular, it was deduced in equation (4.61)-(4.64) that for points $O_{(1,i)}$, $O_{(2,i)}$, $O_{(3,i)}$ and $O_{(4,i)}$, which are also origin of coordinate frames $(1,i)$, $(2,i)$, $(3,i)$, and $(4,i)$, the small displacement from the ideal conditions, represented by $\delta\mathbf{r}_{(\mathbf{1,i})}$, $\delta\mathbf{r}_{(\mathbf{2,i})}$, $\delta\mathbf{r}_{(\mathbf{3,i})}$ and $\delta\mathbf{r}_{(\mathbf{4,i})}$, are in direction of $[0,0,-1]^T$, $[0,0,-1]^T$, $[-\cos(\phi),0,-\sin(\phi)]^T$ and $[-\cos(\phi),0,-\sin(\phi)]^T$ respectively.

Just as a measure of lateral sway in equation (4.65), here too we define a measure lateral sway $\mathcal{C}_i$ as

$$\begin{aligned}\mathcal{C}_i = \begin{bmatrix}0 & 0 & -1\end{bmatrix}^T \left(\boldsymbol{r}_{(1,i)} - \bar{\boldsymbol{r}}_{(1,i)}\right) + \\ \begin{bmatrix}0 & 0 & -1\end{bmatrix}^T \left(\boldsymbol{r}_{(2,i)} - \bar{\boldsymbol{r}}_{(2,i)}\right) + \\ \begin{bmatrix}-\sin\phi & 0 & -\cos\phi\end{bmatrix}^T \left(\boldsymbol{r}_{(3,i)} - \bar{\boldsymbol{r}}_{(3,i)}\right) + \\ \begin{bmatrix}-\sin\phi & 0 & -\cos\phi\end{bmatrix}^T \left(\boldsymbol{r}_{(4,i)} - \bar{\boldsymbol{r}}_{(4,i)}\right) \quad (5.1)\end{aligned}$$

where similar to Chapter 4, $(\boldsymbol{r}_{(j,i)})$, $j = 1,2,3,4$ represent the position vector of the origin of the coordinate frames (j,i), $j = 1,2,3,4$. We have also labelled these origins as $(O_{(j,i)})$, $j = 1,2,3,4$. Further $(\bar{\boldsymbol{r}}_{(j,i)})$, $j = 1,2,3,4$ represents the position vector of these origins in the ideal condition where there is no misalignment and hence no lateral sway.

The objective function that we are taking in the optimization problem of this chapter is $\mathcal{C}_N$ where N represents the last unit of the scissor linkage away from the

ground. Given that loading platform is supported on scissor linkage through revolute joints at $O_{(1,N)}$, $O_{(2,N)}$, $O_{(3,N)}$ and $O_{(4,N)}$, we can describe the objective function as the sum of displacement of the points along their direction of displacements.

5.3.2 Numerical results for the optimization problem

We have to determine the variables such that the objective function is maximized while satisfying both equality and inequality constraints. Thus the mathematical problem we are addressing is a non-linear constrained optimization problem. We solve the same numerically using 'fmincon' solver of MATLAB software.

The optimization problem is solved for different values of parameters to constitute two parametric studies. The common parameter used for both the studies are $l = 0.3\,m$, $\epsilon = 0.1$, $\theta = \pi/3$, $\phi = \pi/3$. The results from the parametric analysis are depicted in plots that contain the following labelled graphs:

- **upper-limit, parallel-plane scissor:** It represents the upper bound of the deflection in the parallel-plane scissor linkage as given in equation (4.69).
- **lower-limit, parallel-plane scissor:** It represents the lower bound of the deflection in the parallel-plane scissor linkage as given in equation (4.74).
- **lateral sway, parallel-plane scissor:** It represents the maximized measure of lateral sway, which is also the objective function, that is obtained by numerically solving the non-linear constrained optimization problem for the parallel-plane scissor linkage.
- **upper-bound, angled-plane scissor:** It represents the upper bound on the lateral sway of the angled-plane scissor linkage as given in equation (4.68).
- **lateral-sway, angled-plane scissor:** It represents the maximized measure of lateral sway that is obtained by numerically solving the non-linear optimization problem for the angled-plane scissor linkage.
- **lateral-sway, triangular-prism-shaped scissor:** It represents the maximized measure of lateral sway that is obtained by numerically solving the non-linear optimization problem for the triangular-prism-shaped scissor linkage.

The two parametric studies we conducted are:

- **Varying connector length:** In this study, the number of units was kept constant at five, and the connector length is varied. The results of the study are depicted in figure (5.3).

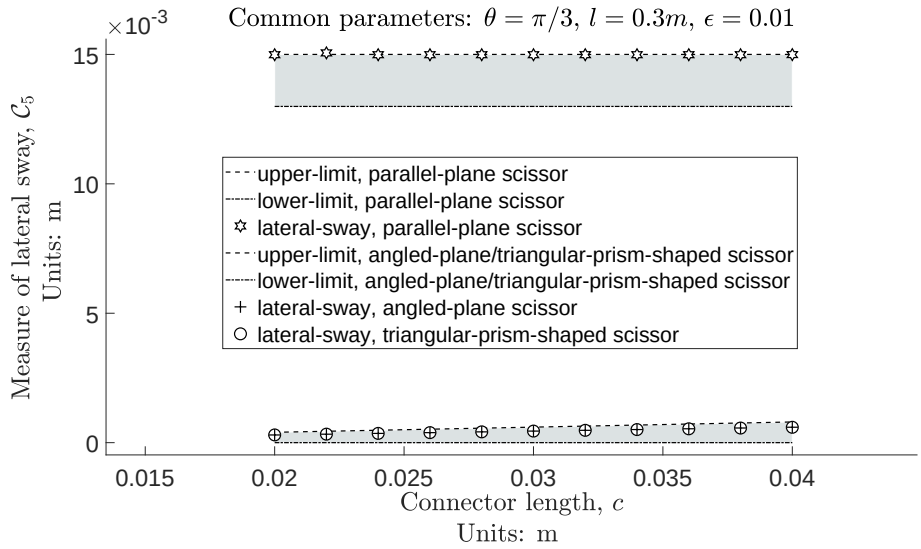

Figure 5.3: Parametric study where connector length is varied.

- **Varying number of units:** In this study, the connector length was kept constant at $0.0302\,m$ and the number of units is varied. The results of the study are depicted in figure (5.4).

5.3.3 Validating observations

The following observations validate the results of the linearized analytical study presented in Section 4.5.

1. In figure (5.3) and (5.4), we see that the results from numerical optimization are almost on the upper bounds derived in equations (4.68) and (4.69) through the linearized analytical study. Any minor violation of the upper bound could be attributed to linearization error.

2. In figure (5.3), the graph corresponding to the numerical solution of the parallel-plane scissor linkage is almost a horizontal line. In contrast, the graph

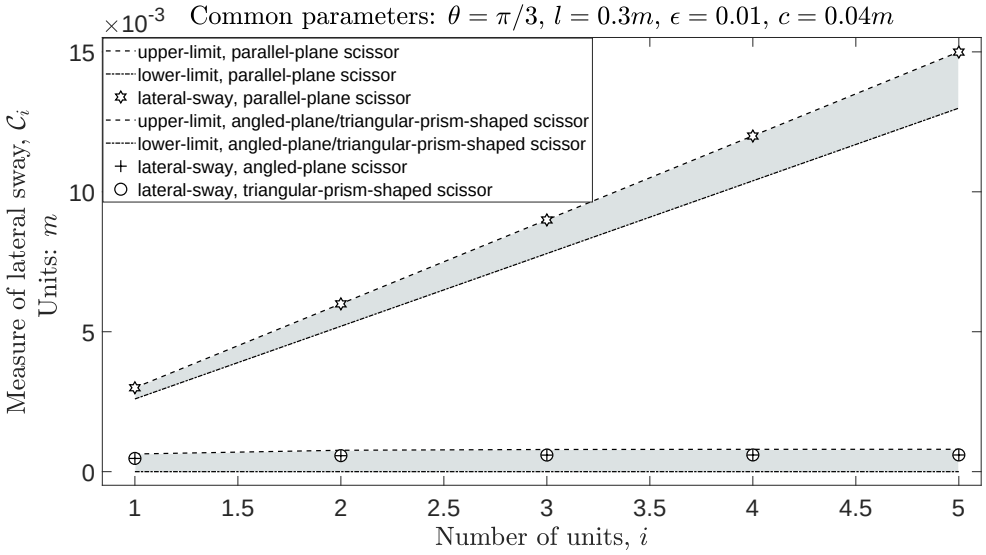

Figure 5.4: Parametric study where the number of units is varied.

corresponding to the numerical solution of the angled-plane scissor linkage and the triangular-prism-shaped scissor linkage has a non-zero slope. This validates the claim made in Section 4.5.1.

3. In figure (5.4), the graph corresponding to the numerical solution of the parallel-plane scissor linkage is increasing in almost a linear manner, which indicates that it does not converge to a finite value. In contrast, the graph corresponding to the numerical solution of the angled-plane scissor linkage is bounded to be less than a finite value irrespective of the number of units. It validates the claim made in Section 4.5.2.

4. The lateral sway of the triangular-prism-shaped scissor linkage is the same or slightly less than that of angled-plane scissor linkage. This validates the claim made in Section 4.1 that

   (a) triangular-prism-shaped scissor linkage can be considered as an additionally constrained angled-plane scissor linkage, and

   (b) the relative resistance against lateral sway of triangular-prism-shaped scissor linkage is arising due to the angled-plane scissor linkage that is embedded in it.

5.4 Conclusion

The major conclusion of this chapter is that for both triangular-prism-shaped scissor linkage and angled-plane scissor linkage, connector length influences the lateral deflection kinematics. Thus, in these scissor linkages, a designer can tune the connector length based on an acceptable lateral sway. The chapter further validated the results from the linearized analytical study of Chapter 4.

Chapter 6

Static balancing of scissor linkage

6.1 Introduction

In Chapter 1, we had stated that we intend to not only fabricate a vertical lift mechanism but also statically balance it. Static balancing of a loaded linkage is the addition of extra potential energy elements like springs or weights so that the net potential energy of the linkage is a constant, i.e., zero gradient potential energy or nearly zero gradient. In the absence of friction, such an addition of elements would eliminate or significantly reduce the actuator force or torque to actuate the linkage. If the actuation effort becomes zero, then the static balancing is called perfect balancing. If the actuation effort is significantly reduced, it is called a partial static balance. Thus, static balancing would let one to use a small capacity motor or actuator for actuation.

Most of the perfect static balancing methods against gravity require a special type of linear spring called as zero-free-length spring [8]. Zero-free-length springs are usually cumbersome to realize. With an intent to keep the fabrication straightforward, we would want to use normally available non-zero-free-length springs and get the best possible partial static-balance against gravity load in scissor linkages. In this chapter, to achieve this, we present a way that is a combination of mathematics

as well as a visual judgment from an interactive graph. When the solution from the interactive graph was implemented on an actual scissor linkage, we realized that friction plays a huge role in determining the actuation effort. We felt that if friction were also to be assessed in the interactive graph, we could have obtained a better static balancing solution. The later part of the chapter is dedicated to assessing the frictional effort on scissor linkage.

Finding dry frictional effort is a little non-trivial. Its direction depends on the direction of impending motion in joints. The concept of friction circle has been proposed long back, and it was popularly used in graphical static analysis [84]. In this chapter, we adopt the same concept into a computer program and use it to assess frictional effort numerically. The programmatic adaption and its usage to assess frictional effort are the contributions of the chapter. While incorporating the numerical solution for frictional effort into the interactive graph remains the scope for future work, we have illustrated the numerical procedure through a few examples.

6.2 Approximate Static balancing of scissor linkage with normal springs

In the scissor linkage shown in figure (3.12b), when a load is applied on the top platform, the linkage comes down to assume minimum potential energy configuration. For spring-based static balancing of this linkage, we have to add extra springs so that the potential energy lost by the load while coming down is transferred to the potential energy of the spring. Similarly, while going up, springs will give back the potential energy to the load. For this transfer of energy to happen, the potential energy of the spring should complement the potential energy of the load so that the sum of the two potential energy functions is constant.

In theory, it is possible to complement the potential energy of the springs with the potential energy of gravity loads when all the springs have zero free-lengths. However, when springs have finite free-lengths, it is possible only approximately to complement the gravity load potential energy function. In this chapter, we decided to use finite free length springs along the horizontal and vertical lines formed by

the revolute joints as shown in figures (6.1) and (6.2). Figure (6.1) shows one face of a unit of the triangular-prism-shaped scissor linkage having the arrangement of horizontal and vertical springs.

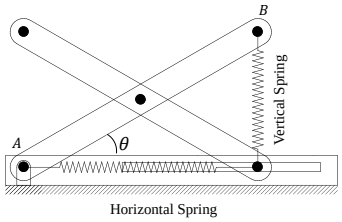

Figure 6.1: Face of the triangular-prism-shaped scissor mechanism with the attached horizontal and vertical springs.

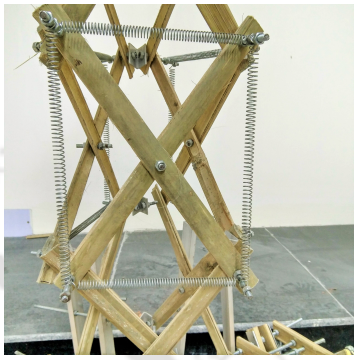

Figure 6.2: Balancing springs added on triangular-prism-shaped scissor linkage in horizontal and vertical lines joining the revolute joints.

The springs that are accessible to us was in the form of the long coil, as shown in figure (6.3). The required springs had to be cut from this long coil. Thus, the property of these springs gets decided by the length of the spring that is cut from the coil. In particular, the spring constant of the spring is inversely proportional to the length of the spring that is cut. Furthermore, since the spring coil does not have pretension, the length of the spring is also the free-length of the spring. Thus, for a spring that is cut,

$$k = \frac{\alpha_p}{f} \tag{6.1}$$

where k is the spring constant of cut spring, and f is the free length of the cut spring. The proportionality constant α_p depends only on the spring coil. Since we had only one kind of coil accessible to us, f parametrizes both free-length and spring constant. In our experimental setup, the value of α_p was found to be 14.9 N.

We have the freedom to chose a multiple numbers of horizontal springs represented by N_h and a multiple numbers of vertical springs represented by N_v. For simplicity, all the horizontal and vertical springs are chosen to have the same free length represented by f.

From figure (6.1) horizontal force F_H and vertical force F_V exerted by the spring

Figure 6.3: Availability of spring in the form of long coil.

are,

$$F_H = \frac{\alpha_p}{f}(l\cos\theta - f) \quad \text{and,} \quad F_V = \frac{\alpha_p}{f}(l\sin\theta - f) \tag{6.2}$$

Where θ is the angle subtended by the link from the ground and l is the length of the links of the scissor linkage, which is equal to length AB as shown in figure (6.1).

Hence, the total horizontal spring force F_h and vertical spring force F_v are

$$F_h = \frac{\alpha_p}{f}(l\cos\theta - f)N_h \quad \text{and,} \quad F_v = \frac{\alpha_p}{f}(l\sin\theta - f)N_v \tag{6.3}$$

So, total spring torque and gravity torque is given as

$$\tau_{spring} = \frac{N_h}{f}\alpha_p l\sin\theta(l\cos\theta - f) + \frac{N_v}{f}\alpha_p l\cos\theta(f - l\sin\theta) \tag{6.4}$$

$$\tau_{gravity} = Wl\cos\theta \tag{6.5}$$

Figure (6.4) shows the plot of gravity torque denoted by $\tau_{gravity}$, spring torque denoted by τ_{spring} and total torque which is $\tau_{gravity} + \tau_{spring}$. For illustration, we take $l = 0.3\ m$, and $W = 10\ Kg$. With this, we have the task of finding acceptable values of N_h, N_v, and f. The problem we are solving is an optimization problem which is summarized in table (6.1). To find the acceptable values, we created an applet in SAGE mathematical software. The applet has the facility to vary N_h, N_v, and f in the form of sliders. By manually varying the parameters N_h, N_v, and f, we obtained the acceptable values as $N_h = 10$, $N_v = 6$, and $f = 0.078\ m$. The plot corresponding to these values is shown in figure (6.4). In the plot, the actuation torque before static balancing got reduced by 90%. We also solved this optimization problem algorithmically using Matlab optimization toolbox, and we got the optimal values as $N_h = 7$, $N_v = 4$, and $f = 0.0632\ m$. The plot corresponding to these optimal values is shown in figure (6.5). Plot (6.5) shows the actuation effort has been reduced by 90% approximately.

Table 6.1: Summary of the optimization problem being solved.

Objective function	$\int_{\theta_1}^{\theta_2} \left(\frac{N_h}{f} \alpha_p l \sin\theta (l\cos\theta - 1) + \frac{N_v}{f} \alpha_p l \cos\theta (1 - l\sin\theta) \right)^2 d\theta + \int_{\theta_1}^{\theta_2} (Wl\cos\theta)^2 \, d\theta$
Constants	$l = 0.3\ m$, $m = 10\ Kg$, $g = 9.81\ m/s^2$, $\alpha_p = 14.9$, $\theta_1 = 10 \times \frac{\pi}{180}$, and $\theta_2 = \frac{\pi}{3}$ (Assumed)
Optimization Variables	N_h, N_v, and f
Optimization constraints	$N_h > 0$, $N_v > 0$, and $f \geq 0$

6.2.1 Practical test of static balancing

To practically test the performance of the acceptable solution, we added springs and weights on the prototype as per the acceptable solution. We then measured the force required in two cases: (1) to lift the mechanism from its bottom position to its top position and (2) to bring down the mechanism from its top position to bottom position. Both sets of forces are plotted in figure (6.6). We see that for the same height of the scissor linkage, multiple forces are possible because of friction in joints. From the graph, it is clear that to handle 10 Kg of load, and we need to apply at most 4 Kg-wt. Thus, by partial static balance, we have reduced the torque or force required from the actuator by about 60%.

In the interactive plot of figure (6.4), the torque shown is the one when no friction is present. Further, we based the selection of parameters of the balancing springs on the same plot. Had we incorporated frictional effort in the same interactive plot, we could have made a better visual judgment in the selection of springs. Equations involving friction force, Coulomb friction force, in particular, are non-linear with discontinuities in higher derivatives. We next discuss a way of obtaining the frictional effort when Coulomb friction is present in revolute joints. The method is based on the concept of a friction circle that is popularly used in graphical static analysis.

6.3 Statics of scissor linkage with friction in revolute joints.

Consider the scissor linkage shown in figure (6.7). It has dry friction in the bearings of the revolute joints. The same figure also shows the free-body diagram of the link and a typical three-force member problem in the presence of revolute-joint friction. Such a problem of the three-force member is generalized in figure (6.8).

In the generalized problem of figure (6.8), a known force $\boldsymbol{f}_P$ acts along a known line of action, which passes through a point P. Further, this force is resisted by revolute joint reaction forces. The center of the revolute joint exists at points Q and R. Since the bearings of these revolute joints have dry friction, the associated friction circles are also shown in the figure, and they have friction circle radii of

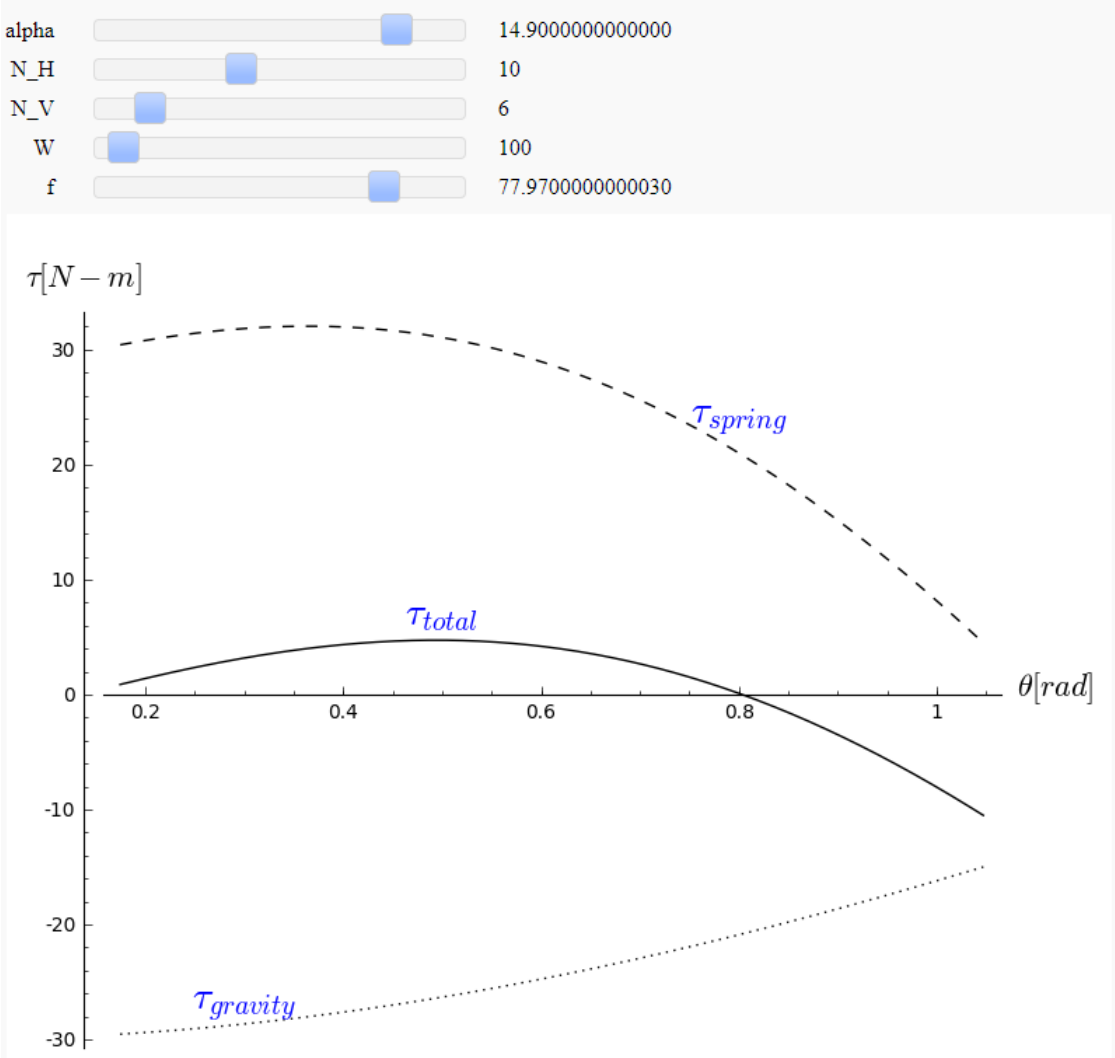

Figure 6.4: Plot between τ_{spring}, $\tau_{gravity}$ and τ_{total} verses θ when $N_h = 10$, $N_v = 6$, and $f = 0.078\ m$.

c_Q and c_R, respectively. Based on the friction circle concept and assuming that there is impending motion, the reaction forces $\boldsymbol{f}_Q$ and $\boldsymbol{f}_R$ have to be tangent to the respective friction circle.

In a typical three-force member problem, one force is known completely in magnitude and line of action; one more force is known only in terms of its line of action; the last force is known only in terms of its point of action. The intersection of lines of action of the first two forces gives the point of concurrency. A line joining point of action of the last force and the point of concurrency gives the line of action of

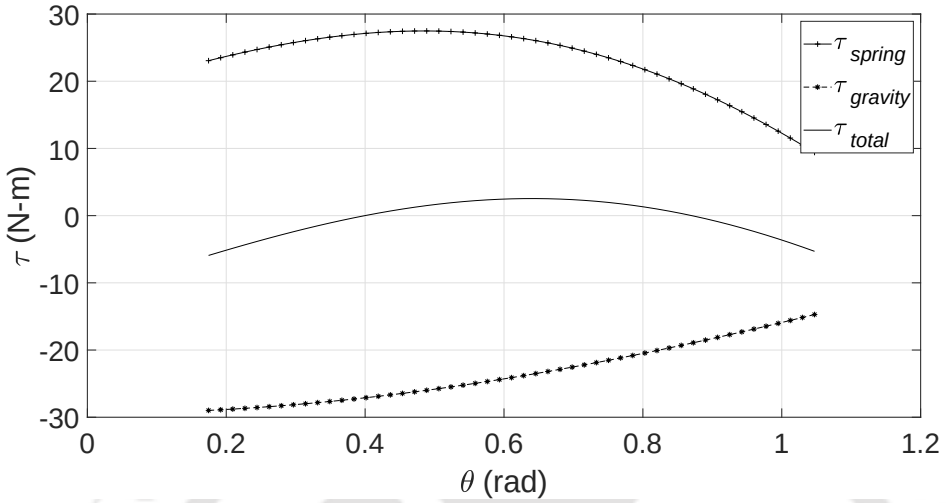

Figure 6.5: Plot between τ_{spring}, $\tau_{gravity}$ and τ_{total} verses θ when $N_h = 7$, $N_v = 4$, and $f = 0.0632\ m$.

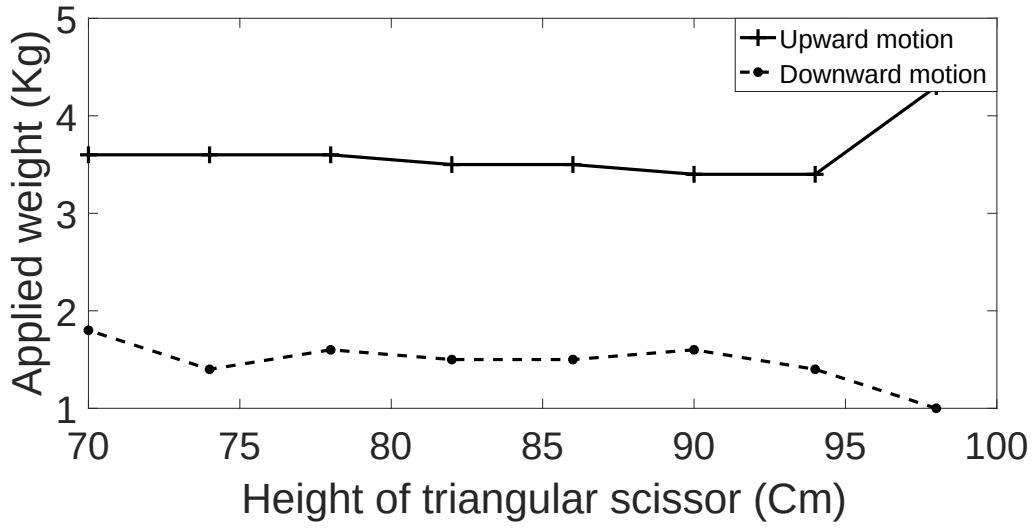

Figure 6.6: Experimental net-torque required for actuation under the load as a function of θ.

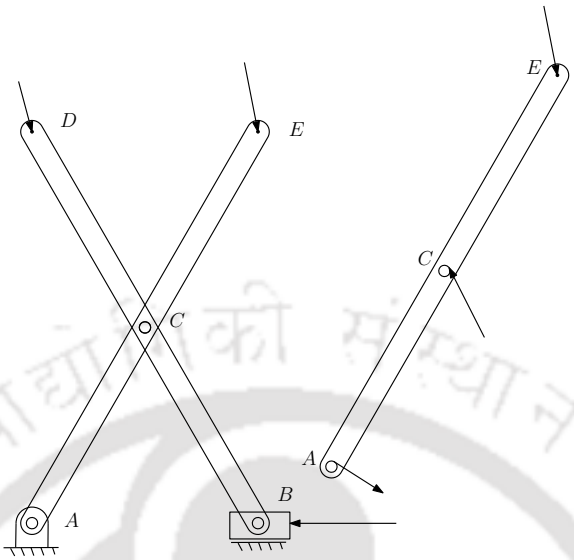

Figure 6.7: A scissor linkage with friction in revolute joints.

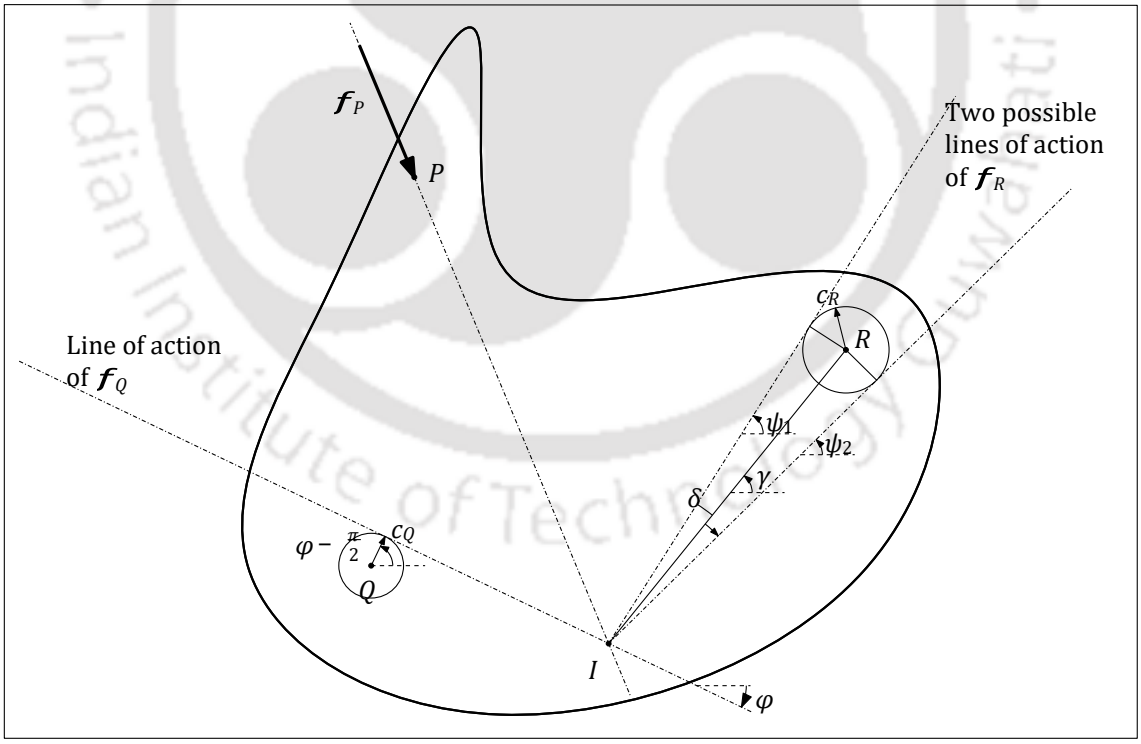

Figure 6.8: A generalized three-force member problem in the presence of dry friction reaction in two revolute joints.

the last force. With this, we have the classic three force triangle problem where the direction of all the forces is known but the magnitude is known only for one force (the first force in this case). However, in the problem of figure (6.8), while we have one force known both in magnitude and line of action, the other two forces are known only in terms of the circle of tangency for the lines of action. Even if the circles are assumed to be of zero radii, we cannot get a unique or finite number of solutions. To address this, we assume the direction of force $\boldsymbol{f}_Q$ to be at an angle of ϕ and tangential to the circle at the radius, which makes an angle of $\phi - \frac{\pi}{2}$. This is depicted in figure (6.8). Thus whatever further quantities we find, they are all functions of ϕ.

6.3.1 Finding point of concurrency

The position vector $\boldsymbol{r}_I$ of point of concurrency I can be written as

$$\boldsymbol{r}_P + \alpha \left[\boldsymbol{f}_P\right] = \boldsymbol{r}_Q + c_Q \begin{bmatrix} \cos\left(\phi - \frac{\pi}{2}\right) \\ \sin\left(\phi - \frac{\pi}{2}\right) \end{bmatrix} + \beta \begin{bmatrix} \cos\phi \\ \sin\phi \end{bmatrix} \tag{6.6}$$

Equation (6.6) can be solved for α and β. Differentiating the equation with respect to ϕ, one can also solve for $\dfrac{d\alpha}{d\phi}$. With this, we obtain

$$\boldsymbol{r}_I = \boldsymbol{r}_P + \alpha \left[\boldsymbol{f}_P\right] \tag{6.7}$$

$$\frac{d\boldsymbol{r}_I}{d\phi} = \frac{d\alpha}{d\phi} \left[\boldsymbol{f}_P\right] \tag{6.8}$$

6.3.2 Finding line of action of $\boldsymbol{f}_R$

The line of action is a tangent from point I in figure (6.8) to the friction circle centered at point R. In general, two tangents are feasible. Both the tangents pass through the point I. Thus, if we find the angles of the two tangents with x-axis, then we would have determined the two possible lines of action. The two angle are represented as $\psi_1 = \gamma + \delta$ and $\psi_2 = \gamma - \delta$, as shown in figure (6.8). Angle γ is made by vector $\boldsymbol{r}_R - \boldsymbol{r}_I$ with x-axis and δ is the half apex angle at I between the two

tangents. They are given by

$$\gamma = \text{atan2}((\boldsymbol{r}_R - \boldsymbol{r}_I)_y, (\boldsymbol{r}_R - \boldsymbol{r}_I)_x)$$

$$\frac{d\gamma}{d\phi} = \frac{\left(-\frac{d\boldsymbol{r}_I}{d\phi}\right)^T \left(\boldsymbol{R}_{\frac{\pi}{2}} (\boldsymbol{r}_R - \boldsymbol{r}_I)\right)}{(\boldsymbol{r}_R - \boldsymbol{r}_I)^T (\boldsymbol{r}_R - \boldsymbol{r}_I)} \tag{6.9}$$

$$\delta = \text{asin}\left(\frac{C_R}{\sqrt{(\boldsymbol{r}_R - \boldsymbol{r}_I)^T (\boldsymbol{r}_R - \boldsymbol{r}_I)}}\right) \tag{6.10}$$

$$\frac{d\delta}{d\phi} = \frac{\left(-\frac{d\boldsymbol{r}_I}{d\phi}\right)^T ((\boldsymbol{r}_R - \boldsymbol{r}_I))}{(\boldsymbol{r}_R - \boldsymbol{r}_I)^T (\boldsymbol{r}_R - \boldsymbol{r}_I)} \tan(\delta) \tag{6.11}$$

$$\frac{d\psi_1}{d\phi} = \frac{d\gamma}{d\phi} + \frac{d\delta}{d\phi} \quad \text{and} \quad \frac{d\psi_2}{d\phi} = \frac{d\gamma}{d\phi} - \frac{d\delta}{d\phi} \tag{6.12}$$

6.3.3 Solving for $\boldsymbol{f}_Q$ and $\boldsymbol{f}_R$

The force summation equation can be written as

$$\boldsymbol{f}_P + \boldsymbol{f}_Q + \boldsymbol{f}_R = \boldsymbol{0} \tag{6.13}$$

$$\text{or} \quad \boldsymbol{f}_P + \begin{bmatrix} \cos\phi & \cos\psi \\ \sin\phi & \sin\psi \end{bmatrix} \begin{bmatrix} a \\ b \end{bmatrix} = \boldsymbol{0} \tag{6.14}$$

By solving equation (6.14), one could obtain a, b and consequently $\boldsymbol{f}_Q$ and $\boldsymbol{f}_R$. Further, by differentiating the same equation, one can obtain $\frac{da}{d\phi}$, $\frac{db}{d\phi}$ and consequently $\frac{d\boldsymbol{f}_Q}{d\phi}$ and $\frac{d\boldsymbol{f}_R}{d\phi}$.

Thus, in the generalized three-force member indicated in figure (6.8), we have expressions to solve all the reaction forces, and they can be programmed as a function ϕ. In the next section, we examine how this can be applied to find reaction forces in a scissor linkage and eventually the effort required at the slider under various conditions of impending motion.

6.4 Evaluation of actuation effort in scissor linkage

Figure (6.9) shows the free-body diagram of each of the links in the scissor linkage, excluding the ground. For each of the links, the methodology described in Section 6.3 can be applied to find $\boldsymbol{f}_{2,1}(\phi)$, and $\boldsymbol{f}_{2,2}(\phi)$. However, we still need to find ϕ. To find ϕ we make use of Newton's third law which require

$$\boldsymbol{f}_{2,1}(\phi) + \boldsymbol{f}_{2,2}(\phi) = \mathbf{0} \tag{6.15}$$

Since same ϕ is used for both force components, the forces would automatically be in the same direction. Thus, we have to focus only on the discrepancy in the magnitude which could be done as follows:

$$\begin{bmatrix} \cos\phi \\ \sin\phi \end{bmatrix}^T \left(\boldsymbol{f}_{2,1}(\phi) + \boldsymbol{f}_{2,2}(\phi)\right) = 0 \tag{6.16}$$

If we write the left hand side of equation (6.16) as $\mathcal{F}(\phi)$, then we have to solve for ϕ in

$$\mathcal{F}(\phi) = 0 \tag{6.17}$$

Based on sensitivity analysis of Section 6.3 and equation (6.16), we can get the derivative $\dfrac{d\mathcal{F}(\phi)}{d\phi}$. Thus, we can use popular equation solving gradient-based numerical algorithms to find the solution. Further, when the method of Section 6.3 was used to find $\boldsymbol{f}_{2,1}(\phi)$, we got two options. Similarly, the there are two options for $\boldsymbol{f}_{2,2}(\phi)$. In total, there are $2 \times 2 = 4$ options. These options have to be resolved by checking whether the frictional moments in the joints at A, B and C are in the appropriate direction. When the impending motion is such that point B is moving to the left, the frictional moment at joint A and C on link 1 should be clockwise and that at point B on link 2 should be anti-clockwise. The frictional moment direction gets reversed when the direction of impending motion changes.

Among gradient-based algorithms to solve $\boldsymbol{f}_{2,1}(\phi) = 0$, one could use Newton-Raphson's method. It may also be recognized that the square of the function, $\left(\boldsymbol{f}_{2,1}(\phi)\right)^2$, has a zero-valued minima at the solutions to $\boldsymbol{f}_{2,1}(\phi) = 0$. In view of this, the equation solving algorithm used in MATLAB's 'fsolve' function finds the minima of the square of the function using gradient-based optimization algorithm.

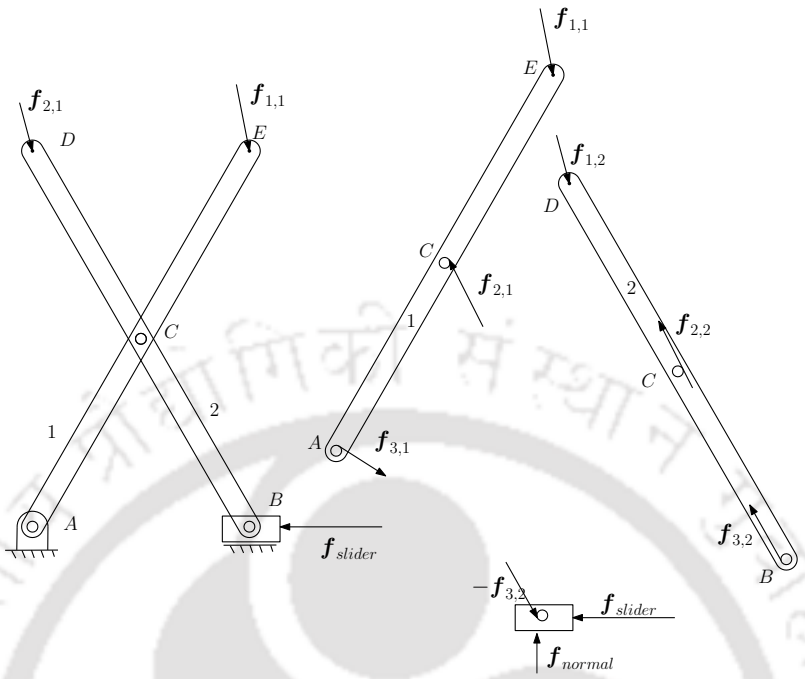

Figure 6.9: Free-body diagram of scissor linkage.

If the minima happen to be zero, then a solution has been found. Otherwise, the algorithm reports failure to find solutions. No matter which algorithm is used, it is not hard to recognize that when the starting guess for the algorithm is in a certain range, the gradient-based algorithm would not be able to converge to a solution. For example, in figure (6.10) that shows a typical profile of $\mathcal{F}(\phi)$, if the starting guess falls between 0.5 and 2.5, the gradient-based algorithm cannot converge to a solution. To circumvent this problem, we apply an equation solving algorithm to multiple starting guesses that are spread over the entire span of ϕ.

We had also received suggestion on using bisection method which does not require computation of gradients. In Appendix D, we compare the gradient-based equation solving method used in this chapter with the bisection method. Also we present a discussion on why we prefer to use the gradient-based method over bisection method.

6.5 Results and discussion

In this chapter, we obtained the approximate balancing solution on scissor linkage using normal springs instead of zero-free-length springs. The balancing solution was

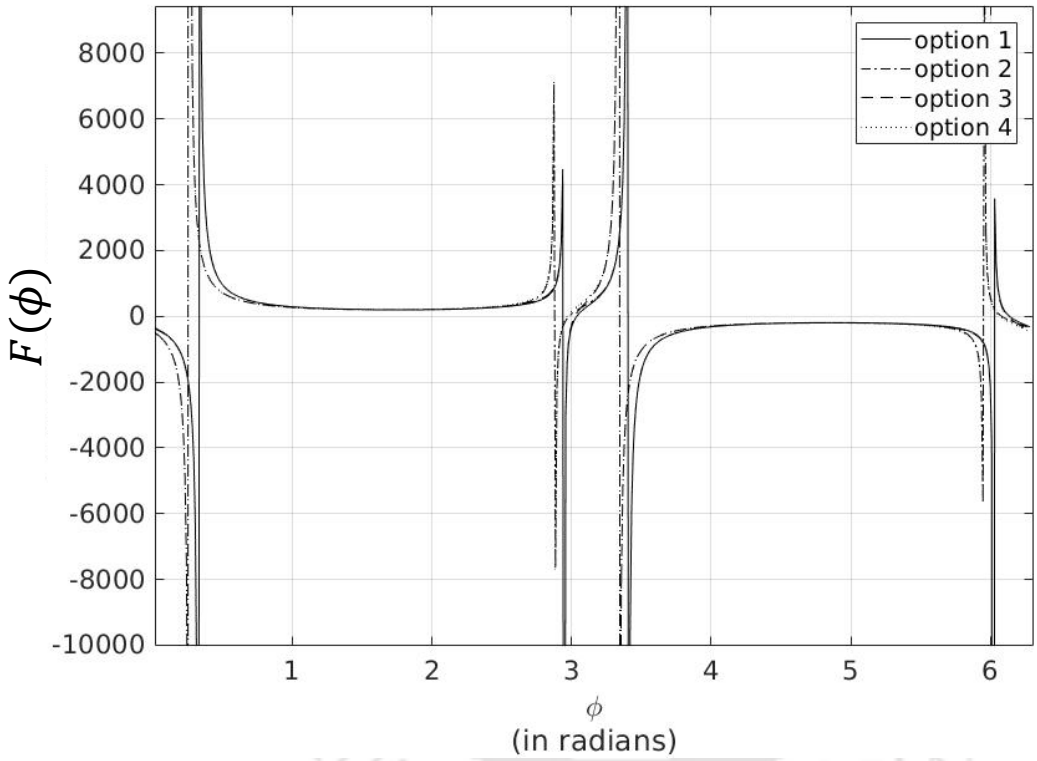

Figure 6.10: Typical profile of $\mathcal{F}(\phi)$.

obtained by varying the free length of the springs that are cut from a long coil. An applet was created in SAGE software to facilitate manual variation of free lengths and the number of springs to arrive at optimal spring parameters where the net torque due to both gravity and springs is minimized through visual judgment. A 90% reduction in torque was accomplished through the minimization. In practice, the reduction was only about 60% due to frictional effects.

These frictional effects can be seen at revolute-joint in the form of dry-frictions. To check the effects of dry friction, we applied the algorithm to find the actuating slider force in a scissor linkage to three different cases. In the first case, the scissor linkage is loaded by gravity at its tips. In later two cases, additional springs are added to balance it statically. We assessed the quality of two static balancing solutions based on frictional force characteristics.

6.5.1 Statically unbalanced scissor linkage

The algorithm was applied on a scissor linkage shown in figure (6.11). The length of each of the links was taken as $0.3\,m$. The point C is the mid-point for both the links. The revolute joints at point A, B and C are considered to have dry friction with a friction circle radius of $5 \times 10^{-3}\,m$. For simplicity, the friction at the slider is neglected. A plot of $\boldsymbol{f}_{slider}$ as function θ when impending motion is 'up' and 'down' are shown in figure (6.12). Here 'up' motion means the tip of the scissor linkage moves in the positive direction of y-axis and 'down' means the tip moves in the negative direction of y-axis. The same figure also shows the plot when the friction circle radius at revolute joints becomes zero. As expected, the plots for friction-less case coincide for both impending-up and impending-down motion.

6.5.2 Statically balanced scissor linkage: case 1

This case is the same as the previous case except that one horizontal spring and one vertical spring is added, as shown in figure (6.13). Both the springs have a spring constant of $1000\,N/m$. The horizontal spring is of zero-free-length whereas the vertical spring has a free length of $0.1\,m$. The plot for this case is shown in figure (6.14).

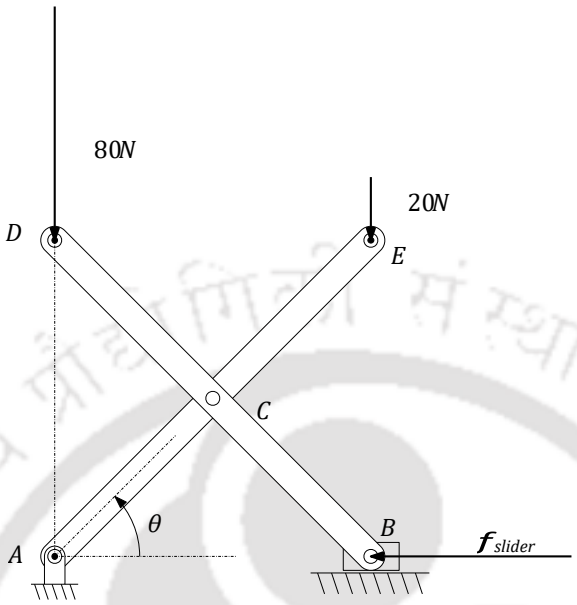

Figure 6.11: A scissor linkage under two vertical loads.

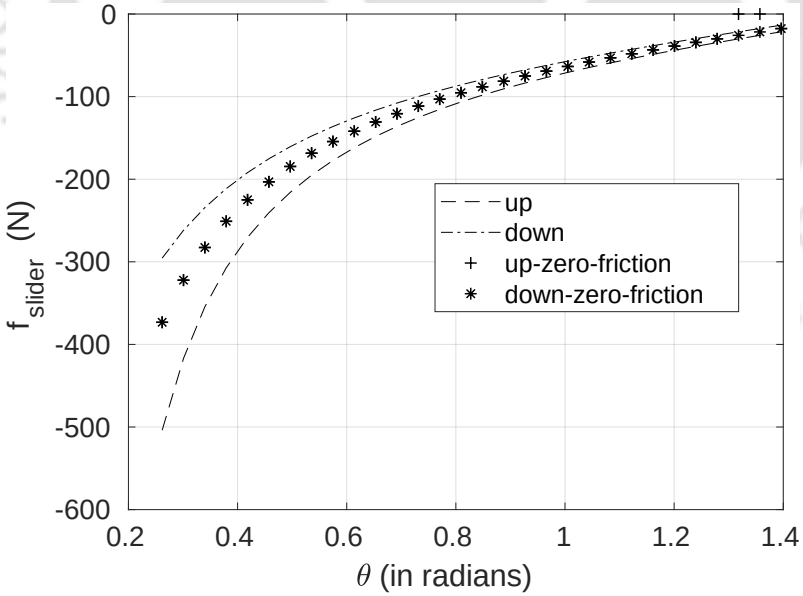

Figure 6.12: The actuation force $\boldsymbol{f}_{slider}$ as function θ for the case shown in figure (6.11).

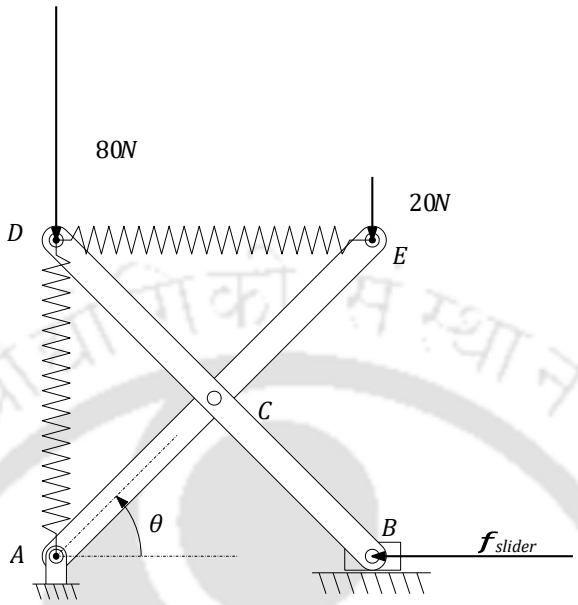

Figure 6.13: A scissor linkage under two vertical loads with balancing springs.

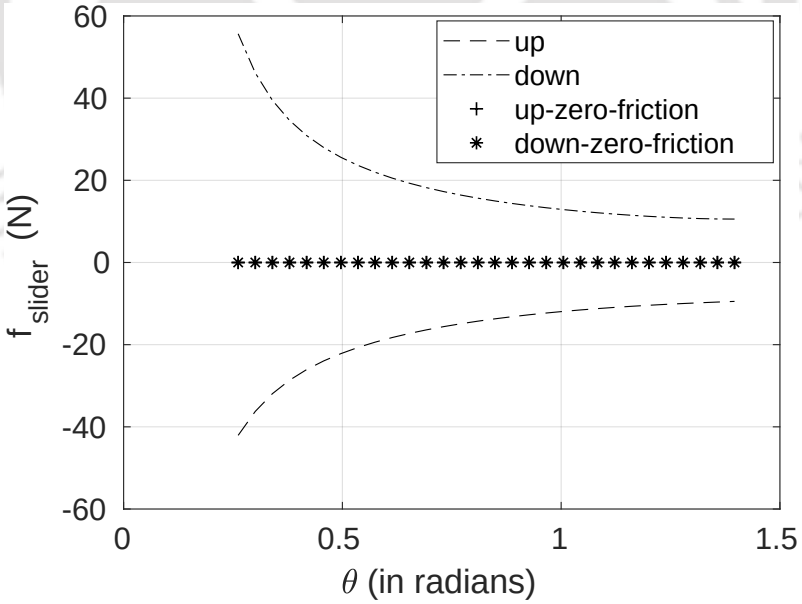

Figure 6.14: The actuation force $\boldsymbol{f}_{slider}$ as function θ for the case shown in figure (6.13).

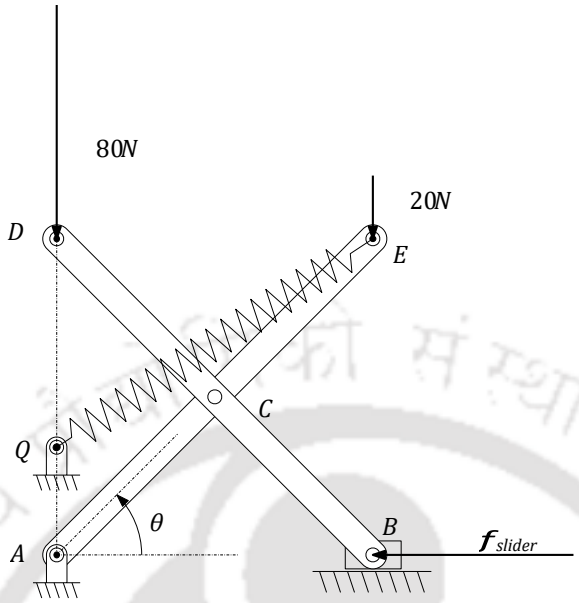

Figure 6.15: A scissor linkage under two vertical loads with a balancing spring.

6.5.3 Statically balanced scissor linkage: case 2

This case is the same as the previous case except that only one spring is used, as shown in figure (6.15). The spring again has a spring constant of $1000\,N/m$. The anchor point of the spring on the ground at point Q is such that it is vertically on the top of point A at a distance of $0.1\,m$. The plot for this case is shown in figure (6.16).

6.5.4 Comparison and future work

While comparing the plot of unbalanced scissor linkage in figure (6.12) with the plots of balanced scissor linkage in figures (6.14) and (6.16), a drastic reduction in the magnitude of the force is quite evident. Nevertheless, there is no drastic difference between the plots in later two statically balanced cases of figure (6.14) and (6.16). Still, some differences, such as the following, can be observed.

1. At 15° of θ, which is also the left extreme of the plot, upward impending motion requires actuation effort in negative y direction that is close to $40\,N$ in case 2 and close to $50\,N$ in case 3.

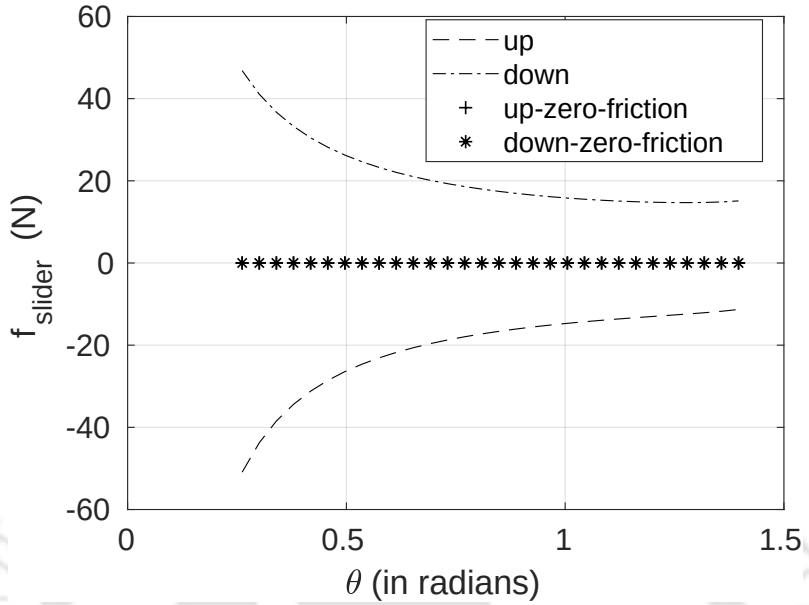

Figure 6.16: The actuation force $\boldsymbol{f}_{slider}$ as function θ for the case shown in figure (6.15).

2. When the angle is closer to 80°, which is also the right extreme of the plot, the magnitude of actuating force under friction is more in case 3 compared to case 2.

Just based on the above two points, it is difficult to say which case can be considered to have less frictional effort. However, this is a universal problem when comparing two functions. Usually, in mathematics, a norm could be calculated to signify the magnitude of the function. However, in this chapter, we leave it to the visual judgment. With similar subjective visual judgment and also based on two points stated above, we marginally say that the static balancing solution in case 3 is better than that of case 2. Nevertheless, more compelling examples need to be investigated to see if the actuation forces due to friction can form a good differentiator of different static balancing solutions for the same mechanism under the same load.

6.6 Closure

In this chapter, we showed how we could optimally choose normal spring with finite free-length to obtain optimal partial static balance through an interactive plot. To incorporate effects of friction in the interactive plot, we described a method to find the frictional force. The method is a programmatic adaptation of the concept of friction circle that is used popularly in graphical statics. The method was illustrated in three cases. Incorporation of the method in the interactive plot remains the scope for future work.

Chapter 7

SUMMARY

7.1 Summary

We abstracted two theoretical problems from a prototyping exercise:

1. For an ideal scissor linkage having one degree of freedom, incorporation of which non-ideality would enable us to demonstrate through equations of mechanics the significantly different lateral sway characteristics between parallel-plane scissor linkage and angled-plane scissor linkage?

2. When there are two competing static balancing methods, could we rank them based on the frictional effort?

The biggest, the most important and the major contribution of the thesis is in solving the first problem stated above through linearized analytical study and numerical study. It is for the first time in the literature that through the equations of mechanics, significantly contrasting lateral sway characteristics between angled-plane and parallel-plane scissor linkage has been demonstrated. The derived analytical expression would also enable a designer to assess the influence of various geometric parameters such as the connector length on lateral sway. Ranking static balancing methods based on frictional effort is a new line of thinking in literature. However,

the results are preliminary, and the contribution is relatively minor. The other minor contribution is from the perspective of bamboo crafts, where we have shown how bamboos, which are famous for making structures, could be used for making mechanisms and thus increasing versatility in bamboo crafts.

In our prototyping exercise, we had the intent of making a height-adjustable device that can move a loaded platform vertically up and down, preferably with as less actuation effort as possible. Towards this intent, we chose to use scissor linkage for vertical lift and also statically balance the same to eliminate or reduce the actuation effort. With an intent to increase the versatility of bamboo crafts, we resolved to fabricate the linkage using bamboo strips with a few additional easily and locally available accessories such as tie rods, nuts and bolts.

When the bamboo-based linkage was fabricated on the lines of an industrial scissor lift, we noted large lateral sway. Furthermore, through a series of trial and error attempts, we found that triangular-prism-shaped scissor linkage has significantly limited lateral sway. We also noted that angled-plane scissor linkage also has a significantly small lateral sway similar to triangular-prism scissor linkage. In fact, we realized that triangular-prism-shaped scissor linkage could be considered as an over-constrained angled-plane scissor linkage. Thus angled-plane scissor linkage is more fundamental, and focusing our investigation on it is appropriate. Given the difficulty of realizing slider joints with bamboo strips, we further demonstrated through fabrication, how straight line generating mechanisms could be used between the scissor linkage and upper as well as lower platforms instead of typical slider joints.

Once we found success in limiting lateral sway through fabrication, we focused on understanding different lateral sway characteristics of parallel-plane scissor-linkage and angled-plane scissor linkage through mathematical modelling. In order to facilitate thoughts, the mathematical model was chosen in a way to keep the number of variables as small as possible. Hence, rather than aiming the mathematical model to realistically represent the fabricated prototype, we aimed the model to represent an ideal scissor linkage with just the right kind of non-ideality incorporated. Misalignment as the non-ideality was our intuitive choice and but we have rigorously shown based on equations of mechanics that the misalignment would lead to significantly different lateral say characteristics between angled-plane scissor linkage and parallel-plane scissor linkage. We have also made certain assumptions (pre-stating the limits on misalignment), which has led us to keep the mathematical model entirely in the

realm of kinematics.

The two scissor linkages were modelled as multibody systems with variables representing the motion of each of the bodies and constraints on the variables representing joints between the rigid bodies. The misalignment in revolute joints was modelled by introducing slack variables in revolute-joint constraints and the slack variables were limited between upper and lower bounds. A function representing lateral sway was also introduced. To assess the resistance of the linkages against the lateral sway, we devised an optimization problem to find the maximum possible lateral sway given equality and inequality constraints among variables. We could not solve the optimization problem analytically. Nevertheless, to get analytical insights, we linearized the constraint equations. Through linearized constraint equations, we could deduce analytical bounds on lateral sway. The analytical study was carried on angled-plane scissor linkage since we found that:

1. parallel-plane scissor linkage can be considered as a subset of angled-plane scissor linkage when the angle between the planes become zero,

2. angled-plane scissor linkage is embedded in triangular-prism-shaped scissor linkage and triangular-prism-shaped scissor linkage can be considered as angled-plane scissor linkage with extra constraints,

3. the angled-plane scissor linkage showed the same resistance against lateral sway as that of triangular-prism-shaped scissor linkage indicating that angled-plane scissor linkage embedded in triangular-prism-shaped scissor linkage is the root cause of resistance against lateral sway.

Through the analytical bounds that were derived, widely different lateral-sway characteristics of parallel-plane scissor linkage on the one hand and triangular-prism-shaped scissor linkage and angled-plane scissor linkage on the other hand were established.

To validate the results and also to avoid linearization errors, non-linear-constraint optimization problem was solved using 'fsolve' function of MATLAB software. The results successfully validated the conclusions of the linearized analytical study. Further, one of the conclusions that unlike parallel-plane scissor linkage, lateral sway for angled-plane scissor linkage and triangular-prism-shaped scissor linkage is de-

pendent on the connector length has a practical implication. The designer could use connector length as a tuning parameter to limit lateral sway to acceptable limits.

Complete elimination of actuation effort of the scissor linkage is typically accomplished by using zero-free-length springs when friction is absent. However, zero-free-length springs are cumbersome to realize, and hence we resolved to use normal springs with finite-free lengths to reduce actuation effort. We proposed a way to parametrize the geometric and elastic features of normal springs. In order to find acceptable values for these parameters, a plot of actuation force versus displacement of the top platform of the scissor lift was created. The plot was also made interactive by allowing interactive changes in the parameters. Through visual judgement in the interactive plot, acceptable parameters of normal springs were chosen. From practice, we realized that friction plays a dominant role in determining actuation effort. To find the frictional effort, we demonstrated a numerical method based on the concept of friction-circle used in graphical static analysis.

7.2 Scope for future works

The prospect of the present work is briefly outlined in the following.

- We have not investigated through experimental measurements the match between the practice and the mathematical models and the results. The experimental investigation would involve estimating three-dimensional rotation, and we think that it is important to set up a reliable computer vision system to carry out the estimation. We could not carry out this work within the constraints of thesis work.
- The prospects of the ranking of static balancing methods based on frictional effort have to be investigated further to see if we could get impactful results.

Appendix A

Background

A.1 Single-plane scissor linkage

A single-plane scissor linkage is a planar linkage as shown in figure (A.1). A mid way reference plane may be identified for the linkage as shown in figure (A.1).

A.2 Two-plane scissor linkage

Two-plane scissor linkage is formed by connecting two identical single-plane scissor linkages as shown in figure (A.2). The reference planes of the two identical single-plane scissor linkage would form the two reference planes of the two-plane scissor linkage.

A.3 Angled-plane scissor linkage and Parallel-plane scissor linkage

In a two-plane scissor linkage, if the reference planes are not parallel, as shown in figure (A.2), then it is called as angled-plane scissor linkage. If the reference planes are parallel, then it is called as parallel-plane scissor linkage as shown in figure (A.3).

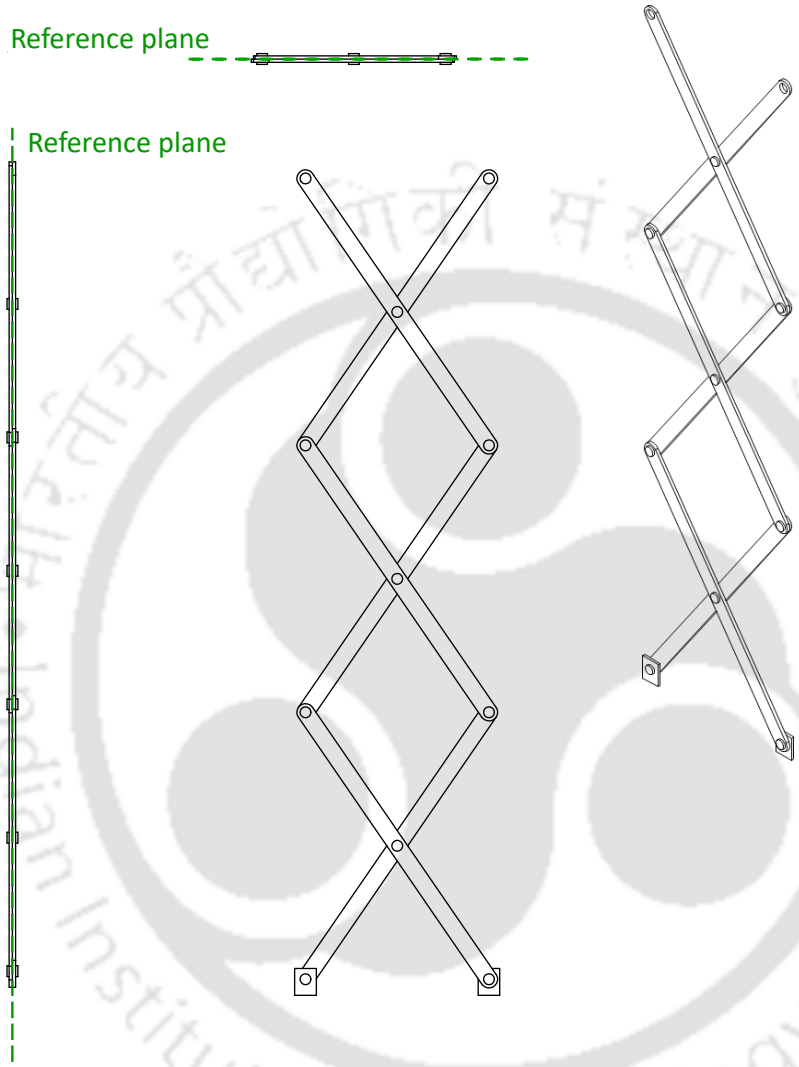

Figure A.1: A single plane scissor linkage and its reference plane.

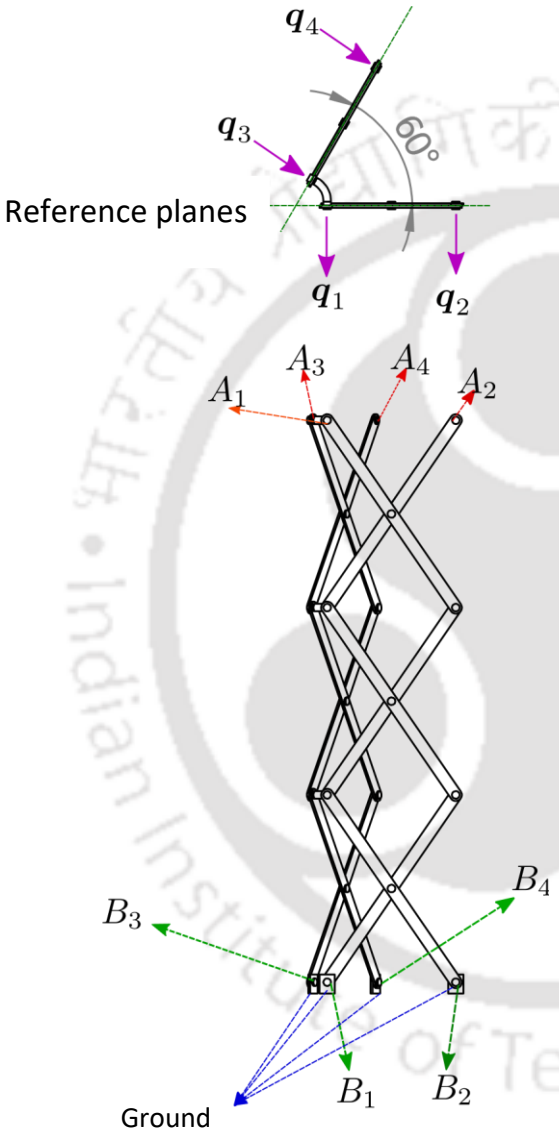

Figure A.2: A two-plane scissor linkage.

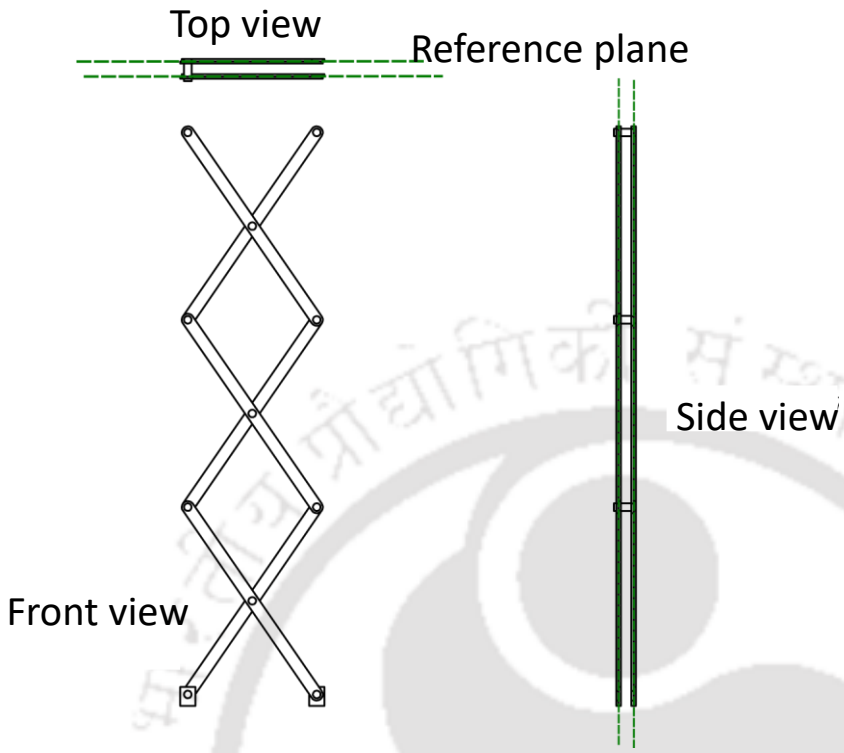

Figure A.3: A parallel-plane scissor linkage.

A.4 Repeating unit of two-plane scissor linkage

The two-plane scissor linkage can be considered as a series of repeating units. A repeating unit of the scissor linkage is shown in figure (A.4).

A.5 Geometry of the linkage

Consider a linkage formed by connecting two identical single-plane scissor linkages into two-plane scissor linkage such as the one shown in figure (A.2). The scissor linkage can be considered as a series of repeating units. The geometry of the linkage is determined by the geometry of the repeating units as shown in figure (A.4). The geometry of the repeating unit is specified by

1. link length l,

2. angle between the reference planes of single-plane scissor linkage ϕ,

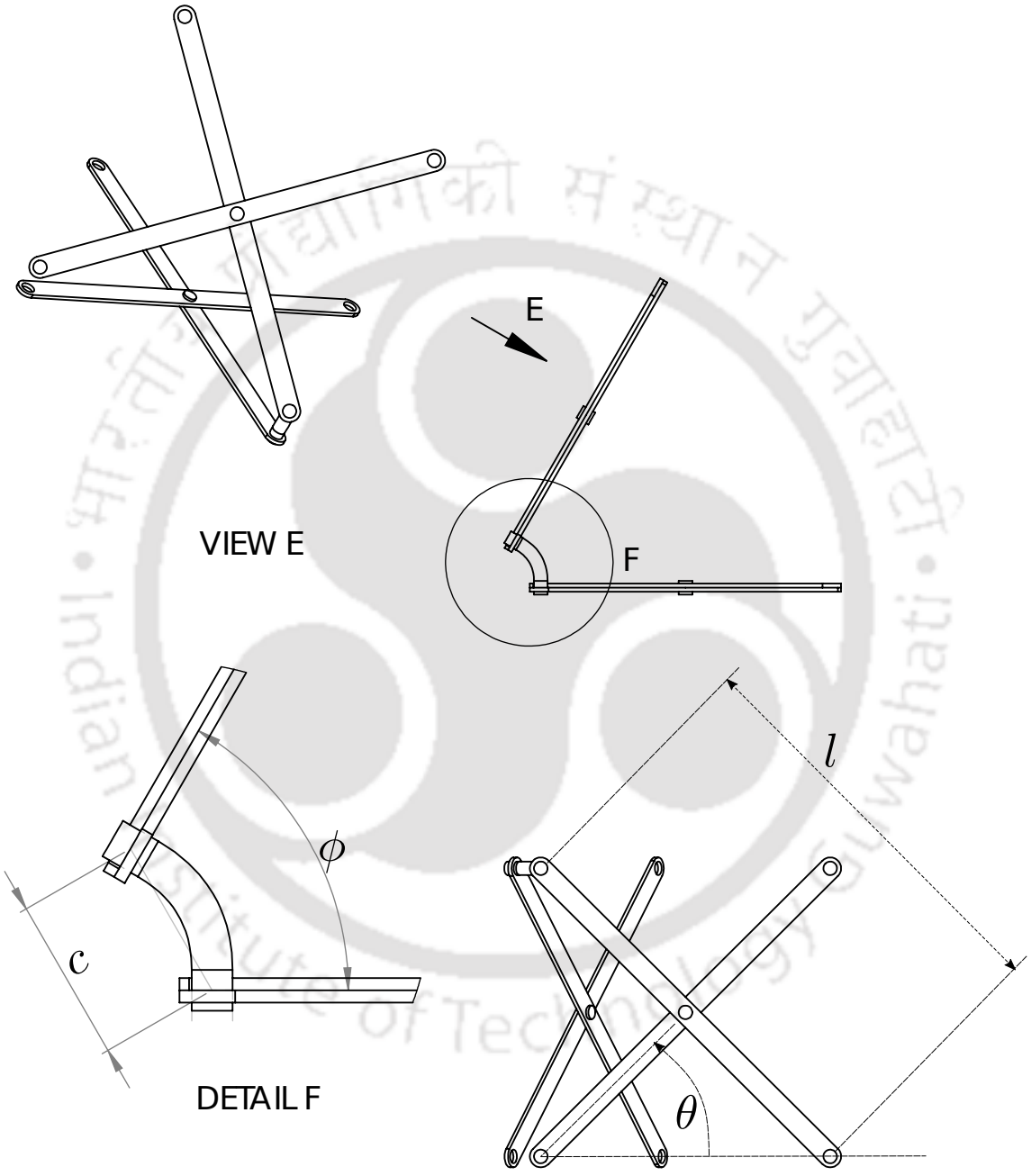

Figure A.4: The repeating unit of two-plane scissor linkage.

3. actuation variable θ,

4. connector length c,

All these variables are depicted in figure (A.4). In addition to these, the number of repeating units i would completely describe the geometry of the two-plane scissor linkage in its ideal condition, i.e., when there is no lateral sway.

A.6 Rigidity of links

All the links in the two-plane scissor linkage are assumed to be rigid. The assumption is intended to reduce the number of variables in the mathematical model.

A.7 Misalignment of revolute joints

In an ideal revolute joint, an axis fixed to one body would be coincident with an axis fixed to the other body. Typically, these axes would be the axis of the hole and the axis of the pin. In misalignment, an angle would be formed between the axes. The point of intersection could be anywhere along the axes. However, to reduce the number of variables in the model to a small number, we assume that the point of intersection does not change its position with respect to either of the links of the revolute joint. We have chosen to make the intersection points lie at the center of the bearing length.

A.8 Limits on misalignment

Typically misalignment in revolute joints is small, and they could arise from 1) clearance in bearing, 2) wear of bearing surface, 3) deformation of bearing surfaces due to load. In this thesis, without getting into the causes of the misalignment, we would merely say that misalignment cannot exceed a pre-specified limit. Then the question is what physical quantity would represent misalignment.

In three-dimensional case, merely stating the angle between lines would not give a full description of the orientation of one line with respect to the other. A complete description can be obtained as:

1. At the point of intersection, draw unit vectors along the intersecting lines.

2. Choosing one of the unit vectors as a reference, consider a plane perpendicular to the unit vector and passing through the intersection point. The projection of the other vector on the plane, which is a two-dimensional quantity, is indicative of the orientation of one line with respect to the other. By choosing a Cartesian coordinate frame on the plane of projection, we can get x, y components of the projection of the unit vector.

The x, y components described above is a two-dimensional quantity describing the relative orientation between lines in 3-dimension. This two-dimensional quantity is also treated as the quantity representing misalignment. If d_x and d_y represent these components, then the limits on misalignment is taken as:

$$|d_x| \leq \epsilon \qquad \text{and} \qquad |d_y| \leq \epsilon \tag{A.1}$$

A.9 Ideal configuration

The configuration of the linkage when the misalignment in all the revolute joints is zero is called an ideal configuration.

A.10 Boundary conditions

In the ideal condition of misalignment being zero, the scissor linkage has one degree of freedom. With the change in actuation variable θ, the scissor linkage would execute its ideal up-and-down motion. However, this ideal motion is not of our focus. Our focus is on the additional motion due to extra degrees of freedom arising out of misalignment. Hence, we would choose such a boundary condition that it

not only supports the scissor linkage but also prevent change in θ. The boundary condition involves revolute joints with the ground at points B_1, B_2, B_3 and B_4 as shown in figure (A.2).

A.11 Measure of lateral sway $\mathcal{C}$

Let us consider the points A_1, A_2, A_3 and A_4 that are located at the other end of the boundary points B_1, B_2, B_3 and B_4 as shown in figure (A.2). It is shown in the thesis, for small displacement, the lateral swaying displacement of points A_1, A_2, A_3 and A_4 from their ideal configuration would be respectively along $\boldsymbol{q}_1$, $\boldsymbol{q}_2$, $\boldsymbol{q}_3$ and $\boldsymbol{q}_4$ as shown in figure (A.2). The vectors $\boldsymbol{q}_1$ and $\boldsymbol{q}_2$ are perpendicular to one reference plane as is evident in figure (A.2). Similarly, $\boldsymbol{q}_3$ and $\boldsymbol{q}_4$ are perpendicular to the other reference plane as shown in figure (A.2). Hence, we take the measure of lateral sway as:

$$\mathcal{C} = \frac{1}{4}\left(\boldsymbol{q}_1 \cdot (\boldsymbol{r}_{A_1} - \bar{\boldsymbol{r}}_{A_1}) + \boldsymbol{q}_2 \cdot (\boldsymbol{r}_{A_2} - \bar{\boldsymbol{r}}_{A_2}) + \boldsymbol{q}_3 \cdot (\boldsymbol{r}_{A_3} - \bar{\boldsymbol{r}}_{A_3}) + \boldsymbol{q}_4 \cdot (\boldsymbol{r}_{A_4} - \bar{\boldsymbol{r}}_{A_4})\right) \tag{A.2}$$

where $\boldsymbol{r}_{A_i}$ represent position vector of point A_i after lateral sway and $\bar{\boldsymbol{r}}_{A_i}$ represents position vector of A_i when there is no lateral sway. Here i varies from 1 to 4.

Appendix B

B.1 Description of misalignment angle in revolute joints

Figure (B.1) shows a pin within the hole. Let hole diameter be D_2 and pin diameter be D_1. Obviously for clearance $D_2 > D_1$. Let the length of pin be 'b'. The length of the hole is greater than or equal to 'b'. Let us assume during misalignment, point 'O' fixed to the pin does not change its location with respect to the hole. Let us further assume that both the pin and the hole are rigid. In these circumstances, from figure (B.1)

$$\theta_1 = \sin^{-1}\left(\frac{D_1}{\sqrt{D_1^2 + b^2}}\right) \tag{B.1}$$

$$\theta_2 = \sin^{-1}\left(\frac{D_2}{\sqrt{D_1^2 + b^2}}\right) \tag{B.2}$$

The maximum possible misalignment is

$$\theta_2 - \theta_1 = \sin^{-1}\left(\frac{D_2}{\sqrt{D_1^2 + b^2}}\right) - \sin^{-1}\left(\frac{D_1}{\sqrt{D_1^2 + b^2}}\right) \tag{B.3}$$

If $D_2 - D_1 = \triangle D$ is small, and $\theta_2 - \theta_1 = \triangle\theta$ is maximum possible misalignment, then from the concept of derivative, we have

$$\triangle\theta = \left[\frac{d}{dD}\left(\sin^{-1}\left(\frac{D}{C}\right)\right)\right]_{D=D_1} \triangle D \tag{B.4}$$

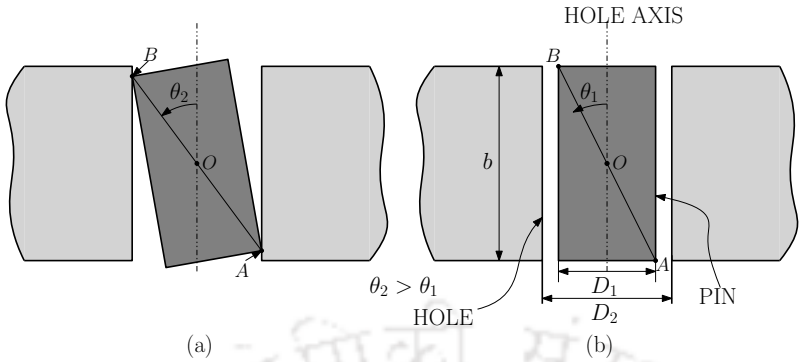

Figure B.1: Misalignment of pin within the hole.

where $C = \sqrt{D_1^2 + b^2}$.

$$\frac{d\theta}{dD} = \frac{d}{dD}\left(\sin^{-1}\left(\frac{D}{C}\right)\right) \tag{B.5}$$

Alternatively,

$$\sin\theta = \frac{D}{C} \tag{B.6}$$

Differentiate the equation (B.6) on both sides with respect to D. We get,

$$\frac{d\theta}{dD} = \frac{1}{\cos(\theta) \times C} \tag{B.7}$$

Further,

$$\begin{aligned}\left.\frac{d\theta}{dD}\right|_{D=D_1} &= \left.\frac{1}{\cos(\theta) \times \sqrt{D_1^2 + b^2}}\right|_{(\theta=\tan^{-1}\frac{b}{\sqrt{D_1^2+b^2}})} \\ &= \frac{1}{\frac{b}{\sqrt{D_1^2+b^2}} \times \sqrt{D_1^2+b^2}}\end{aligned} \tag{B.8}$$

Hence,

$$\left.\frac{d\theta}{dD}\right|_{D=D_1} = \frac{1}{b} \tag{B.9}$$

In other words,

$$\triangle\theta \approx \left(\frac{1}{b}\right)\triangle D \tag{B.10}$$

Thus, misalignment $\triangle\theta$ is approximately inversely proportional to bearing length.

B.2 Understanding the relation between torque on the joint and misalignment through a simple model of deformation

Consider a hole and the pin shown in figure (B.2). We assume that the pin is made of a very rigid material compared to the hole, and it does not undergo deformation. As far as the deformation of the hole is concerned, we take a simple model where deformation is restricted to the enlargement of the diameter of the hole. With this assumption, this case becomes similar to the previous case, and we can write

$$\triangle\theta = \frac{1}{b}\triangle D \tag{B.11}$$

where $\triangle D$ is a change in the diameter of the hole. Our next task is to relate $\triangle D$ to the applied torque. So, let us consider the free-body diagram of the pin and hole. If we presume that the bearing relation forces are focused around the ends of bearing length, then we get a free-body diagram as shown in figure (B.2).

For force balance, we require

$$F \times b = \tau \tag{B.12}$$

Alternatively,

$$F = \frac{\tau}{b} \tag{B.13}$$

If we further presume that the enlargement of the diameter is proportional to force 'F' as

$$\triangle D = (K)F \tag{B.14}$$

where 'K' is the proportional constant. Combining the equation (B.11),(B.13) and (B.14), we have

$$\triangle D = (K) \times \frac{\tau}{b} \tag{B.15}$$

and

$$\triangle\theta = (K) \times \frac{\tau}{b^2} \tag{B.16}$$

Thus, under the simplifying assumption made above, we can say that the misalignment is approximately inversely proportional to the square of the bearing length.

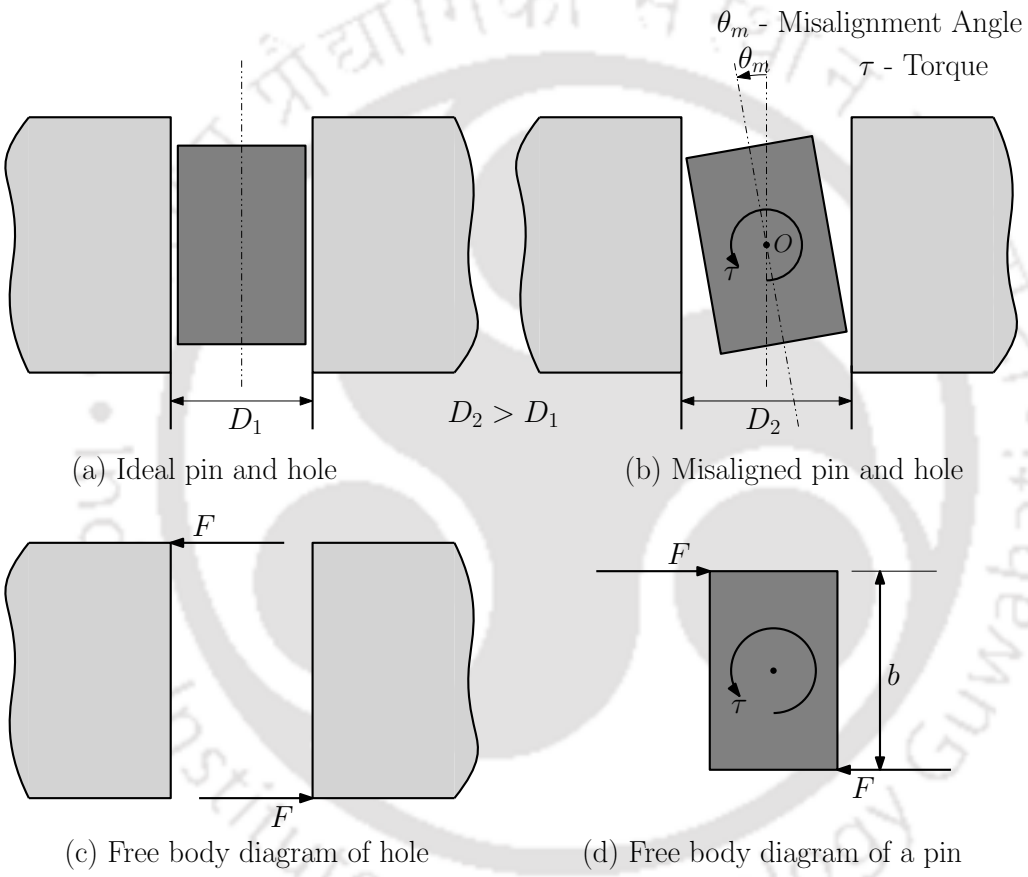

(a) Ideal pin and hole

(b) Misaligned pin and hole

(c) Free body diagram of hole

(d) Free body diagram of a pin

Figure B.2: Misalignment due deformation of hole surface.

Appendix C

C.1 Design process that could involve scissor linkage made of thin strip

If one wants to lift a 100 kg payload from 2 feet above the ground to 4 feet above the ground, the possible design process is as given next.

1. Choose a base mechanism at the base that guides a point on the scissor link in a straight horizontal line. It could be a straight-line generating mechanism as in the case of the prototype made in the thesis or more popularly the slider. Let us say we will use a slider which is more compact.

2. Let us further say that the line of sliding of the slider is half a feet above the ground level.

3. We should have a platform that is to be loaded with a weight of about 100 Kg. We can keep the platform surface flush at 2 feet from the ground. The line of the slider on the loading platform could be at one and a half feet from the ground.

4. See how much longitudinal space is available. Depending on it choose a convenient length of the scissor linkage. (In the thesis, we have labelled it as l.)

5. As far as the angle of the scissor linkage, it would be non-zero to prevent interference between links. The exact angle from the perspective of preventing

interference could be checked in a solid model. The number of stages that can be accommodated within a space of one foot depends upon the width of the links. Make design choices. The choices could be changed later if there is any problem.

6. Add actuator. Ensure that in the range of motion, there is no singularity with respect to the actuator.

7. Perform static analysis.

8. Choose the material of the link and geometry of the link so that the links can sustain compressive or tension forces.

9. Choose manufacturing process.

10. Check the extent of misalignment due to expected tolerance in manufacturing and deformation of bearing surface due to load. A simulation where the bearing surface and the interaction of the pin with the bearing surface is appropriately modelled could be carried out to check the extent of misalignment.

11. One may choose to reinforce joint bearing surface, increase bearing length and incorporate stringent tolerances to decrease misalignment.

12. Alternatively, possibly for saving money, one may change the scissor linkage architecture to angled-plane scissor linkage.

13. Changing the geometry of the linkage to something like C-channel would give a lot of saving in material while increasing rigidity indices such as bending stiffness. However, depending on the thickness of the C-channel, the vulnerability of misalignment may still persist.

14. One could use a simulation that can capture the effects of joint misalignment to estimate the joint misalignment.

15. One could use the expressions for lateral sway derived in the thesis to estimate the lateral sway given the estimate of misalignment in joints. Alternatively, one could directly estimate lateral sway from simulations that can capture the effects of joint misalignment.

16. See if the lateral sway could be tolerated. From the expression in equation (4.51) and equation (4.42), there is also scope for reducing the lateral sway by reducing "c", the connector length. See how much advantage of this could be taken.

17. If the design is not satisfactory, re-iterate the above steps with different design choices. Otherwise, cease the design iterations.

Appendix D

D.1 Comparison between bisection method and the gradient-based equation solving method of Section 6.4

In this appendix, for solving equation (6.17), bisection method is compared with the gradient-based method that was used in Section 6.4. The comparison is made under different issues that are presented next.

D.1.1 Presence of discontinuity

If a function is a discontinuous function within a range of consideration, then both bisection method and the gradient-based method are not guaranteed to converge on a solution even if a solution exists. As seen in figure (6.10), the function $\mathcal{F}(\phi)$ in equation (6.17) is also a discontinuous function and it has a solution.

D.1.2 Stability and boundedness of iterates

Figure (D.1) schematically shows a plus-minus infinity discontinuity in a function to which bisection method is applied. It could be seen that the starting point (A_i) and the ending point (B_i) of the iterates are closing on to the discontinuity. Because of this, the value of the iterates would become unbounded and hence unstable.

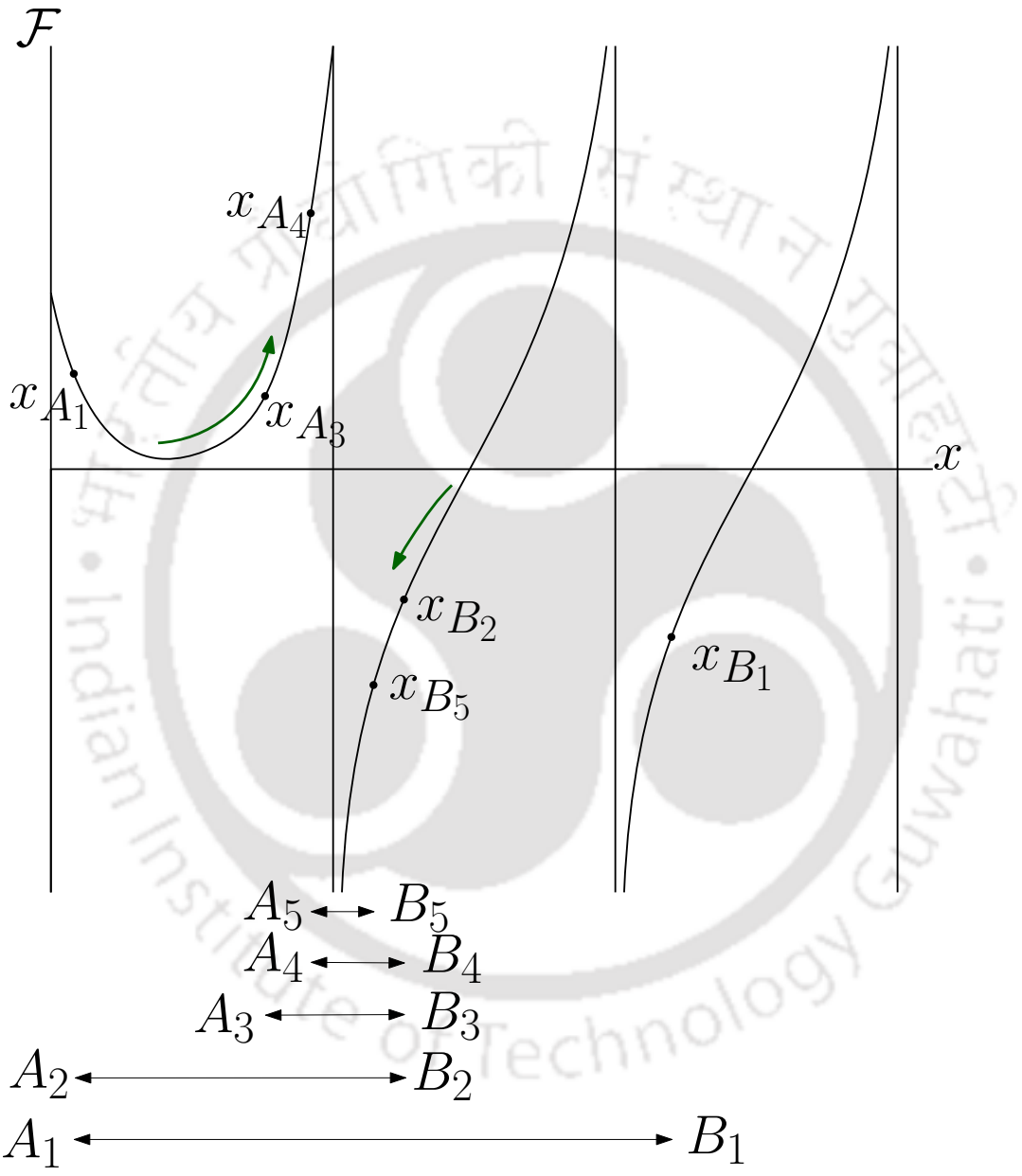

Figure D.1: The progress of iterates in bisection method for finding the solution.

In the gradient-based method that is used in this work, a function to be solved is first squared. In the squared function, minima are found using usual numerical methods for optimization. If one or more minima are zeros, then they are solutions to the function.

Since the gradient-based method is seeking minima of the squared function, the iterates of the method move away from the plus-minus infinity discontinuity as illustrated in figure (D.2). This shields the iterates of the method from becoming unbounded and unstable.

Considering that $\mathcal{F}(\phi)$ also has plus-minus infinity discontinuities as seen in figure (6.10), the gradient-based method adopted in the thesis is more appropriate than bisection method from the perspective of boundedness and stability in the iterates.

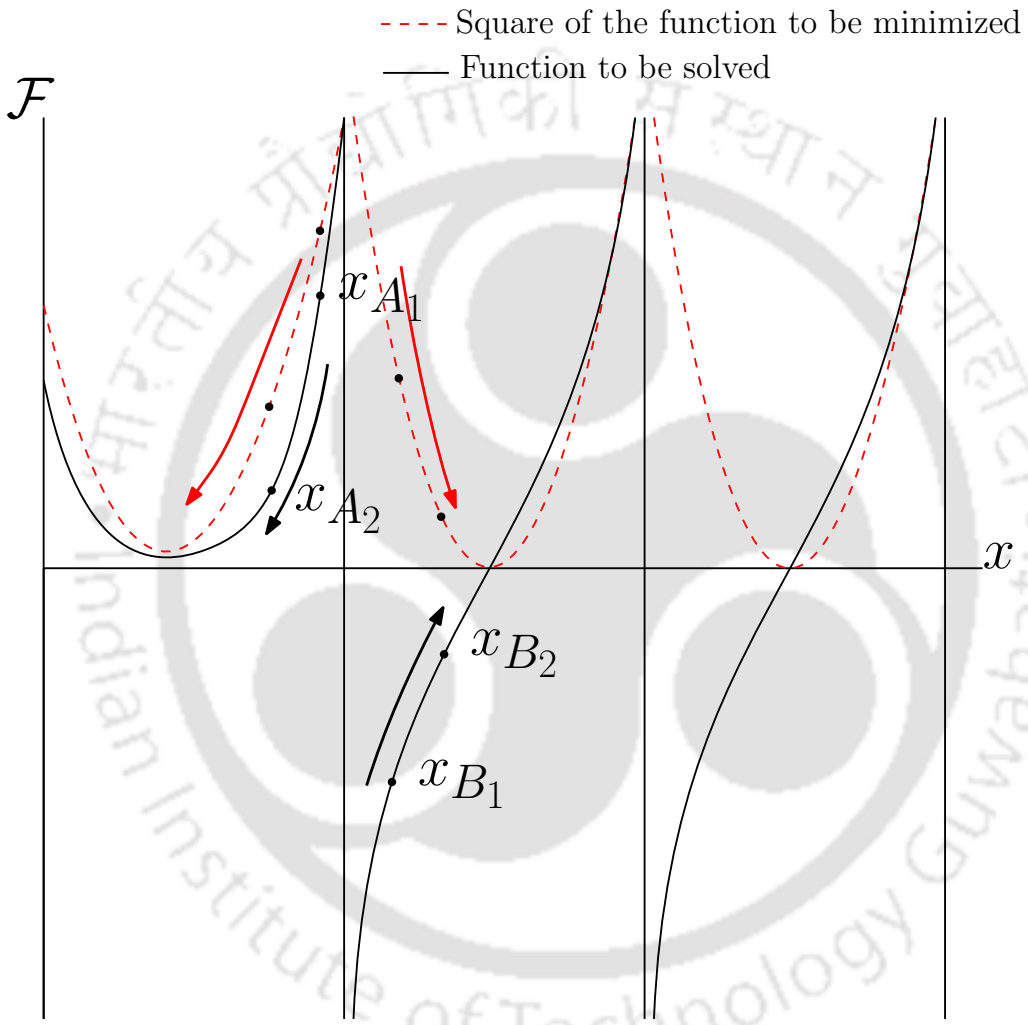

Figure D.2: The progress of iterates in gradient-based method for finding the solution.

Appendix E

In this appendix, we would consider the question of why Euler parameters are used in the thesis instead of Euler angles. Euler angles have three scalar variables. Euler parameters have four scalar variables along with a constraint. At the outset, it appears that we are complicating the situation by using Euler parameters instead of Euler angles. However, there is a theoretical reason why Euler parameters/Euler parameters are used.

Let us consider a map between $\mathbb{C}^3$, which is the set of all possible values of three Euler angles and $SO(3)$, which is the set of all rotation matrices. It is not possible to find a one-to-one, onto homeomorphic map between $\mathbb{C}^3$ and $SO(3)$. Had we gotten such a map, then $SO(3)$ would have been called $\mathbb{C}^3$ itself.

As an illustration, let us consider $z-y-z$ body fixed Euler angles where the first rotation angle is α and the successive rotations are β and γ. The set $\{\alpha, \beta, \gamma\}$ is an element of $\mathbb{C}^3$. From the concept of Euler angles, the following map between $\mathbb{C}^3$, and $SO(3)$ is formed.

$$\begin{bmatrix} \cos\alpha\cos\beta\cos\gamma - \sin\alpha\sin\gamma & -\sin\gamma\cos\alpha\cos\beta - \cos\gamma\sin\alpha & \cos\alpha\sin\beta \\ \sin\alpha\cos\beta\cos\gamma + \sin\gamma\cos\alpha & \cos\alpha\cos\gamma - \sin\alpha\cos\beta\sin\gamma & \sin\alpha\sin\beta \\ -\cos\gamma\sin\beta & \sin\alpha\sin\gamma & \cos\beta \end{bmatrix}$$

Consider a subset in $\mathbb{C}^3$ of the form $\beta = 0$, $\alpha \in \mathbb{C}^1$ and $\gamma \in \mathbb{C}^1$. This subset is clearly two-dimensional. Let us call this subset as set G. Then the set in $SO(3)$ that is mapped by set G is in the following form.

$$\begin{bmatrix} \cos\alpha\cos\gamma - \sin\alpha\sin\gamma & -\sin\gamma\cos\alpha - \cos\gamma\sin\alpha & 0 \\ \sin\gamma\cos\alpha + \cos\gamma\sin\alpha & \cos\alpha\cos\gamma - \sin\alpha\sin\gamma & 0 \\ 0 & 0 & 1 \end{bmatrix} = \begin{bmatrix} \cos(\alpha+\gamma) & -\sin(\alpha+\gamma) & 0 \\ \sin(\alpha+\gamma) & \cos(\alpha+\gamma) & 0 \\ 0 & 0 & 1 \end{bmatrix}$$
$$= \begin{bmatrix} \cos\phi & -\sin\phi & 0 \\ \sin\phi & \cos\phi & 0 \\ 0 & 0 & 1 \end{bmatrix}$$

where $\phi = \alpha + \gamma$.

If we examine the set that G maps to, then it is clearly one-dimensional because it is parametrized by a single parameter ϕ.

Let us take a subset in G by replacing γ with $(-\alpha + \frac{\pi}{3})$. Let the subset be called H. It is a one-dimensional set parametrized by a single parameter α. The set that H maps to is of the form

$$\begin{bmatrix} \cos(\alpha + (-\alpha + \frac{\pi}{3})) & -\sin(\alpha + (-\alpha + \frac{\pi}{3})) & 0 \\ \sin(\alpha + (-\alpha + \frac{\pi}{3})) & \cos(\alpha + (-\alpha + \frac{\pi}{3})) & 0 \\ 0 & 0 & 1 \end{bmatrix} = \begin{bmatrix} \cos\frac{\pi}{3} & -\sin\frac{\pi}{3} & 0 \\ \sin\frac{\pi}{3} & \cos\frac{\pi}{3} & 0 \\ 0 & 0 & 1 \end{bmatrix}$$

We see that the set H map to is a constant. If we take any element in one dimensional H, it maps to a constant element of $SO(3)$ (zero-dimensional). Thus, the map has lost the character of one-one map. The inverse fails to exist for the set that G maps to. When we take derivatives within set G and map to derivative in the set that G maps to, the matrix representing the relation between the derivatives is singular. This would be problematic during simulation. It turns out that no matter what scheme of Euler angle we take, the global map would always be singular at someplace. Hence, Euler angles are avoided in kinematic and dynamic simulation.

In contrast to Euler angles, the map between Euler parameters and $SO(3)$ is one-one, onto and differentiable. So the map is invertible, and the relationship between derivatives in Euler parameters and derivatives in $SO(3)$ is non-singular. Therefore, Euler parameters are widely used in kinematic and dynamic simulations.

Bibliography

[1] https://www.youtube.com/watch?v=hh4r3voHXRg. Accessed December, 2019.

[2] https://www.youtube.com/watch?v=LsRGbfajhjk. Accessed December, 2019.

[3] Jing-Shan Zhao, Fulei Chu, and Zhi-Jing Feng. The mechanism theory and application of deployable structures based on SLE. *Mechanism and Machine Theory*, 44:324–335, 02 2009.

[4] Igor Raskin. *Stiffness and Stability of Deployable Pantographic Columns*. PhD thesis, University of Waterloo, Waterloo, Ontario, Canada, 1998.

[5] Paulo Flores, Ambrósio, Jorge, J.C. Claro, and Hamid Lankarani. *Kinematics and Dynamics of Multibody Systems with Imperfect Joints: Models and Case Studies*, volume 34. 01 2008.

[6] P. Flores. Modeling and simulation of wear in revolute clearance joints in multibody systems. *Mechanism and Machine Theory*, 44(6):1211–1222, 2009.

[7] https://www.youtube.com/watch?v=OrBRpwXt9s8&t=43s. Accessed December, 2019.

[8] J. L. Herder. *Energy-free system. Theory, conception and design of statically balanced spring mechanism.* PhD thesis, Delft University of Technology Delft, The Netherlands, November 2001.

[9] Charles L Larson. Scissor-lift mechanism, 04-19 1966. US Patent US3246876A.

[10] G Coad and J Carter. Scissor lift and drive mechanism therefor, 01-15 1974. US Patent US3785462A.

[11] T King and F Pearne. Platform lift mechanism, 06-28 1974. US Patent US3820631A.

[12] Charles Traficant. High lift mechanism, 06-24 1975. US Patent US3891108A.

[13] Louis L Butler. High lift mechanism, 08-26 1975. US Patent US3901356A.

[14] Duane R. Franklin and Archibald D. Evans. Energy-recycling scissors lift, 17-12 1985. US Patent US4558648A.

[15] Erik Knudsen. Scissor mechanism in particular for lift tables, 08-22 1989. US Patent US4858482A.

[16] Thomas A. Craig. Vehicle scissor lift, 02-13 1990. US Patent US4899987A.

[17] Jr. Angelo Leonaggeo. Hydrotherapy exercising device with scissor lift treadmill, 04-24 1990. US Patent US4918766A.

[18] Ernst Langewellpott. Scissor lift table, 12-09 1997. US Patent US5694864A.

[19] Richard T. Rowan, Leonard G. Sutherland, Gary Cooke, and Paul A. Pedersen. Scissor lift, 03-03 1998. US Patent US5722513A.

[20] Enoch L. Newlin. Work platform lift machine with scissor lift mechanism employing telescopable electro-mechanical based lift actuation arrangement, 04-04 2000. US Patent US6044927A.

[21] George Lawrence Storm. Convertible lift mechanism having a scissor lift linkage, 08-29 2000. US Patent US6109395A.

[22] Donald Watkins. Scissor-lift mechanism, 20-01 2004. US Patent US6679479B1.

[23] Jean-Marie Rennetaud and Tian Zhou. Elevator with a scissor lift mechanism and a spring member serving as virtual counterweight, 03-09 2005. European Patent Office EP1512655A1.

[24] Barry Vaughan and Alvin Vaughan. Portable scissor-lift-assembly, 08-22 2006. US Patent US7093691B1.

[25] Michael Kaufman. Scissor lift mechanism, 05-08 2007. US Patent US7213686B2.

[26] Martin OLESEN. Scissor lift and use of a scissor lift, 11-18 2014. US Patent US8888070B2.

[27] Vincent DeMarco. Tool shelf assembly, 02-26 2019. US Patent US10213915B1.

[28] Todd Humbert and Elizabeth Humbert. Lift and tilt support apparatus, 03-07 2019. US Patent US20190070052A1.

[29] C.J. Gantes. *Deployable structures: analysis and design*. Boston: WIT Press, 2001.

[30] Jing-Shan Zhao, Fulei Chu, and Zhi-Jing Feng. The mechanism theory and application of deployable structures based on sle. *Mechanism and Machine Theory*, 44(2):324–335, 2009.

[31] Tao Liu and Jian Sun. Simulative calculation and optimal design of scissor lifting mechanism. 06 2009.

[32] Yenal Akgün, Charis J. Gantes, Konstantinos E. Kalochairetis, and Gökhan Kiper. A novel concept of convertible roofs with high transformability consisting of planar scissor-hinge structures. *Engineering Structures*, 32(9):2873–2883, 2010.

[33] Yenal Akgün, Charis J. Gantes, Werner Sobek, Koray Korkmaz, and Konstantinos Kalochairetis. A novel adaptive spatial scissor-hinge structural mechanism for convertible roofs. *Engineering Structures*, 33(4):1365–1376, 2011.

[34] Tian Hongyu and Zhang Ziyi. Design and simulation based on pro/e for a hydraulic lift platform in scissors type. *Procedia Engineering*, 16:772–781, 12 2011.

[35] Ren Dong, Christopher S Pan, Jared J Hartsell, Daniel Welcome, Tim Lutz, Anne Brumfield, James R Harris, John Z Wu, Bryan Wimer, Victor Mucino, and Kenneth Means. An investigation on the dynamic stability of scissor lift. *Open Journal of Safety Science and Technology*, 02:8–15, 01 2012.

[36] Lara Alegria Mira, Ashley P. Thrall, and Niels De Temmerman. Deployable scissor arch for transitional shelters. *Automation in Construction*, 43:123–131, 2014.

[37] V.S. Rajashekhar, K. Thiruppathi, and R. Senthi. Modelling, simulation and control of a foldable stair mechanism with a linear actuation technique. *Procedia Engineering*, 97:1312–1321, 2014.

[38] L. Alegria Mira, R. Filomeno Coelho, A.P. Thrall, and N. De Temmerman. Parametric evaluation of deployable scissor arches. *Engineering Structures*, 99:479–491, 09 2015.

[39] Doli Rani, Nitin Agarwal, and Vineet Tirth. Design and fabrication of hydraulic scissor lift. *MIT International Journal of Mechanical Engineering*, 5(2):81–87, 08 2015.

[40] Wei Zhang, Chen Zhang, Jiangbo Zhao, and Chunzhi Du. A study on the static stability of scissor lift. *The Open Mechanical Engineering Journal*, 9:954–960, 10 2015.

[41] Dong-Jie Zhao, Jing-Shan Zhao, and Zheng-Fang Yan. Planar deployable linkage and its application in overconstrained lift mechanism. *Journal of Mechanisms and Robotics*, 8(2):021022 (9 pages), 11 2015.

[42] Andrea Corrado, W Polini, L Canale, and C Cavaliere. To design a belt drive scissor lifting table. *International Journal of Engineering and Technology*, 8(1):515–525, 02 2016.

[43] Anupam Chaturvedi, Jyoti Mishra, and Vijay Parmar. An improved scissor lift working on lead screw mechanism aerial scissor lift and its accessories. *International Journal of Advance Engineering and Research Development*, 4:4–72, 03 2017.

[44] Zhao Na, Yudong Luo, Hongbin Deng, and Yantao Shen. The deformable quad-rotor: Mechanism design, kinematics, and dynamics effects investigation. *Journal of Mechanisms and Robotics*, 10(4):045002 (5 pages), 06 2018.

[45] N. Shrivastava, A. Pande, J. Lele, and K. Kampassi. Embedded control system for self adjusting scissor lift. In *2018 Fourth International Conference on*

Computing Communication Control and Automation (ICCUBEA), pages 1–5, Aug 2018.

[46] Yi Yang, Yan Peng, Huayan Pu, Haijun Chen, Xilun Ding, Gregory S. Chirikjian, and Shengnan Lyu. Deployable parallel lower-mobility manipulators with scissor-like elements. *Mechanism and Machine Theory*, 135:226–250, 2019.

[47] Sangamesh Deepak. *Static balancing of rigid-body linkages and compliant mechanisms*. PhD thesis, Department of Mechanical Engineering Indian Institute of Science Bangalore, 2012.

[48] Jiegao Wang and Clément Gosselin. Static balancing of spatial three-degree-of-freedom parallel mechanisms. *Mechanism and Machine Theory*, 34:437–452, 04 1999.

[49] Lucien J. B. LaCoste. A new type long period vertical seismograph. *Journal of Applied Physics*, 5(7):178–180, 1934.

[50] D A. Streit and Brian Gilmore. perfect spring equilibrators for rotatable bodies. *Journal of Mechanisms Transmissions and Automation in Design*, 111(4):451–458, 12 1989.

[51] D. A. Streit, H. Chung, and B. J. Gilmore. Perfect equilibrators for rigid body spatial rotations about a hooke's joint. *Journal of Mechanical Design*, 113(4):500–507, Dec 1991.

[52] Nathan Ulrich and Vijay Kumar. Passive mechanical gravity compensation for robot manipulators. In *1991 Proceedings - IEEE International Conference on Robotics and Automation*, volume 2, pages 1–5, 1991.

[53] G J. Walsh, D A. Streit, and Brian Gilmore. Spatial spring equilibrator theory. *Mechanism and Machine Theory*, 26(2):155–170, 12 1991.

[54] Ajay Gopalswamy, Pramod Gupta, and M Vidyasagar. A new parallelogram linkage configuration for gravity compensation using torsional springs. volume 1, pages 664–669 vol.1, 06 1992.

[55] T. Rahman, R. Ramanathan, R. Seliktar, and W. Harwin. A simple technique to passively gravity-balance articulated mechanisms. *Journal of Mechanical Design*, 117(4):655–658, Dec 1995.

[56] Just L. Herder. Design of spring force compensation systems. *Mechanism and Machine Theory*, 33(1):151–161, 1998.

[57] Thierry Laliberté, Clément Gosselin, and Martin Jean. Static balancing of 3-dof planar parallel mechanisms. *Mechatronics, IEEE/ASME Transactions on*, 4(4):363–377, 01 2000.

[58] Imme Ebert-Uphoff and Clément Gosselin. Dynamic modeling of a class of spatial statically-balanced parallel platform mechanisms. In *1999 Proceedings - IEEE International Conference on Robotics and Automation*, volume 2, pages 881–888, 02 1999.

[59] Jiegao Wang and Clément Gosselin. Static balancing of spatial four-degree-of-freedom parallel mechanisms. *Mechanism and Machine Theory*, 35:563–592, 04 2000.

[60] Ion Simionescu and Liviu Ciupitu. The static balancing of the industrial robot arms: Part ii: Continuous balancing. *Mechanism and Machine Theory*, 35(9):1299–1311, 01 2000.

[61] M J French and Martin Widden. The spring-and-lever balancing mechanism, george carwardine and the anglepoise lamp. *Proceedings of The Institution of Mechanical Engineers Part C-journal of Mechanical Engineering Science - PROC INST MECH ENG C-J MECH E*, 214:501–508, 03 2000.

[62] Sunil Agrawal and Abbas Fattah. Theory and design of an orthotic device for full or partial gravity-balancing of a human leg during motion. *Neural Systems and Rehabilitation Engineering, IEEE Transactions on*, 12(2):157–165, 06 2004.

[63] Abhishek Agrawal and Sunil K. Agrawal. Design of gravity balancing leg orthosis using non-zero free length springs. *Mechanism and Machine Theory*, 40(6):693–709, 2005.

[64] Andrea Russo, Rosario Sinatra, and Fengfeng Xi. Static balancing of parallel robots. *Mechanism and Machine Theory*, 40(2):191–202, 02 2005.

[65] V. Arakelian and S. Ghazaryan. Improvement of balancing accuracy of robotic systems: Application to leg orthosis for rehabilitation devices. *Mechanism and Machine Theory*, 43(5):565–575, 2008.

[66] R. Saravanan, S. Ramabalan, and P. Dinesh Babu. Optimum static balancing of an industrial robot mechanism. *Engineering Applications of Artificial Intelligence*, 21(6):824–834, 2008.

[67] Theeraphong Wongratanaphisan and Matthew Cole. Analysis of a gravity compensated four-bar linkage mechanism with linear spring suspension. *Journal of Mechanical Design - J MECH DESIGN*, 130(1):011006 (8 pages), 01 2008.

[68] Po-Yang Lin, Graduate Student, Win-Bin Shieh, Assistant Professor, and D.Y. Chen. Design of perfectly static-balanced one-dof planar linkage with revolute joint only. *Proceedings of the ASME Design Engineering Technical Conference*, 2:617–625, 01 2009.

[69] Kenan Koser. A cam mechanism for gravity-balancing. *Mechanics Research Communications*, 36(4):523–530, 06 2009.

[70] Po-Yang Lin, Win-Bin Shieh, and D.Y. Chen. Design of a gravity-balanced general spatial serial-type manipulator. *Journal of Mechanisms and Robotics*, 2(3):031003–010, 08 2010.

[71] Rogier Barents, Mark Schenk, Wouter D. van Dorsser, Boudewijn M. Wisse, and Just Herder. Spring-to-spring balancing as energy-free adjustment method in gravity equilibrators. *Journal of Mechanical Design*, 133(6):061010 (10 pages), 01 2011.

[72] Giuseppe Radaelli, Juan Gallego Sanchez, and Just Herder. An energy approach to static balancing of systems with torsion stiffness. *Journal of Mechanical Design*, 133(9):091006 (8 pages), 09 2011.

[73] Sangamesh Deepak and G.K. Ananthasuresh. Static balancing of a four-bar linkage and its cognates. *Mechanism and Machine Theory*, 48(1):62–80, 2012.

[74] Sangamesh Deepak and G.K. Ananthasuresh. Perfect static balance of linkages by addition of springs but not auxiliary bodies. *Journal of Mechanisms and Robotics*, 4(2):021014 (12 pages), 05 2012.

[75] Po-Yang Lin, Win-Bin Shieh, and D.Y. Chen. A theoretical study of weight-balanced mechanisms for design of spring assistive mobile arm support (mas). *Mechanism and Machine Theory*, 61:156–167, 03 2013.

[76] Simon Perreault, Philippe Cardou, and Clément Gosselin. Approximate static balancing of a planar parallel cable-driven mechanism based on four-bar linkages and springs. *Mechanism and Machine Theory*, 79:64–79, 09 2014.

[77] Sanghyung Kim and Chang-Hyun Cho. Design of planar static balancer with associated linkage. *Mechanism and Machine Theory*, 81:79–93, 11 2014.

[78] Sushant Veer and S. Sujatha. Approximate spring balancing of linkages to reduce actuator requirements. *Mechanism and Machine Theory*, 86:108–124, 2015.

[79] C. Brutti, G. Coglitore, and P.P. Valentini. Modeling 3d revolute joint with clearance and contact stiffness. *Nonlinear Dynamics*, 66(4):531–548, 2011.

[80] Z. Zhang, L. Xu, P. Flores, and H.M. Lankarani. A kriging model for dynamics of mechanical systems with revolute joint clearances. *Journal of Computational and Nonlinear Dynamics*, 9(3):031013 (13 pages), 2014.

[81] E. J. Haug. *Computer Aided Kinematics and Dynamics of Mechanical Systems. Vol. 1: Basic Methods*. Allyn & Bacon, Inc., Needham Heights, MA, USA, 1989.

[82] Parviz E. Nikravesh. *Computer-aided Analysis of Mechanical Systems*. Prentice-Hall, Inc., Upper Saddle River, NJ, USA, 1988.

[83] John J. Craig. *Introduction to Robotics: Mechanics and Control*. Addison-Wesley Longman Publishing Co., Inc., Boston, MA, USA, 2nd edition, 1989.

[84] Systems with resisting force. `http://ocw.metu.edu.tr/pluginfile.php/6467/mod\_resource/content/6/ch6/6-3.html`, (Online; accessed August 17, 2018).

List of publications

International Journal

- S. K. Singh and S. Deepak R, *"Analytical reasons for smaller lateral sway in angled-plane scissor linkage"*, Journal of Mechanisms and Robotics, October 2020; 12(5): 051001.

International conference

- S. K. Singh and S. Deepak R, *"Design and fabrication of a partially statically balanced scissor linkage made of bamboo pieces"*, 3^{rd} International and 18^{th} National Conference on Machines & Mechanisms, BARC Mumbai, December 13-15, 2017.
- S. K. Singh and S. Deepak R, *"Ranking multiple static balancing solutions on the basis of friction overcoming effort"*, 5^{th} International Conference on IFToMM Asian Mechanism and Machine Science, IISc Bengaluru, India, December 17-20, 2018.

Awards

- Awarded 2^{nd} **prize** in **iNaCoMM** students mechanism design contest for the prototype described in thesis, BARC Mumbai, December 13-15, 2017.